JOURNAL OF THE AERONAUTICAL SCIENCES

VOLUME 16 DECEMBER, 1949 NUMBER 12

Combustion Problems in Ram-Jet Design

J. P. LONGWELL*

Standard Oil Development Company

SUMMARY

The requirement of a low frontal area for a ram-jet has made necessary air velocities sometimes greater than 300 ft. per sec. entering the ram-jet combustion chamber. These high velocities make combustion difficult, and a considerable amount of research has been, and still is, necessary to establish the design principles involved in building satisfactory ram-jet combustors. The problems of combustor development can be divided into choice of the best fuel, proper preparation of the fuel-air mixture, ignition of the mixture, and completion of combustion. Factors of interest in choosing the fuel are ease and safety of handling, availability, cost, ease of combustion, volatility, and heat of combustion per pound and per unit volume. Data are presented showing that petroleum hydrocarbons are more difficult to burn than special fuels such as propylene oxide but that the high heat of combustion and availability of the petroleum hydrocarbons make it desirable to develop combustors for their use.

The distribution of fuel in air is of importance in determining the performance of a combustor. It has been found that fuel sprays spread through a turbulent stream of air at a rate proportionate to the concentration gradient. With knowledge of this proportionality constant, it is possible to design an injector system to obtain the desired fuel distribution.

The problems of flame stabilization and flame spreading are more complex, but it has been found that the stability of a flame held in the wake of a baffle is capable of some generalization, and it is felt that further investigation of the variables involved in these phenomena will lead, in time, to a sound design basis for ram-jet combustors.

INTRODUCTION

THE POTENTIALITIES OF THE RAM-JET as a power plant for high-speed flight have led, in recent years, to its extensive investigation under the sponsorship of various Government agencies. The ram-jet seems best suited for supersonic flight, and its characteristic of requiring a high velocity to develop a practical amount of thrust and its simplicity of construction indicate that its most promising application may be in high-speed guided missiles where only a one-way trip is required and the problems of take-off and landing are minimized. Its apparent lack of application to commercial usage, and the military importance of its probable applications prevent public discussion of much of the material now available on ram-jet performance and details of design; however, a brief discussion of a few of the many technical problems involved in combustor development can be given. The bulk of the work discussed in this paper was done in cooperation with the Applied Physics Laboratory of The Johns Hopkins University under contract with the U.S. Navy Bureau of Ordnance.

Because of the importance of frontal area in determining the drag, and therefore the power requirement, at supersonic speeds it is necessary to keep the diameter of a ram-jet as small as possible for a given power output. This results in air velocities entering the combustion chamber sometimes greater than 300 ft. per sec. under normal operating conditions and higher than 600 ft. per sec. under starting conditions for some launching sequences. The combustion problems encountered in turbojet development due to high air velocity are therefore accentuated, since a typical air velocity preceding the combustion chamber of a turbojet would be approximately 50 ft. per sec. While it is permissible to allow 15 velocity heads of pressure drop in a turbojet combustor to obtain satisfactory combustion and mixing, this pressure drop would be disastrous at the higher velocities encountered in a ram-jet. The problem is eased somewhat in a ram-jet by the relative unimportance of having a well mixed stream of hot gases leave the combustion chamber; however, the fact that in a ram-jet it is necessary to burn efficiently in a higher velocity air stream with less drag due to the combustion chamber has given rise to problems and designs differing considerably from those found in turbojet combustion chambers.

The temperature and pressure in the combustion chamber depend on altitude and flight velocity and vary over a wide range depending on operating conditions Air temperatures between 100° and 1,200°F. might be

Presented at the Fourth National Flight Propulsion Meeting, I.A.S., Cleveland, March 18, 1949.

* Supervisor of Special Projects Group, Esso Laboratories, Process Division.

FIGURE 1

COMBUSTION EFFICIENCY AS A FUNCTION OF EQUIVALENCE RATIO

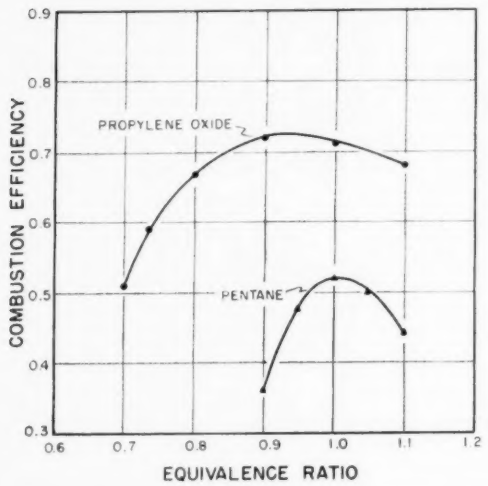

encountered and pressures range from several atmospheres down to a fraction of an atmosphere. While the total range of conditions might not be encountered by any one ram-jet, the general problem of combustor development does cover such a range.

Although the principle of the ram-jet was proposed some time ago in France, the successful application of the principle to flight was not made until 1945 when supersonic flight was maintained by a ram-jet developed by The Johns Hopkins University's Applied Physics Laboratory and associated contractors under the sponsorship of the U.S. Navy Bureau of Ordnance. As in most combustion equipment, development was carried out by trial and error, since the combination of the many important variables involved makes application of the principles of hydrodynamics and reaction kinetics difficult. Facilities for testing the larger sizes of engines, however, are extremely expensive to construct and to operate, and engines of a number of sizes operating under widely different conditions are required. It is therefore important not only to develop engines by trial and error methods but to work out a set of basic design principles that will allow design of large units to give satisfactory operation with a minimum of modification and testing.

Combustor development seems to a great extent, to be a matter of choosing a satisfactory fuel, mixing the fuel properly with the air, igniting it, and then allowing sufficient time for the combustion reaction to run its course. For purposes of the discussion that follows, the subject matter has been divided into the above categories.

FIGURE 2

BURNING VELOCITY AS A FUNCTION OF EQUIVALENCE RATIO

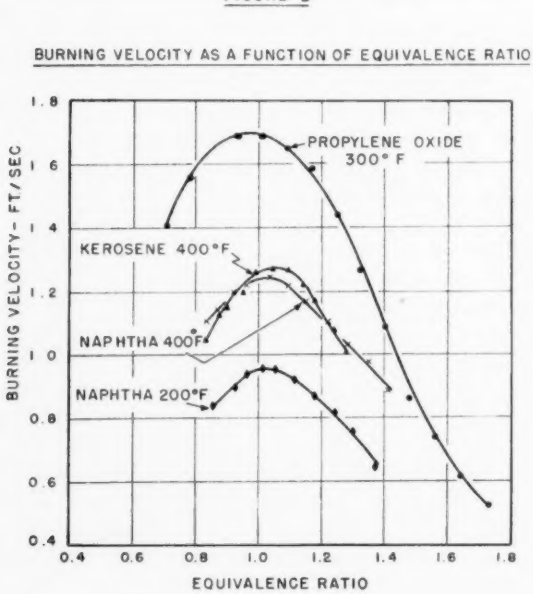

Choice of Fuel

Operational requirements determine, to a great extent, the air temperature, pressure, and velocity, but some choice is allowed in fuel, which also is important in determining the design of the combustion chamber. The ram-jet differs from the turbojet in this respect, since, while an airplane during its lifetime may consume a large quantity of fuel compared to its weight, the ram-jet, if used in a missile, makes only one flight and uses a relatively small quantity of fuel. So, while the problem of supplying sufficient quantities of fuel may control fuel specifications for piloted aircraft, missiles, because of the relatively small quantity of fuel used, could, if desirable, be fueled with more expensive fuels, which, perhaps, could only be produced in limited quantity. On the other hand, it is always desirable to use a cheap and plentiful fuel, so that any special fuel would have to show a distinct advantage.

Aside from availability, a fuel would be judged by the following characteristics: (1) heat of combustion per unit volume of fuel and per pound of air; (2) ease of handling; and (3) ease of combustion.

Ease of handling tends to rule out solid and gaseous fuels, since liquid fuels are much to be preferred by this criterion. Unstable fuels that tend to decompose or to become dangerous in storage would also tend to be ruled out.

Of the stable liquid fuels presently available in reasonably large quantities, petroleum hydrocarbons give the highest heat release per unit volume but are somewhat inferior to some oxygenated hydrocarbons in ease of combustion. This point is illustrated in Fig. 1 (reference 1) where combustion efficiency is plotted as a function of equivalence ratio (stoichiometric air/fuel ratio divided by mixture air/fuel ratio) for a ram-jet type combustor burning pentane and propylene oxide. It is seen that this particular combustor does not burn

pentane so efficiently as propylene oxide. The propylene oxide, on the other hand, has a gross heating value of 14,167 B.t.u. per lb. of fuel as compared to 20,810 B.t.u. per lb. for pentane. Since propylene oxide is also more expensive and less plentiful than pentane, it is desirable to develop a burner capable of successfully burning a hydrocarbon such as pentane.

Several important points are brought out by considering measurements of laminar burning velocity and static inflammability limits. Fig. 2 shows the laminar burning velocity, determined by the Bunsen burner method, of a petroleum naphtha, kerosene, and propylene oxide as a function of equivalence ratio. It is seen that the kerosene and the naphtha have nearly the same burning velocity but that propylene oxide will burn a great deal faster. Maximum burning velocity occurs slightly on the rich side of stoichiometric, indicating greatest ease of burning under rich conditions. It is also noted that, as temperature is reduced from 400° to 200°F., the maximum burning velocity is reduced approximately 24 per cent, so one would expect more difficulty in developing a ram-jet to operate satisfactorily at low air temperatures than at high ones. It is also of interest to note that the highest flame velocity on Fig. 2 is 1.7 ft. per sec., which is small compared to the velocity of the air stream in which the flame is to be stabilized.

Fig. 3 shows static inflammability limits as a function of pressure for several fuels. It will be noted that all of these fuels have a minimum pressure below which ignition cannot be obtained and that this minimum pressure occurs at mixtures somewhat richer than stoichiometric.

Iso-pentane has the narrowest range over which a flame will propagate and also the highest minimum ignition pressure. Propylene oxide can be burned at a lower pressure and over a wider range, and acetylene can be burned over a much wider range of conditions. It would be expected that, under the difficult burning conditions occurring in a ram-jet combustor, one would not quite reach the limits of operating indicated by the static inflammability tests; however, the static inflammability limits probably indicate trends. If the same improvement of minimum ignition pressure were noted in a ram-jet combustor as in inflammability limits, then one might expect to be able to operate at an altitude approximately 35,000 ft. higher if acetylene were used rather than iso-pentane. This advantage would be difficult to realize in practice because of the difficulty in handling acetylene.

The condition of the fuel (whether it is liquid or vapor) when it arrives at the point of ignition also has an effect on its combustion characteristics. It is therefore of interest to know whether a fuel, when injected into the combustion chamber, is capable of evaporating before reaching the point of ignition. It is possible to calculate the equilibrium fraction evaporated of a fuel for various conditions if the distillation

FIGURE 3
STATIC INFLAMMABILITY LIMITS AS A FUNCTION OF PRESSURE

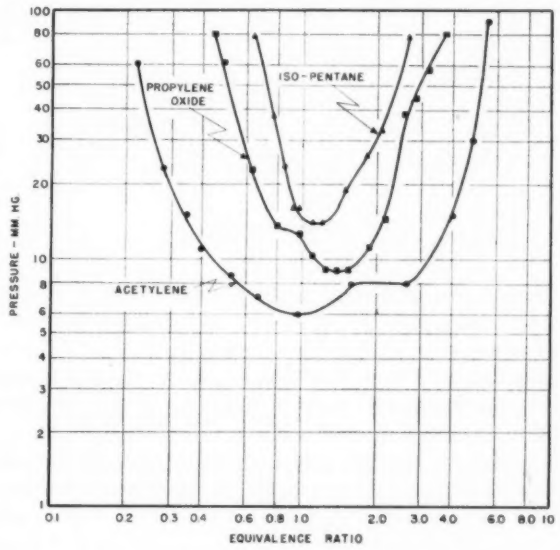

curve and the molecular weight of the various fractions distilled are known. Such information is available for petroleum fuels, and the results of such a calculation are shown in Fig. 4 for a stoichiometric mixture of a typical kerosene-type fuel and air under various conditions of pressure and temperature. The whole range of pressures and temperatures shown on Fig. 4 may be encountered in flights, and it can be seen that under some conditions of flight the kerosene is capable of completely evaporating, while under other conditions only a small fraction can evaporate. It would, of course, be possible to choose a fuel of such low vapor pressure that evaporation would be kept small or a fuel so volatile that substantially complete evaporation would be possible under all operating conditions. Such considerations are of importance in selecting a fuel.

FIGURE 4
EQUILIBRIUM VAPORIZATION OF KEROSENE AS A FUNCTION OF PRESSURE AND TEMPERATURE
STOICHIOMETRIC MIXTURE

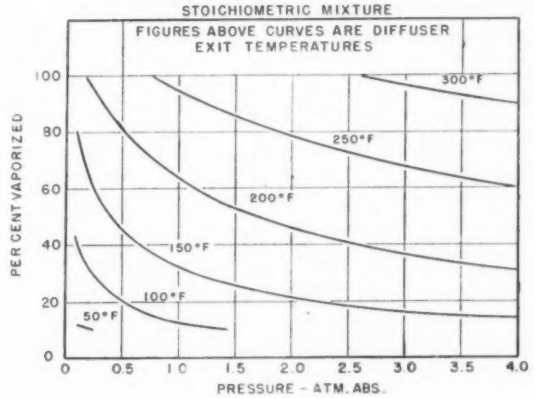

FIGURE 5

DIAGRAMMATIC SKETCH OF A RAM - JET

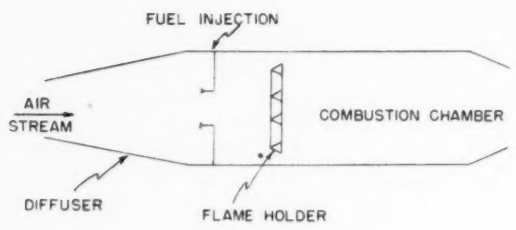

Combustion, in general, proceeds more easily if the fuel is at least partially vaporized at the point of ignition; so it would be desirable to choose a fuel of volatility characteristics such that evaporation is possible under the conditions of flight. Handling characteristics, however, must also be considered, since fuels of extremely low volatility tend to freeze under low-temperature storage conditions and fuels of high vapor pressure tend to evaporate in the fuel tank or cause vapor lock in the pumping system under some conditions of high altitude operation.

In view of the short time elapsing between the time a particle of fuel is injected and the time it reaches the point of ignition, it cannot be expected that equilibrium will be reached; however, such calculations seem to define the limits to which evaporation can go. The extent to which equilibrium is approached is considerably more difficult to determine and is a problem of current interest.

FIGURE 6

FUEL CONCENTRATION DOWNSTREAM FROM A SINGLE CONTRASTREAM INJECTION NEEDLE

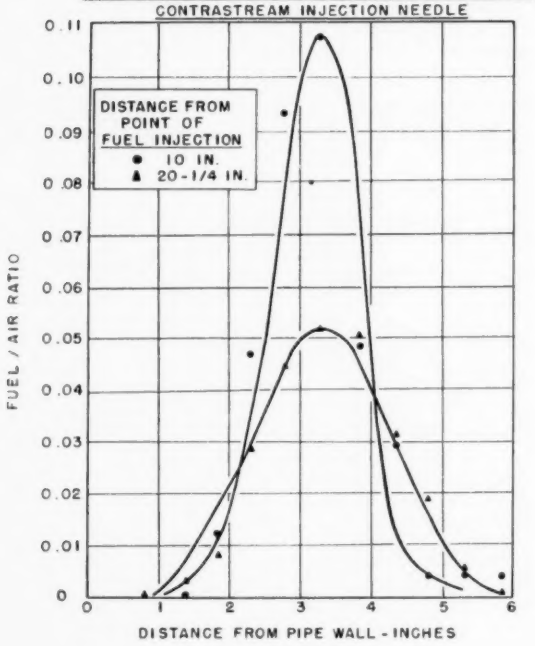

Fig. 5 is a diagrammatic sketch of a common type of ram-jet design. Fuel is injected upstream of the igniting device, which is followed by the combustion chamber in which burning and mixing are completed. These three sections will be discussed separately, since their problems and functions are different.

Mixing of Fuel and Air

The purpose of the fuel injection system is to provide a well-atomized supply of fuel, properly mixed with the air, to the igniting section. The high-velocity stream of air occurring in a ram-jet is an advantage in obtaining good atomization since the impact of the air stream on the entering fuel is quite effective in breaking the fuel up into small particles. One could estimate from the work of Nukeyama and Tanesawa[2] that, with an air stream having a velocity of 300 ft. per sec. relative to the fuel jet, the weight median drop diameter would be approximately 40 microns. In a turbojet, such a high velocity is not readily available, and vortex-type mechanical atomizing nozzles are used. It would be estimated that with 100-lb.-per-sq.in. pressure drop through a typical turbojet vortex nozzle discharging into still air, a median drop diameter of 200 microns would be obtained. Since the vortex nozzle is satisfactory for many high-speed combustion uses, it is apparent that air atomization is promising for use in ram-jets.

As illustrated in Figs. 1–3, the relative proportions of fuel and air are important in determining the ease of combustion. One would not expect flame propagation outside the inflammability limits, and greatest ease of burning would be expected for near stoichiometric mixtures. Since the average fuel/air ratio is determined by operational requirements and may be considerably leaner than stoichiometric and since experience has also shown that stability of operation is dependent on fuel distribution, it is important to be able to determine the distribution of fuel at the point of ignition.

The distribution of fuel downstream from a single contrastream point of fuel injection mounted in a 6-in. diameter pipe is shown in Fig. 6.

The data points were determined by measurement of the fuel/air ratio at various points along a pipe diameter at distances of 10 and 20 in. downstream from the point of injection. The solid lines are plotted from the following equation:

$$f = (W_f u/4\pi C W_a X) e^{-r^2 u/4CX}$$

where

f = fuel/air ratio
W_f = weight rate of fuel flow
W_a = weight rate of air flow per unit of duct area
u = air velocity
r = distance from center of duct

X = distance from point of injection to diameter along which samples were taken
C = diffusion coefficient

A diffusion coefficient of 0.705 sq.ft. per sec. was used, and it is seen that this equation describes the distribution of fuel with sufficient accuracy to be adequate for many purposes. The above equation was derived by assuming that rate of diffusion was proportional to concentration gradient and that injection point was a point source of the diffusing material. A derivation of the equation is given in the Appendix. With knowledge of how this diffusion coefficient varies with other variables such as velocity, pressure, fraction vaporized, etc., it is possible to calculate the fuel distribution for more complicated cases, such as when several injection points are used or when wall effects are important.

Flame Stabilization

It has been found that under most ram-jet operating conditions a flame can be stabilized in the wake of a baffle mounted in the flowing mixture of fuel and air. This method of ignition is the basis of many ram-jet combustor designs and has been given considerable study. It is believed that the flame is stabilized because of a zone of recirculation established in the wake of the baffle. By means of this recirculation, hot combustion products are fed back into the baffle where they serve as a continuous source of ignition for the fresh mixture flowing past the edge of the baffle. Under high-velocity flow conditions with a baffle of circular cross section, material can flow upstream to the baffle from a point as far as 1.7 baffle diameters downstream from the baffle. Under adverse operating conditions, the flame is observed to pinch down at the downstream end of this recirculation zone and seems first to become unstable at this point. It is important to know the range of equivalence ratios over which a stable flame will be maintained in the wake of a baffle as a function of its size and shape and of the operating conditions. This was done in equipment in which some of the complicating factors that occur in a complete ram-jet were eliminated. Instead of an unevenly distributed mixture of fuel and air, as encountered in jet propulsion equipment, a homogeneous mixture of fuel vapors and air flowed past the baffle. The baffle was mounted centrally in the duct so that flow was symmetrical, and an effort was made to avoid large pressure fluctuations by using a short tailpipe. This equipment is diagrammatically illustrated in Fig. 7; in this case the baffle is of a long cylindrical shape mounted axially in the 6-in. pipe.

The results of this study for 1 atmosphere pressure and an entering air temperature of 300°F. are summarized in Fig. 8. In this figure the range of stable operation in terms of equivalence ratio is plotted as a function of the baffle radius (R) divided by the mixture velocity (V) past the baffle. At high values of R/V the curves become almost parallel, the lean limit approaching a value of 0.63 and the rich limit approaching a value of 1.7 indicating that above an R/V of 20×10^{-5} sec. little gain in stability range is to be expected by using larger flameholders for a given mixture velocity. Substantial losses in stability range seem to occur, however, if baffle diameters and velocity are such that R/V is much below this value. It is interesting to note that the lean limit of 0.63 is very near the static lean inflammability limit of 0.58 for this fuel but that the rich limit of 1.7 is much leaner than the static inflammability limit of approximately 3.4 generally reported for this type of fuel.

FIGURE 7

DIAGRAMMATIC SKETCH OF EQUIPMENT FOR STUDYING SIMPLIFIED FLAME HOLDERS

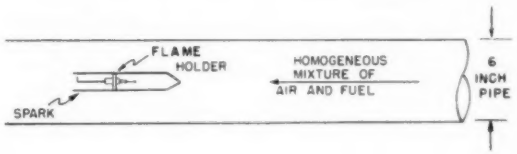

FIGURE 8

EFFECT OF MIXTURE VELOCITY AND BAFFLE DIAMETER ON STABILITY RANGE

PRESSURE 1 ATMOSPHERE INLET AIR TEMP. 300 °F.

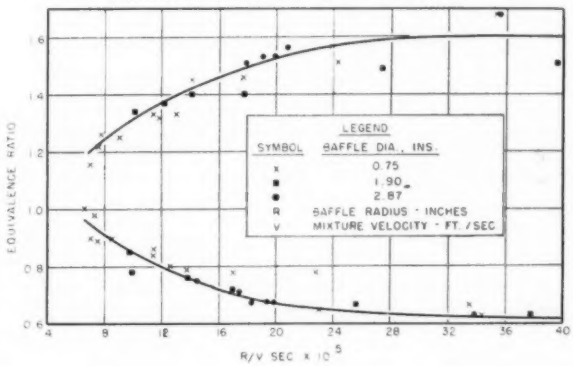

Baffles of other shapes have been tested, and the results can be summarized by stating that, for baffles of circular cross section, streamlining of the downstream face tends to reduce the stability of the flame but that other changes do not have a large effect by this criterion. It was also found that the results for baffles of other cross-sectional shapes can be placed on Fig. 8 by using twice the mean hydraulic radius for the characterizing dimension. A similar study on smaller baffles was carried out at M.I.T.[3] The results were, in general, similar; however, they found that $R^{0.45}/V$ gave the best correlation for their data.

The effect of inlet air temperature is illustrated in Table 1, where it is seen that increasing the inlet air temperature tends to widen the limits. From meas-

FIGURE 9

STABILITY CRITERION AS A FUNCTION OF BLOCKAGE RATIO

COMBUSTION CHAMBER DIAMETER = 6 INCHES

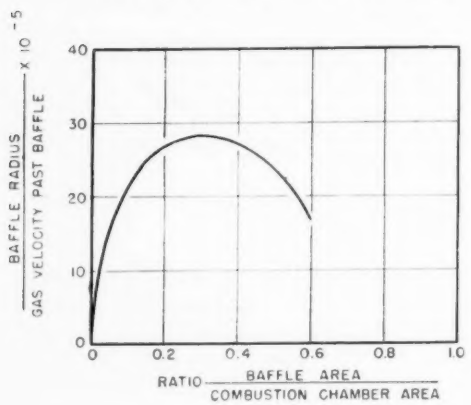

urement of static inflammability limits one would have expected approximately the degree of widening observed.

TABLE 1

Effect of Temperature on Stability Limits

Pressure: 1 Atmosphere; Air Velocity: 275 Ft. per Sec.; Baffle Diameter: 0.75 In.

Inlet Air Temperature, °F.	Stability Limits Equivalence Ratio
205	1.27-0.77
330	1.37-0.76
400	1.37-0.73
500	1.37-0.69

The effect of pressure is indicated by the data in Table 2. A larger effect at the low pressure was observed with smaller flameholders; however, with the larger flameholder, range of operation was quite insensitive to changes in pressure.

TABLE 2

Effect of Pressure on Stability Limits

Inlet Air Temperature: 300°F.; Baffle Diameter: 2.87 In.

Pressure, Lbs. per Sq.In. Absolute	Velocity, Ft. per Sec.	Range of Stable Burning Equivalence Ratio
2.9	470	1.31-0.69
15	400	1.68-0.60
40	400	1.68-0.61

Using R/V as a criterion of stability it is possible to estimate the relative stability of various baffle configurations. For example, if an extremely small baffle is placed in a duct through which a given mass flow of air flows, increasing its size a small amount will result in little change in the velocity past it compared to the increase in R, so a higher value of R/V will be obtained. However, if the process is continued, the blockage of the baffle will become appreciable, the velocity will increase considerably, and the value of R/V will diminish. Fig. 9 shows R/V as a function of blockage ratio, and it is seen that the highest R/V is obtained at a blockage ratio of 0.3.

The above calculation is an example of the current attempt to develop design criteria for ram-jet combustors; however, it is far from a complete study, since the data used were taken under idealized conditions, and other considerations of equal importance such as drag and combustion efficiency enter into flame stabilizer design.

Flame Spreading

The combustion chamber receives a mixture of air and fuel in which combustion has been started at a number of points, and it is necessary that sufficient space be allotted for the flame to spread through the fuel-air mixture. One would expect that the rate of combustion depends on the burning velocity normal to the flame front and on the area of the flame front.

While the laminar burning velocity, determined by the Bunsen-burner technique, is measured under flow conditions quite different from those occurring in a ram-jet, data indicate that the laminar burning velocity will, under some conditions, serve as a measure of the relative amount of combustion of a fuel in a ram-jet. This was pointed out by Scurlock,[3] who compared, by time exposure photographs, the rate of spread of city gas-air and propane-air flames under simulated ram-jet operating conditions. He found that the rate of spread of the flame was greater for the city gas-air mixture, which had approximately twice the laminar burning velocity of the propane-air mixture, approximately in proportion to the ratio of laminar burning velocities. This effect is also illustrated by Figs. 1 and 2. In Fig. 1 it is shown that the combustion efficiency for a particular ram-jet is highest for mixture ratios near stoichiometric and that propylene oxide gives a higher combustion efficiency than a paraffin hydrocarbon. Examination of Fig. 2 shows the same trend for the laminar burning velocities of these fuels.

Since the thickness of the flame front under laminar burning conditions is of the order of 0.1 mm., the scale of turbulence existing in large equipment would be expected to be considerably larger than this. In this case the area of the flame front is increased by the distortion of the surface due to turbulent flow. Photographic evidence presented by Scurlock[3] indicates that, under ram-jet conditions, the turbulence of the air upstream from the igniters has relatively little effect on the rate of flame spreading as compared to the mixing introduced by the flow past the igniters and the mixing caused by the acceleration of the burned gases. High-speed photographs of flame fronts show that the surface of the flame is extremely ragged. Determination of the area is therefore difficult, and the tendency has been to report a flame velocity based on time exposure photographs of the flame. Such a value would be high if used to calculate the rate at which the mixture is

burned, since a large amount of unburned fuel may be included within the boundaries indicated by such a photograph. Quantitative data on actual rates of burning are not available; however, this problem is of considerable theoretical and practical interest.

Since the flame spreads through the unburned mixture from the surface of the flame held in the wake of the flame stabilizers, one would expect that the length of combustion chamber would then depend on the distance between flame stabilizers. In order to keep this distance to a minimum, one would want to use a large number of flame stabilizers, but to keep the blockage of the stabilizer low it would be necessary to use small stabilizers. In the preceding section, however, it was pointed out that as the size of a baffle is reduced the stability range is also reduced; so it is necessary to compromise between the shorter combustion chamber possible with a large number of small baffles and the loss of igniter stability resulting from reducing the baffle size. In order to arrive at the best compromise for the great variety of possible ram-jet motors, it can be seen that accurate data on baffle stability and on combustion rates are necessary.

One of the outstanding problems encountered when the combustion chamber is added to the flame stabilization section is the rough and explosive burning that sometimes occurs. Knowing the fuel distribution and the stability range of the baffles, one could attempt to predict the range of air/fuel ratios over which stable operation can be maintained; however, rough and unstable burning sometimes occurs within this predicted range This phenomenon is apparently a consequence of spreading the flame throughout the high-velocity gas stream and might be expected from the following reasoning. Since the pressure at the inlet to the combustion chamber can, under some circumstances, be twice that at the exit, because of the heating of the gas stream, a change in the amount of combustion will change the pressure, and this change in pressure can change the flow through the diffuser, the rate of fuel flow, and other variables of importance to the combustor. With such a situation many opportunities for resonance phenomena and instability exist, depending on the exact relation between these variables, and, while rules of thumb that allow one to avoid this situation are being developed through experience, this is another phenomenon that needs study and generalization.

Conclusions

While the data and discussion given in this paper have perhaps raised more questions than they have given answers, it is felt that indications exist that generalization of many of the processes involved in ram-jet combustion is possible. Development of a firm basis for the various phases of combustor design will require a large amount of further research, which, it is felt, is justified in view of the great expense of testing large ram-jets and the variety of conditions under which it appears ram-jets will operate.

References

[1] Mullen, J. W., II, Unpublished Data, Experiment Incorporated, Richmond, Va.

[2] Lewis, H. C., *et al.*, *Atomization of Liquids in High Velocity Gas Streams*, Ind. & Eng. Chem., Vol. 40, No. 1, pp. 67–74, January, 1948.

[3] Scurlock, A. C., *Flame Stabilization and Propagation in High Velocity Gas Stream*, Project Meteor Report No. 19, M.I.T., May, 1948.

Appendix I

Derivation of Equation for Fuel Concentration Downstream from a Point Source

If it is assumed that the rate of spreading of fuel in a ram-jet downstream from a point of fuel injection is proportional to the concentration gradient, it is possible to calculate the shape of the fuel distribution curve as follows:

$$\partial V/\partial t = -CA(\partial f/\partial r) \tag{1}$$

where

V = the volume of diffusing material
t = time
C = diffusion coefficient
f = fuel/air ratio
A = area normal to the direction r

This equation can be applied to the case where fuel is injected at a point making the following assumptions: (1) steady flow in the system; (2) a flat velocity distribution; (3) the amount of mixing in the direction of flow (x) negligible in comparison with the mixing in a radial direction (r); (4) the mixing coefficient (C) constant at all points in the system; and (5) the duct is extremely large in diameter.

Applying a material balance to this system, Eq. (1) becomes:

$$\partial f/\partial x = (C/u)[(1/r)(\partial f/\partial r) + (\partial^2 f/\partial r^2)] \tag{2}$$

where u is the stream velocity.

A solution of the equation which will also describe the boundary conditions is

$$f = (1/ax)e^{-br^2/x} \tag{3}$$

where a and b are constants

By differentiating Eq. (3) and substituting in Eq. (2), one finds that

$$b = u/4C \tag{4}$$

Substituting Eq. (4) into Eq. (3), we have

$$f = (1/ax)e^{-ur^2/4Cx} \tag{5}$$

(*Continued on page 760*)

Basic Studies on Flame Stabilization

GLENN C. WILLIAMS*

Massachusetts Institute of Technology

ABSTRACT

This is a report of initial studies to determine the mechanism of anchoring flame in high-velocity air-fuel streams. Simple bluff shapes were used as flame stabilizers in a constant area 1- × 3-in. rectangular duct carrying homogeneous mixtures of air and gaseous fuel. The limiting gas velocity above which flames blew off the stabilizers were studied as it was affected by:

(1) The approach gas stream variables. (a) Fuel-air ratio (over the whole range of inflammability). (b) Turbulence (intensities from 0.3 to 8 per cent of the approach stream velocity). (c) Fuel type (commercial propane and city gas).

(2) Stabilizer variables. (a) Size (Characteristic dimension from 0.02 to 0.5 in.) (b) Shape (simple, faired, and shortened rods, flat plates, gutters, spheres). (c) Addition or extraction of heat from stabilizer.

On the basis of experimental evidence, the following conclusions were reached:

(1) Flame stabilization behind bluff obstacles depends on the presence of a recirculating eddy region that is filled with hot combustion products and furnishes continuous ignition to the approaching unburned gases.

(2) Over the range of stabilizer sizes studied, the blowout velocity under steady flow conditions was found to be affected primarily by the properties of the approach gas stream and the stabilizer thickness.

(a) For span-thickness ratios greater than 2, the blowout velocity at a given air-fuel ratio in the absence of approach stream turbulence was independent of the stabilizer shape and proportional to the thickness to the 0.45 power.

(b) For span-thickness ratios less than 2, the corresponding blowout velocity was roughly proportional to the first power of the thickness.

(c) The stability limits for a stabilizer of given characteristic dimension are unaffected by variation (simulated) of ratio of chamber width to stabilizer thickness over the range 10 to 80.

(3) Increasing turbulence in the approach gas stream decreased both the velocity and air-fuel ratio ranges over which flame could be maintained. The effect of imposing turbulence of a given scale and intensity diminishes with increasing ratio of stabilizer thickness to turbulence scale.

(4) Heating the stabilizer other than by the flame markedly increases the stability limits, and externally cooling the stabilizer markedly decreases the stability limits.

(5) The maximum blowout velocities occur with slightly leaner than stoichiometric mixtures of city gas (26 per cent H_2) and richer than stoichiometric for propane. This is attributed to the different ratios of molecular diffusivity to that of air for the two fuels.

(6) Flame blowoff usually proceeds stepwise, flame propagation throughout the main stream ceasing before the eddy zone behind the stabilizer is quenched.

NOMENCLATURE

a, c = dimensionless constants
Cp = mass specific heat at constant pressure
f = mass ratio of fuel to air
n = stabilizer thickness
T = absolute temperature
V = velocity
δ_t = thickness of preignition zone
ν = kinematic viscosity
0 = subscript indicating entrance conditions
i = subscript indicating ignition conditions

Presented at the fourth National Flight Propulsion Meeting, I.A.S., Cleveland, March 18, 1949.

* Professor of Chemical Engineering.

(I) INTRODUCTION

OF THE PERFORMANCE PARAMETERS used to evaluate combustion chamber performance for aircraft propulsion application, one of the most critical is the limitation of operating ranges of air-fuel ratio and flow velocity due to inability to maintain stable combustion. In order to attack the problem of designing combustion chambers having desirably wide ranges of operability, it is in order to attempt to discover the laws governing the mechanism of flame stabilization or at least to determine empirically the variables affecting flame stability in high-output systems, as well as quantitative information on the effects of variation of these variables. It is well known[3, 5] that, at the gas velocity ranges of interest in the operation of Bunsen-type flames, the criterion for flame stabilization on a surface parallel to the gas flow calls for the existence of a particular gas velocity profile in a plane normal to the surface. This profile must include, at a distance no less than a certain minimum value (the quenching distance) from the stabilizing surface, a gas velocity no greater than laminar flame velocity. Since laminar flame velocities for most fuel-air mixtures of general interest are less than a few feet per second and since laminar boundary layers on surfaces in high-velocity streams are usually much thinner than the minimum allowable quenching distance, flame-holding on flat surfaces is obviously unsuited to high-output systems that may operate with inlet gas velocities as high as 500 ft. per sec. Early experiments[5–7] with flames stabilized downstream of blunt-ended wires showed that flames could be stabilized on these wires at higher gas velocities than on flat surfaces. In contrast to experiments on normal Bunsen flames, no correlation appears to exit between the gas velocity at which flame blew off the blunt ends of the wires and the velocity gradient at the wire surface. The most successful steady-flow propulsive combustion chambers developed to date have exploited the superior flame-holding abilities of bluff shapes. Attempts to isolate separate effects of the various variables presumed to influence

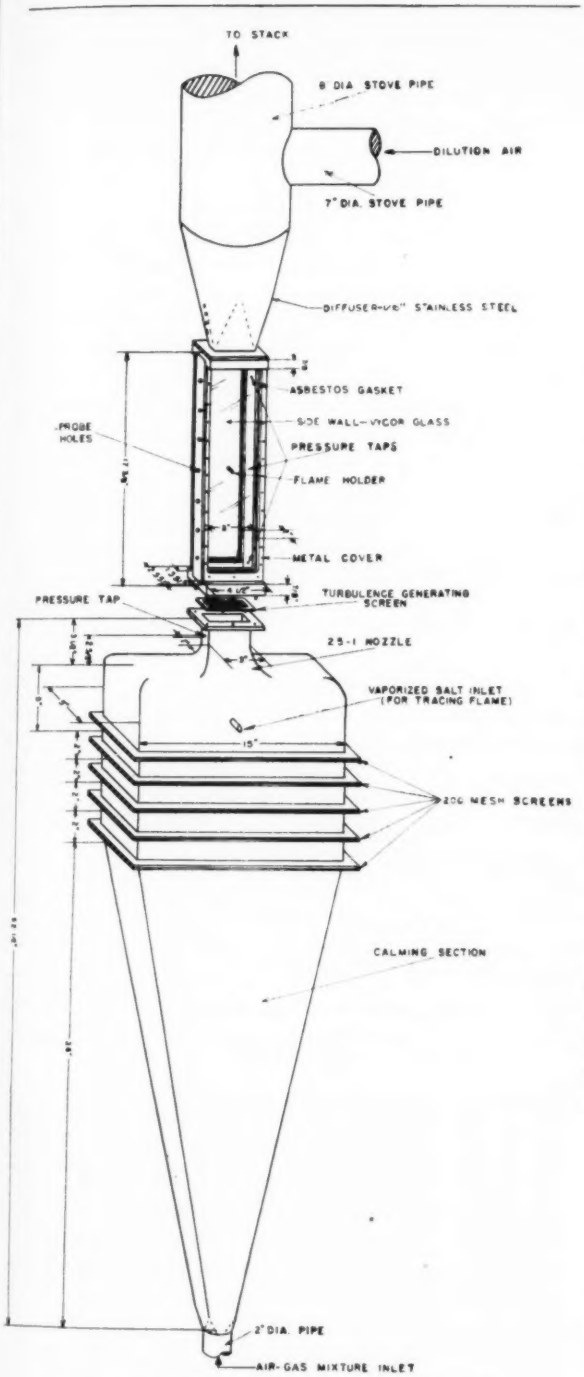

FIG. 1. Combustion chamber and calming section.

burner performance by studies on complete combustion chambers have been unsuccessful.

The purpose of this investigation was to study flame stabilization on bluff shapes in experiments designed to allow independent study of several variables while eliminating or holding constant those variables not under study. The variables studied were air-fuel ratio, approach gas velocity, turbulence in the approach gas stream, flame stabilizer size and shape, and fuel type (Cambridge city gas and commercial propane).

(II) Apparatus and Procedure

The experimental apparatus, Fig. 1, consisted of a constant cross section, 3 by 1 in., low turbulence duct, 17 in. long, through which homogeneous mixtures of gaseous fuel in air could be flowed steadily with entrance pressure and temperature of about one atmosphere and 300°K. and at entrance velocities from 20 to 350 ft. per sec.

As shown in Fig. 1, the mixture flows through a calming section—consisting of a diffuser, five 200-mesh screens, and a 25 to 1 contraction-ratio nozzle—and enters the combustion chamber. The turbulence intensity at entry is less than 0.5 per cent of the mean velocity, and the velocity profile is flat. Screens of different mesh and wire diameter were placed at the combustion chamber entrance to raise the turbulence level in the chamber. The rectangular combustion chamber had two 3-in. wide opposing walls of Vycor glass to allow observation and photography of the flame. Flame stabilizers of simple shape and of various sizes were supported with axes normal to the direction of flow between the opposing glass sidewalls. The stabilized flame when viewed along the axis of a stabilizer gave an appearance of two-dimensionality.

The parameters chosen for study were varied as follows: air-fuel ratio, lean limit to rich limit blowout; combustion chamber entrance velocity, 20–350 ft. per sec.; entering stream turbulence intensity, 0.4–8.0 per cent; turbulence scale, 0.01–0.08 in.; flame stabilizer thickness, 0.016–0.5 in.. span, 0.1–1.0 in.; flame stabilizer shapes, single cylindrical rods, shortened rods with rounded ends, rods with wedge-shaped upstream fairings, spheres, 30° closed-edge and open-edge gutters, flat plates, multiple rods.

Characteristics of the fuel-gases used were:

Cambridge City Gas		Commercial Propane	
CO_2	7.3%	C_3H_8	2.4
Illuminants	9.8%	C_3H_6	83.8
O_2	0.6%	C_2H_6	13.3
CO	21.8%	C_4H_{10}	0.5
CH_4	14.7%		
H_2	26.8%		
N_2	19.0%		
Pounds air per pound gas required to make stoichiometric mixtures	6.51		15.6

Runs were made to obtain blowout limits and photographs of the flame at various air-fuel ratios and combustion chamber entrance velocities, with different sizes, shapes, and locations of the flame stabilizer, and for different turbulence levels.

Prior to making runs with flame, the gas flow through the chamber was examined in some detail, with turbulence generated by one of three screens of mesh 3, 8, and 55 per in.; wire diameter, 0.063, 0.025, and 0.007

in.; and fractional blocked area, 0.342, 0.360, and 0.629, respectively, as well as with no screen present. Figs. 2 and 3 show the results of calculations and measurements of turbulence. The calculations were made using Dryden's equation[2] for decay of turbulence downstream from screens, assuming in the case of the no-screen runs that the turbulence was that existing 6 in. from a 200-mesh screen (in the calming section), reduced twenty-five-fold in intensity by contraction but unchanged in scale. Experimental measurements of turbulence were made with a two-probe hot-wire anemometer designed for use up to frequencies of 20,000 cycles per sec. The measured per cent turbulence falls below the calculated values for all three screens except near the exit end of the chamber, where the measured values begin to increase because of diffusion out into the main stream of turbulence generated in the boundary layer.

With no screen at the chamber entrance the measured values of turbulence are considerably above the calculated values (0.4 per cent measured, 0.02 per cent calculated). That this discrepancy is probably due to pulsations from the air compressor is shown by comparison of the 0.07 per cent turbulence measured with the air supplied to the chamber by blowing down a large surge tank, with a reading 0.3 per cent obtained under the same conditions except with the compressor on. The measured values of scale are in every case larger than the calculated values. Comparison of measured and calculated values of scale and intensity in Figs. 2 and 3 suggests that the hot wire was not sufficiently compensated for time lag in these tests. Other possible reasons for disagreement are the presence of small oil droplets and the vibratory effects of the air compressor.

The critical velocity for boundary-layer turbulence was determined with the turbulence probe at three locations along the chamber length. Corresponding Reynolds Numbers based on the distance from the end of the converging section of the nozzle were about 10,[6] independent of location. At all velocities greater than about 20 ft. per sec., the boundary layer in the major portion of the chamber is turbulent with a measured intensity of about 3 to 5 per cent. No systematic change in boundary-layer thickness or ratio of local to mean velocity V_0 was observed with changes in V_0.

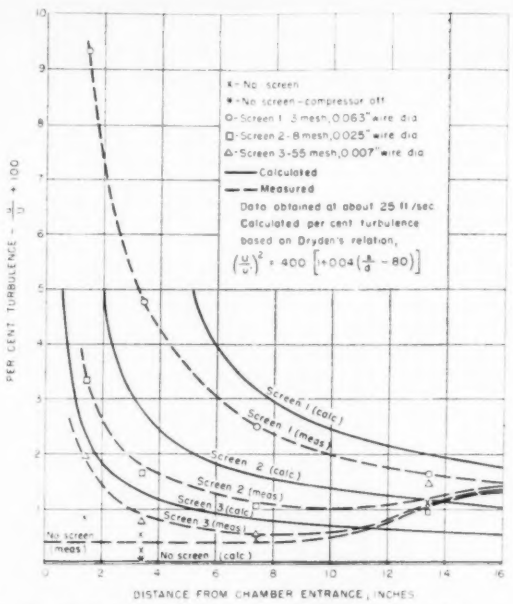

FIG. 2. Turbulence intensity in chamber with cold flow.

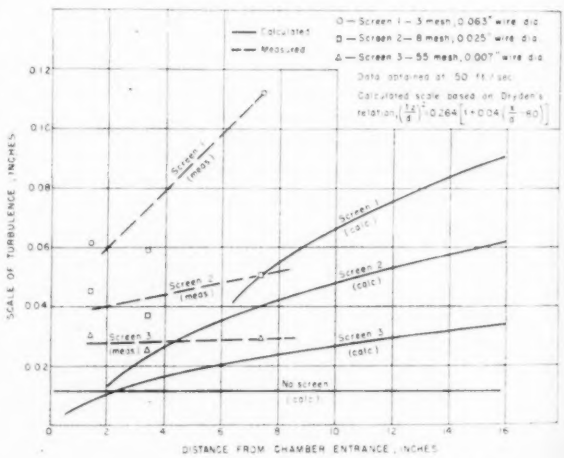

FIG. 3. Turbulence scale in chamber with cold flow.

(III) THEORETICAL CONSIDERATIONS

As the cold approach stream gases pass around a bluff shape, separate from it, and then contact the hot gases in the eddy region, heat and chain carriers are transferred from the eddy zone to the portion of the cold unburned stream nearest the eddy region. This cold gas soon reaches its ignition temperature and burns. During the time that this recently ignited gas parcel flows past the rest of the eddy region, heat and chain carriers flow back into the eddy region and replenish the previous depletion. The recirculation of the hot gases in the eddy region thus furnishes a continuous source of ignition for the unburned gases. Assuming thermally controlled ignition, the required heat supply rate for ignition of the approach stream increases with V_0, with the difference $(T_i - T_0)$ between the ignition temperature and the approach stream temperature, the thickness of the preignition zone δ_i and the heat capacity per unit volume ρCp. The rate of heat supply necessary to assure continuous ignition is then proportional to

$$V_0[\delta_i(\rho Cp)(T_i - T_0)] \qquad (1)$$

If δ_i is assumed proportional to the ratio of thermal diffusivity $k/\rho Cp$ to laminar flame speed S_L, relation 1 becomes

$$V_0 k/S_L\,(T_i - T_0) \qquad (2)$$

From heat-transfer considerations the rate of heat supply from the eddy region (size assumed proportional to n, the stabilizer thickness) to the unburned gas prior to ignition is proportional to the product of the transfer area, the coefficient, and the temperature difference between burned and unburned gases,

$$[(nV_0/\nu)^c(k/n)]n(T_b - T_0) \qquad (3)$$

The bracketed term in relation (3) allows for the factors affecting the heat-transfer coefficient (ν is the kinematic viscosity of the gases), and the other two terms allow for area and temperature difference. For blowout to occur, the heat supply rate must be infinitesimally less than the heat required. Equating relations (2) and (3) and rearranging so that all quantities thought to be a function of air-fuel ratio appear on the right-hand side, the following relation results:

$$\frac{V_{B_0}}{n^a} \propto \frac{1}{\nu^a}\left[\frac{S_L(T_b - T_0)}{T_i - T_0}\right]^{1+a} = \phi\left(\frac{1}{f}\right) \qquad (4)$$

where the new exponent a replaces $c/(1-c)$ and f is the mass fuel-air ratio.

It is interesting to note the only effect of pressure on the blowout limits as predicted by Eq. (4) is that on density through its effect on the kinematic viscosity ν, which varies inversely with the pressure. Thus, the blowout velocity should be reduced as pressure is decreased.

(IV) Experimental Results

Visual observation of the flames leads to the conclusion that the eddy region just downstream of the stabilizer consists of completely burned gases.

Examination of flame photographs similar to those of Fig. 4 shows no effect of air-fuel ratio or of approach-stream velocity on the location with respect to the stabilizer of the first appearance of reaction.

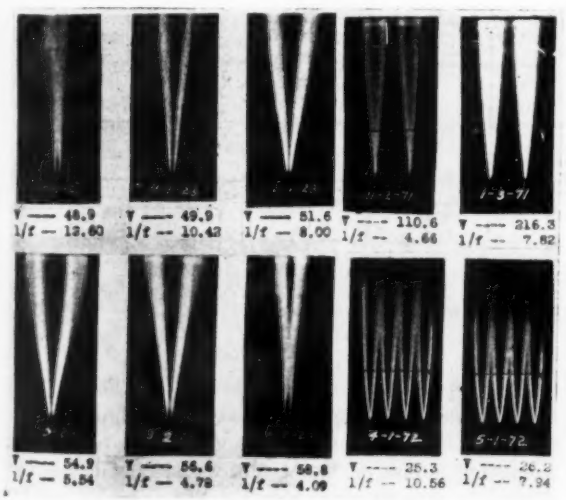

FIG. 4. Typical flames on rod flameholders.

Inability to hold flame in a high-velocity stream on an unheated surface that does not provide an eddy region was demonstrated by failure of all attempts to stabilize flame on a $^1/_2$-in. long flat plate lying parallel to the flow.

Mechanism of Blowout

It is postulated that flame blows out when the eddy region regains less heat from the newly ignited gases than is required to ignite these gases. At constant approach velocity, as the mixture ratio is changed to reduce the flame temperature, the average temperature of the eddy region drops, finally reaching so low a temperature that continuous ignition is no longer maintained and the flame dies. Flame does not immediately cease, however, but continues for a few revolutions of the eddy region until it cools sufficiently to be impotent.

Examination of high-speed movies of blowout shows that the last region where flame exists is near the rod, indicating that the flame extinguishes by first ceasing to propagate into the main stream and then shortening until the eddy region temperature becomes too low for ignition.

Considerable quenching occurs when the burned gases just to the rear of the eddy region are rapidly accelerated as they move farther downstream in a constant area duct. This quenching action must account for the failure of the residual flame to propagate into the main stream. It appears that the propagation of the flame above the stabilizer into the unburned gases (which fails to take place in the case of the residual flame) and the stabilization mechanism itself are independent of one another. Residual flames appeared in only a few instances—on the lean side of stoichiometric when city gas was used as the fuel and on the rich side with propane. With the fuels and stabilizers employed in these tests it appears that failure of the flame to stabilize, rather than its failure to propagate, is in most instances the controlling phenomenon. Heating the stabilizer should tend to make propagation controlling; this was verified.

Blowout limits of city-gas flames stabilized on nine rods varying thirty-fold in diameter from 0.016 to 0.498 in. were obtained both with and without a screen at the chamber entrance. Fig. 5 presents the results, which are seen to be consistent with Eq. (4) except in the range of extremely lean mixtures where the effect of rod size reverses. This effect is thought to be due to the increased cooling of the eddy region by the large stabilizers; experiments with water-cooled rods support this view.

In contrast with the small effect of approach-stream turbulence on propagation reported elsewhere,[8] the reduction in stability is pronounced (Fig. 6) except on the two largest rods. It is believed that the effect of turbulence on stability limits is primarily due to the intensity and size of the gusts characterizing the variation from the mean value of the local velocity at the stabi-

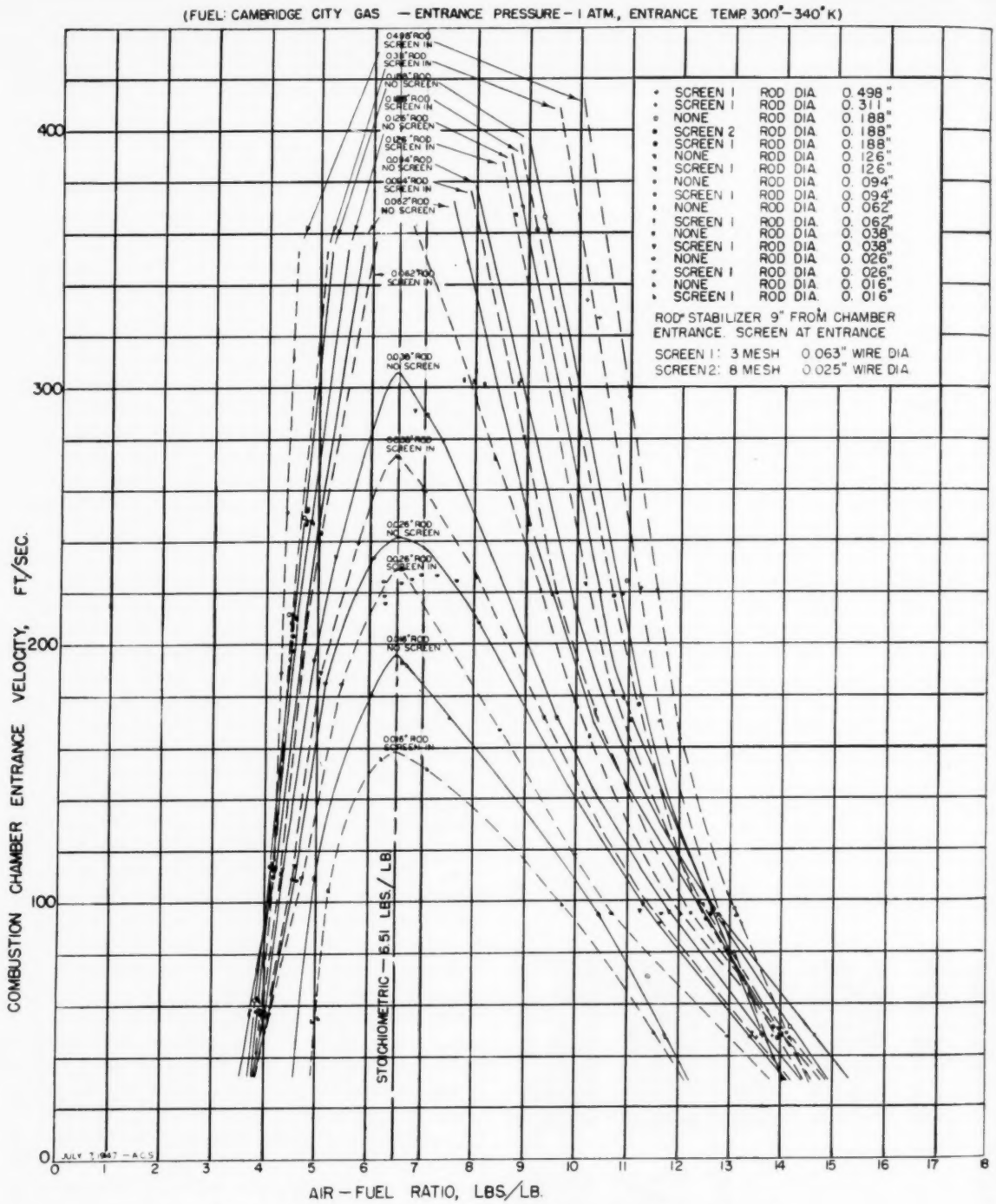
(FUEL: CAMBRIDGE CITY GAS — ENTRANCE PRESSURE — 1 ATM., ENTRANCE TEMP. 300°–340° K)
SCREEN 1 ROD DIA. 0.498"
SCREEN 1 ROD DIA. 0.311"
NONE ROD DIA. 0.188"
SCREEN 2 ROD DIA. 0.188"
SCREEN 1 ROD DIA. 0.188"
NONE ROD DIA. 0.126"
SCREEN 1 ROD DIA. 0.126"
NONE ROD DIA. 0.094"
SCREEN 1 ROD DIA. 0.094"
NONE ROD DIA. 0.062"
SCREEN 1 ROD DIA. 0.062"
NONE ROD DIA. 0.038"
SCREEN 1 ROD DIA. 0.038"
NONE ROD DIA. 0.026"
SCREEN 1 ROD DIA. 0.026"
NONE ROD DIA. 0.016"
SCREEN 1 ROD DIA. 0.016"
ROD STABILIZER 9" FROM CHAMBER ENTRANCE. SCREEN AT ENTRANCE
SCREEN 1: 3 MESH 0.063" WIRE DIA.
SCREEN 2: 8 MESH 0.025" WIRE DIA.
STOICHIOMETRIC — 6.51 LBS./LB.
COMBUSTION CHAMBER ENTRANCE VELOCITY, FT/SEC.
AIR — FUEL RATIO, LBS./LB.

FIG. 5. Stability limits of flames stabilized on rods. (Fuel: city gas.)

lizer. Turbulence of a given scale and intensity should then have less influence on the stability limits of large stabilizers. The data confirm this.

To test Eq. (4), a best value of the exponent a, 0.45, was found by plotting V_{B_0} vs. n to logarithmic coordinates. Blowout limit data for rods replotted with $(V_{B_0})^{0.45}$ as ordinate are shown in Fig. 7. The correlation is satisfactory, but, as expected, the points scatter somewhat on the lean side at low velocity because of the quenching action of the stabilizer itself, which is not taken into account in the heat balance on which Eq. (4) is based.

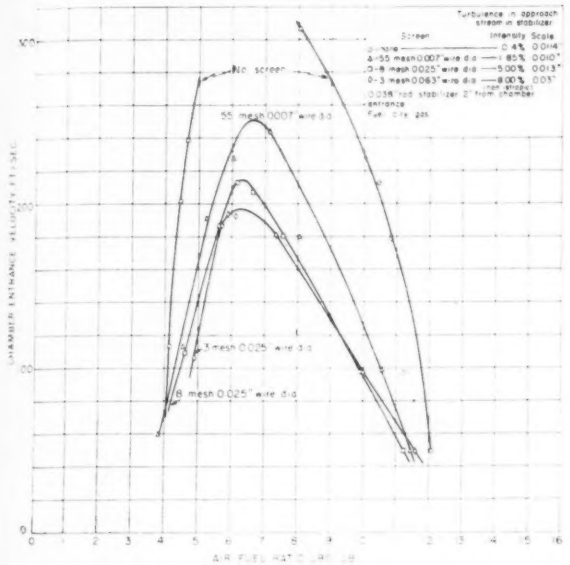

FIG. 6. Effect on stability limits of different turbulence scales and intensities.

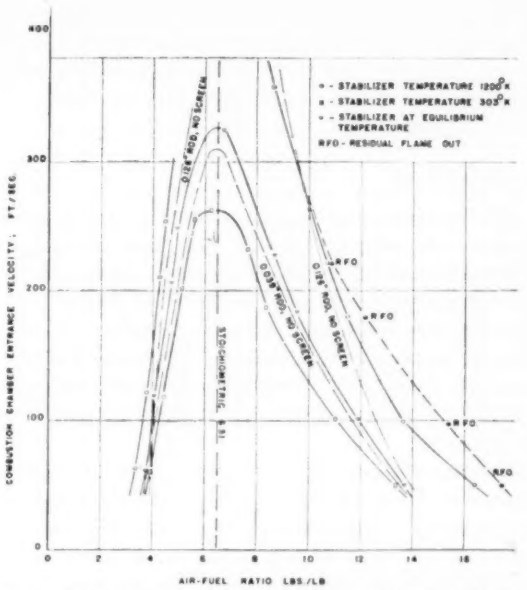

FIG. 8. Effect of stabilizer temperature on blowout limits of 0.032-in. tube stabilizer. (Fuel: city gas.)

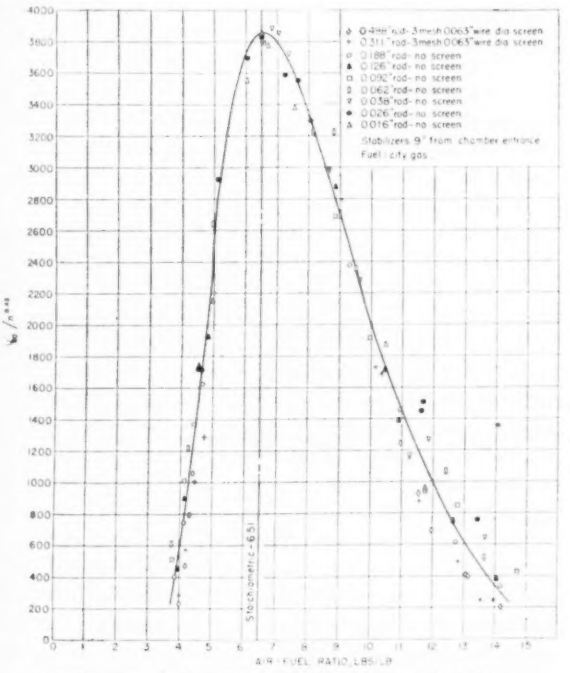

FIG. 7. Correlation of rod stabilizer blowout limit data.

The effects of heating and cooling the stabilizer are shown graphically in Fig. 8 for city gas-air mixtures. Blowout velocities obtained with a 0.038-in. tube maintained at 1,200°K. match those for a 0.126-in. unheated

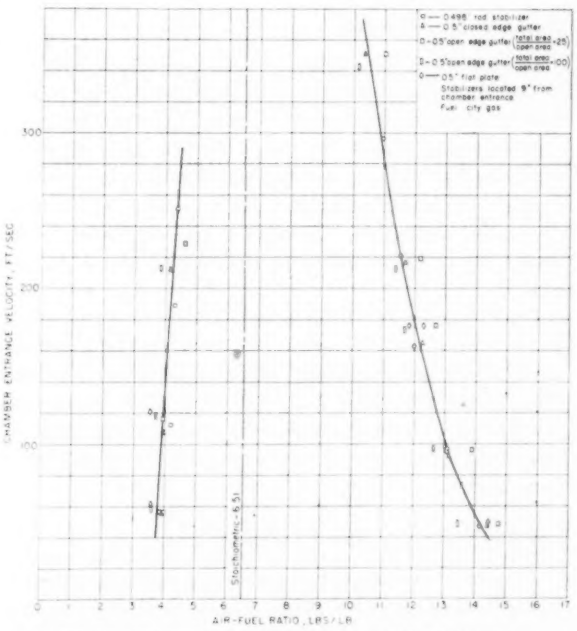

FIG. 9. Blowout limits for half-inch thick stabilizers.

rod at an air-fuel ratio of 9.5. As the mixture ratio approaches stoichiometric, the unheated rod rises in temperature, and the effect of the artificial heating becomes less. As expected, blowout limits for the unheated tube were wider than for an unheated rod of equal diameter. Similar results were obtained with propane-air mixtures.[1]

Stabilizer Shape

Closed-edge-gutter blowout-limit data for city gas-air mixtures were obtained with five gutters ranging in width from 0.025 to 0.5 in. Comparison of the stability-limit curves for closed-edge gutters with similar curves for rods shows that, although they both have the same general shape and appearance, lean-side limits are leaner for the gutters. This is due, it is presumed, to the relatively smaller cooling action of the gutters on the eddy region.

It has been already been shown that the blowout limits for flames stabilized on rods and closed-edge gutters were approximately the same. Blowout limit data were obtained with a rod, a closed-edged gutter, open-edge gutters with a ratio of total area to open area of 100 and 25, and a flat plate, all having approximately the same characteristic dimension of 0.5 in. That a single curve be drawn through all these data without great dispersion is shown in Fig. 9. On the basis of the blowout limit data it is concluded that the length of the eddy region behind gutters, rods, and plates of the same characteristic dimension is approximately the same.

Multiple Rod Stabilizers

Blowout limit data obtained with 1, 2, 4, and 8, 0.038-in. rod stabilizers placed in a single plane normal to the flow in the chamber are plotted in Fig. 10. A single curve fits all except the 8-rod data. The effect of changing the ratio of chamber width to stabilizer width over a simulated eightfold ratio is shown to be substantially negligible. Blowout as determined by visual observation occurred simultaneously from all rods.

Under similar conditions the stability of propane-air flames on rods was found to be considerably less than that of city gas-air flames, a result expected from the lower value of laminar flame velocity. The marked reduction in stability caused by the introduction of approach-stream turbulence was again noted with propane as fuel.

Effect of Stabilizer Span-Thickness Ratio

Longwell[6] obtained blowout data with naphtha-air mixtures flowing in the range of gas velocities from 300 to 1,000 ft. per sec., with flames stabilized on axially symmetrical flameholders axially located in a cylindrical duct 6 in. in diameter. His blowout data appear to correlate reasonably well either as a function of stabilizer characteristic dimension to the 0.45 power or to the

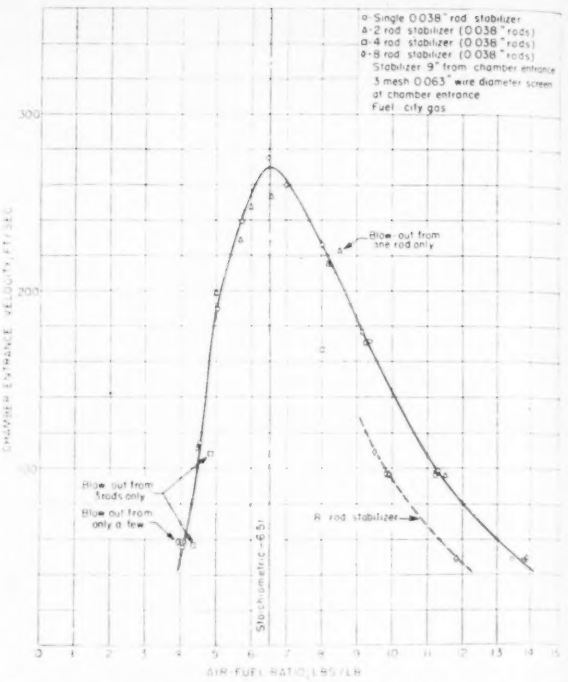
o-Single 0.038" rod stabilizer
Δ-2 rod stabilizer (0.038" rods)
□-4 rod stabilizer (0.038" rods)
◊-8 rod stabilizer (0.038" rods)
Stabilizer 9" from chamber entrance
5 mesh 0.063" wire diameter screen at chamber entrance
Fuel: city gas
Blow out from one rod only
Blow out from 5 rods only
Blow out from only a few
8 rod stabilizer
Stoichiometric-6.5
AIR-FUEL RATIO, LBS/LB

FIG. 10. Blowout limits for multiple rod stabilizers. (Simulated variation of chamber width.)

first power. Because of the existence of Longwell's data for larger size flameholders than those studied in this investigation and because doubts were cast upon the approach to two-dimensionality of the present experiments, a program of investigation[1] of this phase was initiated in which tests were made of stability limits in propane-air mixtures of rods progressively shortened from the full 1-in. depth of the test chamber to a span-thickness ratio of unity. Each of the rods shorter than 1 in. in span was fitted with hemispherical ends and supported by a wire of small diameter passing through the axis of the rod. As shown by Fig. 11, the effect on blowout velocity of shortening the span of 0.1-in. diameter rods is negligible until the ratio of span to thickness is less than 2. Similar results were obtained with 0.188-in. diameter rods. Data obtained with spheres are shown in Fig. 12 to give reasonable correlation with the first power of the sphere diameter as first proposed by Longwell. It should be noted that blowout limits for rods proportional to the 0.45 power of rod diameter and blowout limits for spheres proportional to the first power of sphere diameter call for a sphere of a large size to produce more stable flames than a rod of the same diameter. If it is visualized that the superior stability limits of a rod having a length diameter ratio greater than 2 are due to the ability of the rod to sustain flame when a quenching gust of size equal to rod diameter passes across the eddy region, whereas a similar sized quenching gust passing across the eddy region of a sphere would leave no fire to restart the eddy region, it does not appear that the relative exponents on

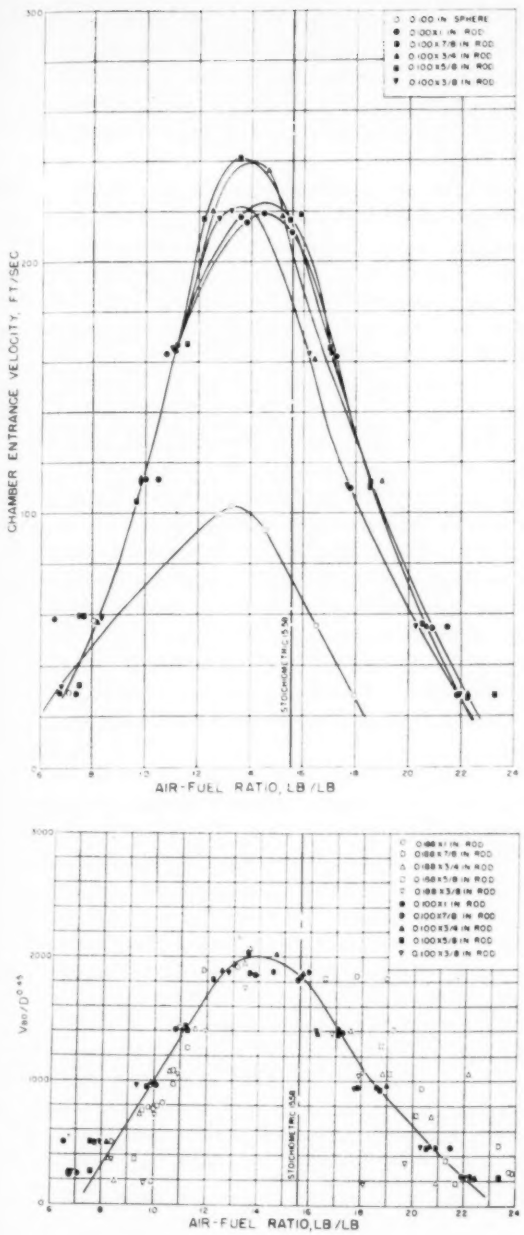

FIG. 11. Effect of span-thickness ratio on stability limits. (Fuel: propane.)

size for spheres and rods are valid outside the range of experimental variables covered here.

Stabilizer Boundary-Layer Thickness

The stabilizer used in initial boundary-layer studies[9] consisted of a rod mounted with its axis normal to the direction of gas flow and with a wedge pointing upstream attached to its upstream surface. Wedge fairings of various lengths were used to control the boundary layer on the stabilizer at the point of entry of the cold approach gases into the preignition and combustion zones. The length of the wedge fairing was increased progressively to increase boundary-layer thickness, and long fairings were used to deliver a turbulent boundary layer to the combustion zone. The faired section was externally cooled and insulated from the hot portion of the stabilizer in an attempt to find only those effects due to boundary-layer variation. Unfortunately, the scatter of the blowout data taken in this series of tests was so great as to mask any effects of boundary-layer variation. It can be concluded that, if the effects of changes in wedge fairing length were confined to changes in boundary-layer thickness and turbulence alone, the effect of change in boundary layer is not nearly so pronounced as that of changing stabilizer temperature. It can be argued that changing the length of wedge fairing not only changed the boundary-layer thickness and turbulence at entry to the eddy zone but

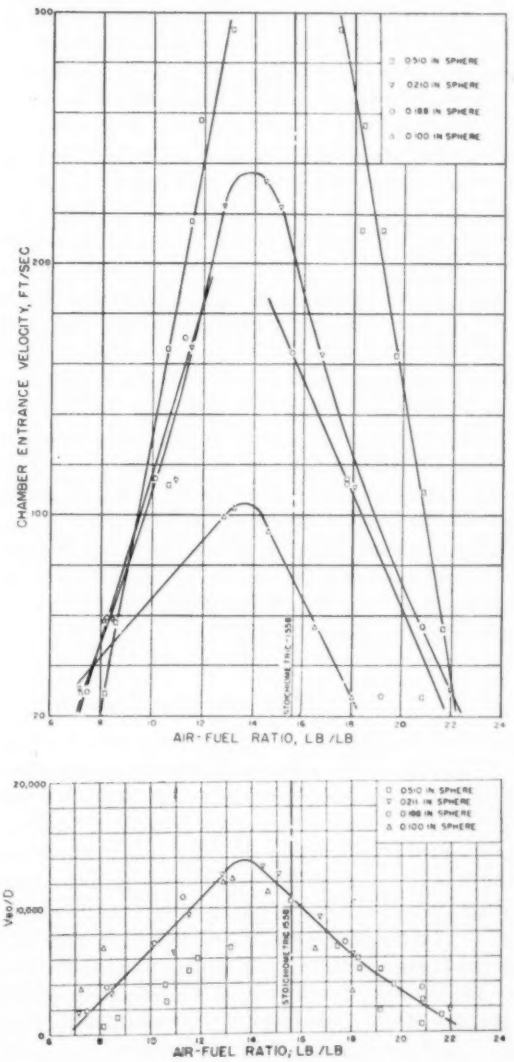

FIG. 12. Effect of sphere size on stability limits. (Fuel: propane.)

also changed the approach angle of the boundary layer. That the effect of such a change in approach angle is probably small is militated for in the negligible effect on stability shown by changes from gutter to rod to flat plate in Fig. 9.

Molecular Diffusion

Most of the observations of the characteristics of flame stabilization on bluff shapes can apparently be explained on the basis of a thermal ignition theory and the gross aerodynamics of the system. Failure to correlate blowout velocity data for different fuels in terms of the laminar flame velocity, however, and some visual observation on differences in the character of flames of city gas and of propane lead to the tentative conclusion that molecular diffusion plays a role of some importance in determining the air-fuel ratio range over which stable flames are obtained. The appearance of residual flames only on the rich side of stoichiometric for propane-air mixtures and only on the lean side of stoichiometric for city gas-air mixtures argues in favor of this hypothesis. Since the molecular diffusivity of propane is less than that of oxygen and since those of hydrogen and methane (the major combustible constituents of the city gas) are greater than that of oxygen, it can be argued that in the case of propane the mixture in the eddy region is always leaner in fuel than that of the main stream and in the case of city gas the eddy region is always richer in fuel than the main stream. This thesis is supported by the fact that the peaks of blowout velocity curves for propane-air mixtures always appear on the fuel-rich side and those of city gas-air mixtures always slightly on the fuel-lean side, plus the fact that the color of the eddy region of propane flames was always characteristic of a leaner mixture than that of the burning main stream. It would be expected, in the absence of concentration gradients of fuel-air ratio, that maximum blowout velocity would occur for stoichiometric mixtures, since maximum flame velocity and maximum heat generation per unit volume are expected near the stoichiometric ratio.

(V) Conclusions

(1) Flame stabilization in high velocity, premixed gaseous fuel-air streams is not possible on unheated surfaces that do not produce recirculating eddy zones. Flame stabilization in the wake of an eddy-producing stabilizer depends on the presence of an eddy region filled with combustion products sufficiently hot to furnish continuous ignition to the approaching unburned gases.

(2) Over a range of stabilizer sizes from 0.016 to 0.50 in. in thickness and from 0.1 to 1.0 in. in span, the blowout velocity for a given fuel in air was affected primarily by the gas stream variables of air-fuel ratio and turbulence and by the stabilizer thickness:

(a) For span-thickness ratios greater than 2, the blowout velocity at a given air-fuel ratio and stream turbulence was independent of stabilizer shape-cylindrical rods, rods with wedge-shaped upstream fairings, hemispherically ended cylindrical rods, open-edged gutters, flat plates. The blowout velocity was proportional to the 0.45 power of the stabilizer thickness.

(b) For span-thickness ratios less than 2, the corresponding blowout velocity was roughly proportional to the first power of the thickness.

(c) The stability limits for a stabilizer of given thickness are unaffected by simulated variation from 10 to 80 of the ratio of stabilizer thickness to chamber width.

(d) Increasing turbulence in the approach gas stream decreases the range of approach velocity and air-fuel ratio over which flame can be maintained. The effect of approach stream turbulence of a given scale and intensity diminishes with increasing ratio of stabilizer thickness to turbulence scale.

(3) Heat addition externally to a stabilizer holding flame in a gaseous combustible mixture markedly widens the stability limits. Removal of heat from such a stabilizer narrows the stability limits.

(4) Flame blowoff from a bluff stabilizer usually proceeds stepwise. Flame propagation downstream from the eddy zone usually ceases before the eddy zone itself is quenched.

(5) Shifting of the peak velocity of stable burning away from the stoichiometric fuel-air ratio normally expected to give maximum blowout velocity is attributed to the mechanism of molecular diffusion operating to change the fuel-air ratio in the eddy zone from that in the main gas stream.

(6) The effect on stability limits of changing fuel type is in the direction of the accompanying change in laminar flame speed.

References

[1] Baddour, R. F., and Carr, L. D., S. M. Thesis in Chemical Engineering, Massachusetts Institute of Technology, 1949.

[2] Dryden, H. L., *Turbulence and Diffusion*, Ind. Eng. Chem., Vol. 31, pp. 416–425, April, 1939.

[3] von Elbe, G., and Mentser, M., *Further Studies of the Structure and Stability of Burner Flames*, J. Chem. Phys., Vol. 13, pp. 89–100, February, 1945.

[4] Goss, W. H., and Cook, Emory, *The Ramjet as a Supersonic Propulsion Plant*, Trans. S.A.E., Vol. 2, No. 4, pp. 642–657, October, 1948.

[5] Lewis, B., and von Elbe, G., *Stability and Structure of Burner Flames*, J. Chem. Phys., Vol. 11, pp. 75–97, February, 1943.

[6] Longwell, J. P. (see reference 4), Standard Oil Development Company.

[7] Mache, H., *Die Physik der Verbrennungserscheinungen*, Veit und Comp., pp. 25–54, Leipzig, 1918.

[8] Scurlock, A. C., Sc.D. Thesis in Chemical Engineering, Massachusetts Institute of Technology, 1948; abstracted in *Flame Stabilization and Propagation in High-Velocity Gas Streams*, Meteor Report No. 19, Fuels Research Laboratory, Massachusetts Institute of Technology, July, 1948.

[9] Kellogg, W. W., S.M. Thesis in Aeronautical Engineering, Massachusetts Institute of Technology, 1949.

Equations for the Approximate Solution of Dynamic Problems for Stable Linear Systems

KURT H. HOHENEMSER*
McDonnell Aircraft Corporation

SUMMARY

In generalization of the "square wave" formulas, presented recently in this magazine,[1] a number of equations are derived which are applicable in the approximate analysis of complicated linear systems or in the analysis of dynamic test data of a linear system. A summary of the obtained equations is given in the Appendix.

(1) INTRODUCTION

IN THE ANALYSIS AND SYNTHESIS of linear systems, for example of aircraft automatic controls, it is often desirable to use approximate numerical or graphical methods for the calculation of a transient if the frequency response of the system is given or for the calculation of the frequency response function if a transient is given. Approximate methods are indicated if either the exact analytical solution is too involved (for example, in systems where the characteristic equation has more than four roots) or if the system is given by measurements of the frequency response or of a transient rather than by its physical constants. In reference 1 it was shown how well the frequency response function, calculated by an approximate method from the measured airplane motion after an elevator step displacement, fitted the frequency response function as measured in flight. The advantage of substituting the laborious measurements of the airplane response to harmonic control displacements over the entire necessary frequency range by a single measurement of a transient, following a step displacement of the control, is obvious.

It is often of importance to know the relations between transient and frequency response in case of a gradual transition from one position of the control to another position with finite rate of change of the stick position. This procedure may be called oblique step displacement of the control, contrary to the rectangular step displacement. Finally, an alternative method of exciting a transient of an airplane is the use of an impulse control deflection instead of a step deflection. The impulse method consists of deflecting the control for a short time and going back to the original position.

In the following, a number of approximate formulas is developed appropriate for numerical or graphical determination of the frequency response from a given transient and of a transient from a given frequency response covering the two cases of oblique step input and of impulse input. The case of rectangular step input, treated in reference 1, is included in the more general equations for oblique step input.

Received March 4, 1949. Revised and received July 15, 1949.

* Chief of Aerodynamics, Helicopter Division.

(2) APPROXIMATE CALCULATION OF A TRANSIENT WHEN THE FREQUENCY RESPONSE IS GIVEN

(2.1) *Oblique Step Input*

Let η be the input variable (for example, control deflection) and y be the responding variable (for example, pitch or rate of pitch or translational velocity of the aircraft).

For the input variable $\eta(t)$ as a function of time t, we assume the periodic function shown in Fig. 1 with a period $T = 2\pi/\omega$ large enough to be sure that the transient of the responding variable $y(t)$ at the end of the half period $T/2$ is practically subsided. (See Fig. 2.)

We first expand the periodic function shown in Fig. 3 in a Fourier series. Since the function $\eta(x)$ is antisymmetrical with respect to the point $x = 0$, only sine terms are present in the Fourier expansion:

$$\eta(x) = \sum_{n=1}^{\infty} c_n \sin(nx) \tag{1}$$

with

$$c_n = (1/\pi)\int_0^{2\pi} \eta(x) \sin(nx)dx \tag{2}$$

Only the odd terms of the series (1) are different from zero, and Eq. (2) may be written

$$c_n = (4/\pi)\int_0^{\pi/2} \eta(x) \sin(nx)dx, \quad n = 1, 3, \ldots \tag{3}$$

The result of the integration is

$$c_n = (4b/\pi a)[\sin(na)/n^2]$$

and the Fourier series (1) reads

$$\eta(x) = (4b/\pi a) \sum_{n=1,3,\ldots}^{\infty} [\sin(na) \sin(nx)]/n^2 \tag{4}$$

For some purposes it is more convenient to write the series in complex form. Substituting

$$\sin(nx) = (1/2i)(e^{inx} - e^{-inx})$$

the series (4) reads

$$\eta(x) = (b/\pi a) \sum_{\substack{n=1,3,\ldots \\ -1,-3,\ldots}}^{\infty} [e^{in(x-a)} - e^{in(x+a)}]/n^2 \tag{5}$$

The summation is to be taken over all positive and negative odd integers n.

In order to obtain the series for $\eta(t)$, shown in Fig. 1, we substitute in Eq. (5)

$$x = \omega\left(t - \frac{\tau}{2}\right), \quad a = \omega\frac{\tau}{2}, \quad b = \frac{1}{2}$$

and add the mean value $^1/_2$ (compare Fig. 3 with Fig. 1):

$$\eta(t) = \frac{1}{2} + \frac{1}{\pi\omega} \sum_{\substack{n=1,3,\ldots \\ -1,-3,\ldots}}^{\infty} \frac{e^{in\omega t}}{n^2}\left(\frac{e^{-in\omega\tau} - 1}{\tau}\right) \qquad (6)$$

ω is the fundamental circular frequency of the periodic input function $\eta(t)$ and of the response function $y(t)$; τ is the time for the change of input position (control deflection) from $\eta(0) = 0$ to $\eta(\tau) = 1$, the rate of change being uniform between $t = 0$ and $t = \tau$; and i denotes $\sqrt{-1}$.

Eq. (6) in real form reads

$$\eta(t) = \frac{1}{2} + \frac{2}{\pi\omega} \sum_{n=1,3,\ldots}^{\infty} \frac{\cos\left[n\omega(t-\tau)\right] - \cos\left[n\omega t\right]}{\tau n^2} \qquad (7)$$

and the summation is to be taken for positive odd integers n only.

In order to obtain the response $y(t)$ of the system to the input $\eta(t)$, every harmonic term in Eq. (6) has to be multiplied by the value of the frequency response function corresponding to the frequency $n\omega$. In complex notation the frequency response function, also called transfer function, $F(in\omega)$, is the complex amplitude ratio $y(in\omega)/\eta(in\omega) = F(in\omega)$, obtained by solving the equations of motion of the system for a steady state harmonic oscillation $e^{in\omega}$.

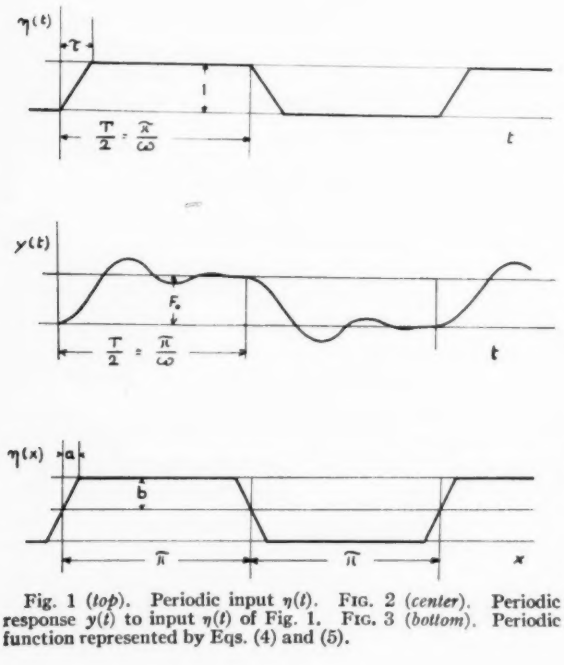

Fig. 1 (*top*). Periodic input $\eta(t)$. Fig. 2 (*center*). Periodic response $y(t)$ to input $\eta(t)$ of Fig. 1. Fig. 3 (*bottom*). Periodic function represented by Eqs. (4) and (5).

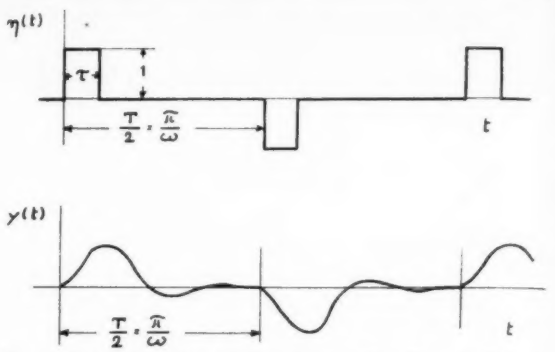

Fig. 4 (*top*). Periodic impulse input $\eta(t)$. Fig. 5 (*bottom*). Periodic response $y(t)$ to impulse input $\eta(t)$ of Fig. 4.

The transfer function is a complex rational function of the imaginary variable $in\omega$ with real coefficients. Therefore, $F(in\omega)$ and $F(-in\omega)$ are conjugate complex numbers, and

$$F(in\omega) = \begin{cases} F_n e^{i\varphi_n} \text{ for positive } n \\ F_n e^{-i\varphi_n} \text{ for negative } n \end{cases} \qquad (8)$$

F_n (amplitude ratio) and φ_n (phase difference) are real numbers.

Multiplying the harmonic terms of Eq. (6) with the corresponding values of the transfer function,

$$y(t) = \frac{F_0}{2} + \frac{1}{\pi\omega} \sum_{\substack{n=1,3,\ldots \\ -1,-3,\ldots}}^{\infty} \frac{F_n}{n^2} e^{i(n\omega t + \varphi_n)}\left(\frac{e^{-in\omega\tau} - 1}{\tau}\right) \qquad (9)$$

F_0 is the static amplitude ratio for zero frequency. Considering Eq. (8), the series (9) may be written in the real form:

$$y(t) = \frac{F_0}{2} + \frac{2}{\pi\omega\tau} \sum_{n=1,3,\ldots}^{\infty} \times \frac{F_n}{n^2}\left\{\cos\left[n\omega(t-\tau) + \varphi_n\right] - \cos\left(n\omega t + \varphi_n\right)\right\} \qquad (10)$$

and the summation is to be taken again for positive odd integers n only. The amplitude ratio F_n decreases with n if $n\omega$ is higher than the highest natural frequency of the system; the coefficient F_n/n^2 decreases still faster with n; therefore, the series (9) or (10) converge rapidly once $n\omega$ is beyond the highest natural frequency of the system. The fundamental frequency ω of series (9) or (10) must be chosen as a fraction of the lowest natural frequency and must be the smaller the less damped the transient is, because otherwise the solution for a periodic input as shown in Fig. 1 would not be an approximation to the step input. The number of terms to be carried in series (9) or (10) depends on

the characteristics of the system. For a well-damped system with a not-too-wide natural frequency spectrum, seven to nine terms may be entirely satisfactory. The summation may be performed numerically or graphically by adding vectors with the length proportional to F_n/n^2 and the direction with respect to a reference line given by the angles $n\omega(t-\tau)+\varphi_n$ and $n\omega t+\varphi_n$ and by projecting the resultant vector on the reference line.

For τ approaching zero (rectangular step function), Eq. (6) is reduced to

$$\eta(t) = (1/2) + (1/\pi) \sum_{\substack{n=1,3,\ldots \\ -1,-3,\ldots}}^{\infty} (e^{in\omega t}/in) \qquad (11)$$

and Eq. (9) is reduced to

$$y(t) = (F_0/2) + (1/\pi) \sum_{\substack{n=1,3,\ldots \\ -1,-3,\ldots}}^{\infty} (F_n/in)e^{i(n\omega t+\varphi_n)} \qquad (12)$$

or in real form [consider Eq. (8)]:

$$y(t) = (F_0/2) + (2/\pi) \sum_{n=1,3,\ldots}^{\infty} (F_n/in) \sin(n\omega t+\varphi_n) \qquad (13)$$

This equation was used in reference 1.

(2.2) *Comparison with Exact Solution*

If we take two discrete points on the frequency response curve which are close together, then the interval between them for n odd will be denoted

$$(n+2)i\omega - ni\omega = 2i\omega = \Delta s$$

Further, $ni\omega = s$. Then, as $\omega \to 0$, Eq. (11) becomes

$$\eta(t) = \frac{1}{2} + \frac{1}{2\pi i}\left[\int_{-i\infty}^{-\Delta s/2} \frac{e^{st}}{s}\,ds + \int_{\Delta s/2}^{i\infty} \frac{e^{st}}{s}\,ds\right] \qquad (14)$$

We connect the two paths of integration along the positive and negative imaginary axes from $\Delta s/2$ to $-\Delta s/2$ by the right half circle around the pole of the integrand at $s=0$. The residue of the integrand at $s=0$ (coefficient of $1/s$ in the expansion of the integrand) is one, and the value of the integral along the small half circle is

$$\int (e^{st}/s)\;ds = \pi i \qquad (15)$$

Combining Eqs. (14) and (15),

$$\eta(t) = (1/2\pi i) \int_{-i\infty}^{+i\infty} (e^{st}/s)\,ds \qquad (16)$$

It is to be understood that the path of integration along the imaginary axis passes the pole of the integrand at $s=0$ at the right. Eq. (16) is the well-known inverse Laplace transform of the rectangular unit step function $\eta(t)$.

Assuming that the complex transfer function $F(s)$ has no poles on the imaginary axis or to the right of this axis (stable systems) and assuming further that, for $s=0$, $F(0)$ has the real value F_0 (static deflection), one obtains, by the same method indicated above for ω approaching zero instead of Eq. (12), the following equation:

$$y(t) = (1/2\pi i) \int_{-i\infty}^{+i\infty} [F(s)/s]e^{st}\,ds \qquad (17)$$

This is the inverse Laplace transform of the response $y(t)$ caused by a rectangular unit step input.

Writing again $2i\omega = \Delta s$ and $ni\omega = s$, Eq. (6) reads, for ω approaching zero,

$$\eta(t) = \frac{1}{2} + \frac{1}{2\pi i}\left(\int_{-i\infty}^{\Delta s/2} \frac{e^{st}}{s^2}\frac{1-e^{-s\tau}}{\tau}\,ds + \int_{\Delta s/2}^{i\infty} \frac{e^{st}}{s^2}\frac{1-e^{-s\tau}}{\tau}\,ds\right) \qquad (18)$$

Expanding the integrand

$$\frac{e^{st}}{s^2}\frac{1-e^{-s\tau}}{\tau} = \frac{1+st+\ldots-1-s(t-\tau)\ldots}{s^2\tau} = \frac{1}{s}+\ldots$$

results again in a residue one, and the value of the integral along the small right half circle around the pole at $s=0$ is again πi; therefore, Eq. (18) may be written:

$$\eta(t) = \frac{1}{2\pi i}\int_{-i\infty}^{+i\infty} \frac{e^{st}}{s^2}\frac{1-e^{-s\tau}}{\tau}\,ds \qquad (19)$$

By the same method and assuming the above-mentioned properties of the complex transfer function $F(s)$, Eq. (9) may be written, for ω approaching zero in the form:

$$y(t) = \frac{1}{2\pi i}\int_{-i\infty}^{+i\infty} F(s)\frac{e^{st}}{s^2}\frac{1-e^{-s\tau}}{\tau}\,ds \qquad (20)$$

Eq. (19) is the inverse Laplace transform of the oblique unit step function, as may be easily verified by evaluating the integral

$$\mathfrak{L}[\eta(t)] = \int_0^\infty \eta(t)e^{-st}\,dt = \int_0^\tau \frac{t}{\tau}e^{-st}\,dt + \int_\tau^\infty e^{-st}dt$$

with the result

$$\mathfrak{L}[\eta(t)] = (1-e^{-s\tau})/\tau s^2 \qquad (21)$$

Eq. (20) is the inverse Laplace transform of the response caused by an oblique unit step input.

Of course, the approximate formulas [Eqs. (9) and (10)] could have been derived by starting with the Laplace transform (21) and by subdividing the integrals (19) and (20) in a constant part along the small half circle around the pole at $s=0$ and in the remaining two parts along the positive and negative imaginary axes, excluding the pole, and by approximating these two latter integrals by an infinite series. Formulas for

an approximate method of calculating the transient from a given frequency response function, different from those discussed here, were derived in reference 2 on the basis of an approximate evaluation of the inverse Laplace integral. Though the method of reference 2 is more general and requires only the Laplace transform of the input function in order to be applicable to any given input, it seems that the use of Eqs. (9) and (10) or their equivalent has the advantage of a closer connection to a physical picture. The basis of Eqs. (9) and (10) is the substitution of the oblique step input by a periodic input, Fig. 1, and it is easy to visualize the conditions for good or bad approximation or convergence of the method without needing considerable experience with the method.

(2.3) *Impulse Input*

For the input variable $\eta(t)$ as a function of time t, we now assume the periodic function shown in Fig. 4. The response is shown in Fig. 5.

The Fourier series for the input function in Fig. 4 is obtained by subtracting the equation

$$\eta(t) = (1/2) + (1/\pi) \sum_{\substack{n=1,3,\ldots \\ -1,-3,\ldots}}^{\infty} [e^{in\omega(t-\tau)}/in] \quad (11a)$$

from Eq. (11), with the result:

$$\eta(t) = (1/\pi) \sum_{\substack{n=1,3,\ldots \\ -1,-3,\ldots}}^{\infty} (e^{in\omega t} - e^{in\omega(t-\tau)})/in \quad (22)$$

The periodic unit impulse is obtained from this equation by multiplication with a factor K and by letting the time τ approach zero but keeping the product $K\tau$ equal to one.

Multiplication of Eq. (22) with $K = 1/\tau$ and letting $\tau \to 0$ results in an indeterminate form. After applying L'Hospital's rule, one obtains

$$\eta(t) = (\omega/\pi) \sum_{\substack{n=1,3,\ldots \\ -1,-3,\ldots}}^{\infty} e^{in\omega t} \quad (23)$$

or in real notation

$$\eta(t) = (2\omega/\pi) \sum_{n=1,3,\ldots}^{\infty} \cos(n\omega t) \quad (24)$$

The response $y(t)$ is obtained by multiplying every term in the series (23) with the transfer function $F(in\omega) = F_n e^{i\varphi_n}$:

$$y(t) = (\omega/\pi) \sum_{\substack{n=1,3,\ldots \\ -1,-3,\ldots}}^{\infty} F_n e^{i(n\omega t + \varphi_n)} \quad (25)$$

or, considering Eq. (8), in real notation,

$$y(t) = \frac{2\omega}{\pi} \sum_{n=1,3,\ldots}^{\infty} F_n \cos(n\omega t + \varphi_n) \quad (26)$$

The transition to the case where ω is approaching zero is again made by substituting $2\omega i = \Delta s$ and $n\omega i = s$. Since the integrand has no pole on the imaginary axis one obtains directly, instead of Eqs. (23) and (25), the following equations:

$$\eta(t) = (1/2\pi i) \int_{-i\infty}^{+i\infty} e^{st} ds \quad (27)$$

$$y(t) = (1/2\pi i) \int_{-i\infty}^{+i\infty} F(s) e^{st} ds \quad (28)$$

Eq. (27) is the well-known inverse Laplace transform for a unit impulse. For a unit input during a finite time τ, as shown in Fig. 4, Eq. (25) reads

$$y(t) = \frac{1}{\pi} \sum_{\substack{n=1,3,\ldots \\ -1,-3,\ldots}}^{\infty} \frac{F_n}{in} e^{i(n\omega t + \varphi_n)} [1 - e^{-in\omega\tau}] \quad (25a)$$

or in real notation, considering Eq. (8),

$$y(t) = \frac{2}{\pi} \sum_{n=1,3,\ldots}^{\infty} \frac{F_n}{n} \{\sin(n\omega t + \varphi_n) - \sin[n\omega(t-\tau) + \varphi_n]\} \quad (26a)$$

(3) Approximate Calculation of the Frequency Response When a Transient Is Given

(3.1) *Oblique Step Input*

The given response to an oblique displacement may be represented by the curve in Fig. 6 between $t = 0$ and $t = T/2$. The response curve is extended beyond the time $t = T/2$ as a periodic function with the period T. This period must be chosen so that at the end of the half period the transient is practically subsided. The response curve $y(t)$ is now approximated by adding K periodic functions consisting of elementary trapezoids of the kind shown in Fig. 6.

Each of these elementary periodic functions is expanded in a Fourier series according to Eq. (6), with $t - t_m$ instead of t. The result is the following sum of K Fourier series:

$$y(t) = \sum_{m=1}^{K} \Delta_m y \left[\frac{1}{2} + \frac{1}{\pi\omega} \sum_{\substack{n=1,3,\ldots \\ -1,-3,\ldots}}^{\infty} \frac{e^{in\omega(t-t_m)}}{n^2} \times \left(\frac{e^{-in\omega\tau_m} - 1}{\tau_m}\right)\right] \quad (29)$$

Eq. (9) gives the same curve $y(t)$ in terms of the transfer function $F(in\omega)$. Comparing Eqs. (9) and (29), the following expressions for the transfer function are found:

$$F_0 = \sum_{m=1}^{K} \Delta_m y \quad (30)$$

$$F_n e^{i\varphi_n} = \frac{\tau}{e^{-in\omega\tau} - 1} \sum_{m=1}^{K} \Delta_m y e^{-in\omega t_m} \left(\frac{e^{-in\omega\tau_m} - 1}{\tau_m}\right) \quad (31)$$

For each frequency $n\omega$ in the interesting frequency range, the summation of the K complex numbers on the right side of Eq. (31) must be performed.

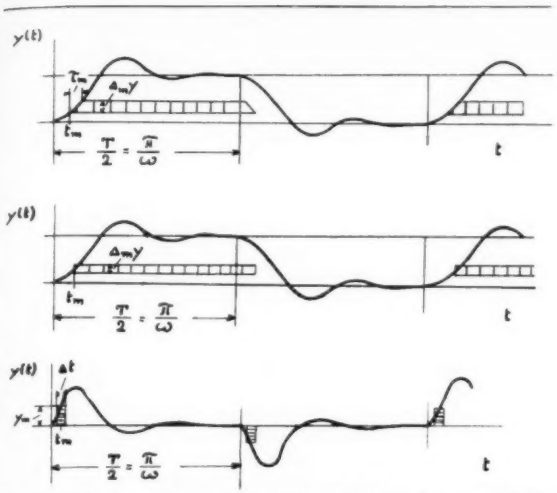

FIG. 6 (*top*). Response $y(t)$ with mth element of series (29).
FIG. 7 (*center*). Response $y(t)$ with mth element of series (32).
FIG. 8 (*bottom*). Response $y(t)$ with mth element of series (43).

If all the τ_m are approaching zero, Eq. (29) is reduced to

$$y(t) = \sum_{m=1}^{K} \Delta_m y \left[\frac{1}{2} + \frac{1}{\pi} \sum_{\substack{n=1,3,\ldots \\ -1,-3,\ldots}}^{\infty} \frac{e^{in\omega(t-t_m)}}{in} \right] \tag{32}$$

In this case t_m is better chosen as the midpoint of each time interval—see Fig. 7. For $\tau_m \to 0$, Eq. (31) is reduced to

$$F_n e^{i\varphi_n} = \frac{n\tau\omega}{i(e^{-in\omega\tau} - 1)} \sum_{m=1}^{K} \Delta_m y e^{-in\omega t_m} \tag{33}$$

For a rectangular step input, $\tau \to 0$, Eq. (31) is reduced to

$$F_n e^{i\varphi_n} = \frac{i}{n\omega} \sum_{m=1}^{K} \Delta_m y e^{-in\omega t_m} \left(\frac{e^{-in\omega\tau_m} - 1}{\tau_m} \right) \tag{34}$$

If the elementary steps are assumed to be rectangular, $\tau_m \to 0$ (see Fig. 7), Eq. (34) is further reduced to

$$F_n e^{i\varphi_n} = \sum_{m=1}^{K} \Delta_m y e^{-in\omega t_m} \tag{35}$$

For equal time intervals $t_{m+1} - t_m$, this equation is identical with that used in reference 1.

The formulas that use elementary trapezoids allow a smoother approximation of the given response curve than those that use elementary rectangles, and, therefore, less elements are necessary for the approximation.

In order to obtain, in the case of rectangular unit step input, the connection with the exact solution, we substitute in Eq. (35) $in\omega = s$ and approach the limits $\Delta_m y \to 0$ and $T \to \infty$:

$$F(s) = \int_0^\infty (dy/dt) e^{-st} dt \tag{35a}$$

This equation indicates that $F(s)$ is the Laplace transform of dy/dt. Since the system is at rest before the unit step input, Eq. (35a) may also be written:

$$F(s)/s = \int_0^\infty y(t) e^{-st} dt \tag{35b}$$

which is the inverse to Eq. (17) and which is the well-known Laplace transform of the response $y(t)$ caused by a rectangular unit step input. Going to the same limits in Eq. (33) for the oblique unit step input, we obtain

$$F(s) = \frac{\tau s}{1 - e^{-s\tau}} \int^\infty \frac{dy}{dt} e^{-st} dt \tag{33a}$$

or

$$F(s) \frac{1 - e^{-s\tau}}{\tau s^2} = \int_0^\infty y(t) e^{-st} dt \tag{33b}$$

This is the inverse of Eq. (20), and it was shown in Section (2.2) that Eq. (33b) represents the correct Laplace transform of the response $y(t)$ caused by an oblique unit step input.

(3.2) *Impulse Input*

We assume again that the response to a periodic impulse input, Fig. 4, is approximated by the sum of K elementary trapezoids, Fig. 6, and is represented by Eq. (29). Comparison of Eq. (29) with Eq. (25a) leads to the following equation for the transfer function:

$$F_n e^{i\varphi_n} = \frac{i}{n\omega(1 - e^{-in\omega\tau})} \sum_{m=1}^{K} \Delta_m y e^{-in\omega t_m} \left(\frac{e^{-in\omega\tau_m} - 1}{\tau_m} \right) \tag{36}$$

If the periodic response curve is approximated by the sum of K elementary rectangles, Fig. 7, all the τ_m in Eq. (36) are approaching zero and one obtains

$$F_n e^{i\varphi_n} = \frac{1}{1 - e^{-in\omega\tau}} \sum_{m=1}^{\infty} \Delta_m y e^{-in\omega t_m} \tag{37}$$

In case of a unit impulse of infinitely small duration, Eqs. (36) and (37), by multiplication with τ and letting τ approach zero, are reduced to

$$F_n e^{i\varphi_n} = \frac{1}{n^2\omega^2} \sum_{m=1}^{K} \Delta_m y e^{-in\omega t_m} \left(\frac{e^{-in\omega\tau_m} - 1}{\tau_m} \right) \tag{38}$$

$$F_n e^{i\varphi_n} = \frac{1}{in\omega} \sum_{m=1}^{K} \Delta_m y e^{-in\omega t_m} \tag{39}$$

In order to obtain the connection with the exact solution for a unit impulse, we substitute in Eq. (39) $in\omega = s$ and approach the limits $\Delta_m y \to 0$ and $T \to \infty$:

$$F(s) = (1/s) \int_0^\infty (dy/dt) e^{-st} dt \tag{40}$$

This equation indicates that $sF(s)$ is the Laplace transform of dy/dt, or, since the system is at rest before the impulse is applied,

$$F(s) = \int_0^\infty y(t) e^{-st} dt \tag{41}$$

which is the inverse to Eq. (28) and expresses the well-known fact that the transfer function of a system is equal to the Laplace transform of the transient caused by a unit impulse. Eqs. (36) and (38), which are based on the approximation of the periodic response curve $y(t)$ by trapezoids, allow less elements than Eqs. (37) and (39) because of the smoother approximation.

Finally, a third set of approximate formulas may be obtained by using vertical strips instead of horizontal strips for the approximation of the given response curve $y(t)$, see Fig. 8.

Each of these elements is expanded in a Fourier series according to Eq. (23), with $t - t_m$ instead of t. The result is:

$$y(t) = \sum_{m=1}^{K} y_m \, \Delta_m t(\omega/\pi) \sum_{\substack{n=1,3,\dots \\ -1,-3,\dots}}^{\infty} e^{in\omega(t-t_m)} \qquad (42)$$

Comparing Eq. (42) with Eq. (25a),

$$F_n e^{i\varphi_n} = \frac{in\omega}{1 - e^{-in\omega\tau}} \sum_{m=1}^{K} y_m \Delta_m t e^{-in\omega t_m} \qquad (43)$$

This equation is valid for the case of a unit input during a time τ. In the limit for an infinitely short time τ, but assuming a unit input impulse, Eq. (43) is reduced to

$$F_n e^{i\varphi_n} = \sum_{m=1}^{K} y_m \Delta_m t e^{-in\omega t_m} \qquad (44)$$

Substituting $in\omega = s$ and approaching the limits $\Delta_m t \to 0$ and $T \to \infty$ transforms Eq. (44) directly into Eq. (41). The vertical strip method may be inferior to the horizontal strip method when analyzing the response to a step input (Fig. 7), but it may be more convenient when analyzing the response to an impulse (Fig. 8).

References

[1] Seamans, R. C., Jr., Bromberg, B. G., and Payne, L. E., *Application of the Performance Operator to Aircraft Automatic Control*, Journal of the Aeronautical Sciences, Vol. 15, No. 9, pp. 535–555, September, 1948.

[2] Brown, G. S., and Campbell, D. P., *Principles of Servomechanisms*, John Wiley and Sons, New York, 1948.

(5) Appendix—Summary of Formulas

(5.1) *Approximate Calculation of Transients for a Given Frequency Response*

(5.1.1) Oblique Unit Step Input.—

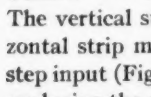

$$y(t) = \frac{F_0}{2} + \frac{2}{\pi\omega\tau} \sum_{n=1,3,\dots}^{h} \frac{F_n}{n^2} \times \{\cos[n\omega(t-\tau) + \varphi_n] - \cos(n\omega t + \varphi_n)\}$$

(5.1.2) Rectangular Unit Step Input.—

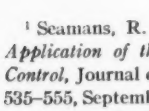

$$y(t) = (F_0/2) + (2/\pi) \sum_{n=1,3,\dots}^{h} (F_n/n) \times \sin(n\omega t + \varphi_n)$$

(5.1.3) Temporary Unit Input.—

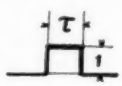

$$y(t) = \frac{2}{\pi} \sum_{n=1,3,\dots}^{h} \frac{F_n}{n} \times \{\sin(n\omega t + \varphi_n) - \sin[n\omega(t-\tau) + \varphi_n]\}$$

(5.1.4) Unit Impulse Input.—

$$y(t) = (2\omega/\pi) \sum_{n=1,3,\dots}^{h} F_n \cos(n\omega t + \varphi_n)$$

(5.2) *Approximate Calculation of the Frequency Response for a Given Transient*

Modes of approximation are:

(A) The given response function is approximated by horizontal elementary trapezoidal strips.

(B) The given response function is approximated by horizontal elementary rectangular strips.

(C) The given response function is approximated by vertical elementary rectangular strips.

(5.2.1.) Oblique Unit Step Input.—

(A) $$F_n e^{i\varphi_n} = (1/A_n) \sum_{m=1}^{k} A_{mn} \Delta_m y e^{-in\omega t_m}$$

(B) $$F_n e^{i\varphi_n} = (n\omega/iA_n) \sum_{m=1}^{k} \Delta_m y e^{-in\omega t_m}$$

(5.2.2.) Rectangular Unit Step Input.—

(A) $$F_n e^{i\varphi_n} = (i/n\omega) \sum_{m=1}^{k} A_{mn} \Delta_m y e^{-in\omega t_m}$$

(B) $$F_n e^{i\varphi_n} = \sum_{m=1}^{k} \Delta_m y e^{-in\omega t_m}$$

(5.2.3.) Temporary Unit Input.—

(A) $$F_n e^{i\varphi_n} = (\tau/in\omega A_n) \sum_{m=1}^{k} A_{mn} \Delta_m y e^{-in\omega t_m}$$

(B) $$F_n e^{i\varphi_n} = (\tau/ - A_n) \sum_{m=1}^{k} \Delta_m y e^{-in\omega t_m}$$

(C) $$F_n e^{i\varphi_n} = \frac{in\omega\tau}{-A_n} \sum_{m=1}^{k} y_m \Delta_m t e^{-in\omega t_m}$$

(5.2.4.) Unit Impulse Input.—

(A) $$F_n e^{i\varphi_n} = (1/n^2\omega^2) \sum_{m=1}^{k} A_{mn} \Delta_n y e^{-in\omega t_m}$$

(B) $$F_n e^{i\varphi_n} = (1/in\omega) \sum_{m=1}^{k} \Delta_m \dot{y} e^{-in\omega t_m}$$

(C) $$F_n e^{i\varphi_n} = \sum_{m=1}^{k} y_m \Delta_m t e^{-in\omega t_m}$$

Abbreviations:

$$\frac{e^{-in\omega\tau} - 1}{\tau} = A_n; \quad \frac{e^{-in\omega\tau_m} - 1}{\tau_m} = A_{mn}$$

Present Status of Research on Boundary-Layer Control

A. E. VON DOENHOFF* AND L. K. LOFTIN, JR.*

National Advisory Committee for Aeronautics

SUMMARY

A survey has been made of the present status of research on boundary-layer control and its possible applications in aeronautics. Although the number of possible applications of boundary-layer control is large, only those that have received the most attention recently or show the most promise of producing useful results are considered in the present paper. The possible applications of boundary-layer control considered are:

(1) Reduction of profile drag by the elimination of turbulent separation and by increasing the relative extent of laminar flow.

(2) Increase of the maximum lift coefficient through control of laminar and turbulent separation.

(3) The use of suction and blowing slots near the trailing edge of an airfoil as a means of lateral control.

(4) The use of boundary-layer control as a means of increasing the efficiency of diffusers and bends.

(5) The use of boundary-layer control to influence shock boundary-layer interaction at high speed.

The possible improvements in airplane characteristics resulting from these applications of boundary-layer control are discussed, and the general lines of future research are indicated.

INTRODUCTION

SINCE PRANDTL'S FIRST PAPER on boundary layers, removal of a portion of the boundary layer or the injection of high energy air under the boundary layer have been considered as possible means for avoiding boundary-layer separation. More recently, removal of a portion of the laminar boundary layer, either through discrete slots or through a permeable surface, has been proposed as a means of increasing the stability and thereby the relative extent of the laminar layer at high Reynolds Numbers so that the skin friction drag is reduced. It has been suggested that the effects on the potential flow field of withdrawing or ejecting small quantities of air near the trailing edge be used as a means of varying the lift of an airfoil.

A great deal of research has been conducted on various phases of boundary-layer control, but few results of this vast quantity of research have found practical application. The purposes of the present paper are to state briefly the present status of information regarding various types of boundary-layer control, to discuss the possibility of improving the characteristics of aircraft by boundary-layer control, and to indicate the general lines of future research on this subject that appear to offer the greatest promise of producing useful results.

The possibility of using boundary-layer control exists each time that the avoidance of separation or the maintenance of extensive laminar flow becomes a problem. Because of the large number of ways in which boundary-layer control can conceivably be applied, no general conclusions regarding the applicability of boundary-layer control can be drawn. The scope of the present paper is, therefore, limited to the consideration of proposed methods of boundary-layer control as they affect the individual aerodynamic characteristics of an aircraft. The applications considered are:

(1) Reduction of profile drag by the elimination of turbulent separation and by increasing the relative extent of laminar flow.

(2) Increase of the maximum lift coefficient through control of laminar and turbulent separation.

(3) The use of suction and blowing slots near the rear portion of the airfoil as a means of lateral control.

(4) The use of boundary-layer control as a means of increasing the efficiency and the range of efficient operating conditions of diffusers and bends.

(5) The use of boundary-layer control to influence shock boundary-layer interaction at high speeds and, in particular, to eliminate boundary-layer separation following the shock.

The use of slots represents in all cases one method of applying boundary-layer control, and in such cases the gains resulting from the use of boundary-layer control may depend in large measure on the design of the slots. For this reason, a short discussion of the status of research on the development of efficient slots is included at the end of the paper.

SYMBOLS

A	= aspect ratio (b^2/S)
b	= wing span
c	= chord
x	= distance along chord
t	= airfoil maximum thickness
S	= wing area
W	= airplane weight
V	= free-stream velocity
Q	= volume flow per unit span
v/V	= ratio of local velocity to free-stream velocity
W/S	= wing loading, lbs. per sq.ft.
L/D	= lift-drag ratio
c_d	= section drag coefficient
c_l	= section lift coefficient
C_L	= wing lift coefficient

Presented at the Aircraft Design Session, Seventeenth Annual Meeting, I.A.S., New York, January 24–27, 1949.

* Aeronautical Research Scientist, Langley Aeronautical Laboratory.

c_Q = section flow coefficient (Q/cV)
R = Reynolds Number
α_0 = section angle of attack
$max.$ = subscript indicating maximum

Drag

As mentioned in the introduction, reductions in the profile drag can be achieved by boundary-layer control through control of the turbulent layer and through extending the length of the laminar layer. Numerous design calculations have indicated the comparatively large improvements in airplane performance to be expected from reductions in the profile drag. The improvement in performance which can be expected from reductions in the profile drag through the maintenance of extensive laminar layers is shown to be even more marked for jet than for propeller-driven aircraft.[1] The effectiveness of control of the turbulent boundary layer as a means of reducing the profile drag is considered first.

Control of the Turbulent Layer

In the absence of separation, theoretically, some reduction in the net drag can be obtained by sucking the boundary layer into the interior of the airfoil at the trailing edge and discharging the air thus withdrawn at free-stream total pressure. It seems unlikely that any net gain could result from such a process because of the necessary losses associated with the internal flow. If, however, fairly extensive regions of separated flow exist, controlling the turbulent boundary layer in such a way as to eliminate separation results in substantial reduction of the profile drag even when the necessary pumping power is included in the drag coefficient.[2, 3] Such separation occurs on airfoils of moderate thickness at lift coefficients approaching the maximum and on extremely thick airfoil sections throughout the entire range of operating lift coefficients. The reduction in drag observed at the higher lift coefficients for the thin sections usually comes about as a by-product of attempts to improve the maximum lift by boundary-layer control. For wings having aspect ratios less than 10 or 12 and airfoil sections of less than 20 per cent thickness, such savings in drag are particularly marked only for lift coefficients above those for maximum L/D and, hence, are of relatively minor importance.

The use of aspect ratios of the order of 15 to 25 has always appeared attractive from the point of view of lower induced drag but has not been practical because, for structural reasons, the root sections of such wings are fairly thick so that flow separation occurs at all useful lift coefficients and the associated increase in profile drag equals or exceeds the saving in induced drag. Under such circumstances, the prevention of separation by boundary-layer control would seem to offer the possibility of realizing net drag savings and increased values of L/D on wings of high aspect ratio. With this thought in mind an experimental investigation has recently been made at the N.A.C.A. of the characteristics of three NACA 6-series airfoils of 24, 32, and 40 per cent thickness ratio employing boundary-layer control by suction to prevent separation of the turbulent boundary layer. The airfoils were cambered to have theoretical design lift coefficients of 0.4. The suction was applied through a single slot at or slightly behind the mid-chord position of the airfoil sections. In order that the results should correspond approximately to the limited extent of laminar flow that is usually obtained on airplane wings under practical operating conditions, the tests were made with the leading edges of the models roughened sufficiently to cause immediate transition. Lift and drag data are now available for the 24 per cent thick section[2] and are being prepared for publication for the 32 and 40 per cent thick sections. The data for the three thick sections, together with those for airfoils of 12 to 21 per cent thickness employing boundary-layer control,[4–6] are sufficient to enable designers to determine the desirability of employing boundary-layer control for the purpose of improving the characteristics of high-aspect-ratio wings. In order to supply detailed design information, however, further research will be necessary to determine optimum slot shapes, pitching-moment characteristics, and the behavior of three-dimensional wings employing boundary-layer control.

In order to give some indication of the possible improvement in wing characteristics which can be realized by employing boundary-layer control on wings of high aspect ratio, a comparison is made in Fig. 1 of a group of wings having a taper ratio of 0.4 and a varying aspect ratio with and without boundary-layer control. The wings are composed of NACA 6-series airfoils with leading edges roughened sufficiently to cause immediate transition. The root section thickness ratios were based on the structural design criterion that the ratio of the span to root thickness should be 35 to 1, but in no

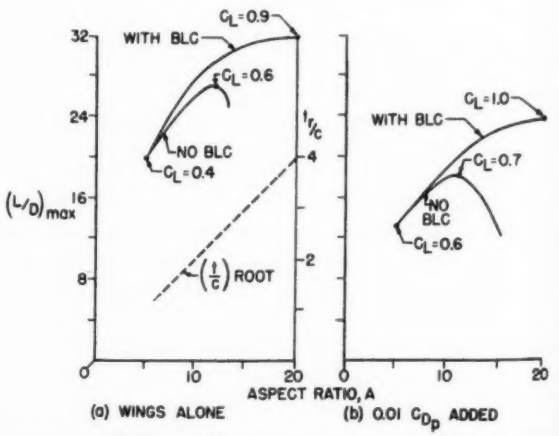

FIG. 1. Effect upon $(L/D)_{max.}$ of controlling turbulent separation on the thick root sections of high-aspect-ratio wings with leading-edge roughness. (a) Wings alone. (b) 0.01 parasite-drag coefficient added.

case was the root section thickness ratio made less than 12 per cent. In all cases the tip had a 12 per cent thickness ratio. A linear spanwise distribution of thickness ratio was assumed. The drag values used in computing the values of L/D included the wake drag plus the drag equivalent of the suction power.

A comparison of the data for the wings shown in Fig. 1 indicates that the optimum aspect ratio for maximum L/D is increased from approximately 11 to 20 by the use of boundary-layer control with an accompanying increase in L/D of approximately 19 per cent. The suction power considered in the calculations is that required to remove the necessary quantity of air from the surface of the wing through the slot but does not include any estimate of the losses that would occur in the ducting and pumping equipment of an airplane. The results for the two sets of wings given in Fig. 1 are, however, strictly comparable if the net efficiency of the pumping system from the boundary-layer control slot to the discharge outlet is equal to the propulsive efficiency of the main driving unit.

Despite the fact that the L/D of the wing with boundary-layer control is higher than that of the wing without boundary-layer control, the value of the profile-drag coefficient at $(L/D)_{max.}$ is greater for the wing with boundary-layer control. Consequently, the addition of a given increment of parasite drag coefficient will make the comparison more favorable for the wing with boundary-layer control. Fig. 1b gives a comparison between the two sets of wings when an arbitrary increment of parasite drag coefficient of 0.0100 has been added to each. Inspection of the data of Fig. 1b indicates that the optimum aspect ratio is now slightly higher than 20 for the wings with boundary-layer control and that the use of boundary-layer control gives an increase in $(L/D)_{max.}$ of approximately 30 per cent.

It should be noted that the maximum lift coefficients of the thick sections are high, and, as is shown subsequently, it is on wings of high aspect ratio that high maximum lift coefficients can be most effectively employed.

This application of boundary-layer control would be of primary interest for relatively low-speed airplanes where range is of the greatest importance. For example, the critical Mach Number obtained from low-speed pressure-distribution diagrams for the 40 per cent thick airfoil section at conditions corresponding to maximum L/D of the wing is 0.450. In spite of a number of obvious difficulties, it is thought that the possibility of increasing this limiting speed somewhat by the use of a moderate amount of sweep should be investigated.

Control of the Laminar Layer

The first attempts to obtain reductions in the profile drag by increasing the relative extent of laminar flow consisted of the design of new airfoil shapes having the position of minimum pressure far back along the surface. The rearward practical limit of the position of minimum pressure was dictated by the avoidance of turbulent separation over the rear portion of the airfoil, particularly for lift coefficients outside the low-drag range. Three general types of boundary-layer control have been proposed to increase the possible relative extent of laminar flow: first, multiple slots to limit the growth of the boundary-layer thickness and eliminate laminar separation; second, special airfoil sections having the position of minimum pressure extremely far back together with a single suction slot to eliminate separation at a pressure discontinuity; third, continuous boundary-layer suction through a porous surface.

The Use of Multiple Slots

Multiple slots have two distinct and interrelated effects on the boundary layer; they decrease the value of the boundary-layer Reynolds Number and delay or prevent laminar separation. Work on this problem has been carried out by Holstein[7, 8] in Germany; by Pfenninger[9] and Ackeret, Ras, and Pfenninger[10] in Switzerland; and by the N.A.C.A. in the United States. These investigations showed, in general, that it was possible to extend the laminar layer in a region of adverse pressure gradient practically to the trailing edge with a small expenditure of power such that extremely large net drag savings were realized. The most favorable results were obtained at a fairly low value of the Reynolds Number. For example, Pfenninger's best results, which showed a net drag saving of 50 per cent, were obtained at a Reynolds Number of 2.0×10^6. In both Pfenninger's and Holstein's experiments, however, the saving in drag disappeared when an attempt was made to repeat the tests at higher Reynolds Numbers. Pfenninger attributed this adverse scale effect to increasing turbulence in the tunnel as the speed was increased. Holstein[8] was able to maintain extensive laminar flow up to Reynolds Numbers of 3.2×10^6. However, he found that, if the slot spacing was not decreased as the Reynolds Number was increased, the power required to limit the growth of the laminar boundary layer would become excessive. He gave no explanation of his failure to achieve extensive laminar flow at Reynolds Numbers above 3.2×10^6.

An investigation is currently being carried out by the N.A.C.A. on a symmetrical NACA 64A010 airfoil section of 3-ft. chord designed to maintain laminar flow to the trailing edge by means of suction slots up to Reynolds Numbers of the order of 25.0×10^6. The model is being tested at zero lift in the Langley two-dimensional low-turbulence pressure tunnel.

The following considerations dictated the slot spacing and slot size: First, the boundary-layer Reynolds Number should not be allowed to exceed a definite value. Boundary-layer Reynolds Numbers corresponding to transition (based on displacement thickness) of 6,000 to 7,500 have been measured in flight,[11] and values of 5,000 to 6,000 have been measured on another wing section in the Langley two-dimensional low-turbu-

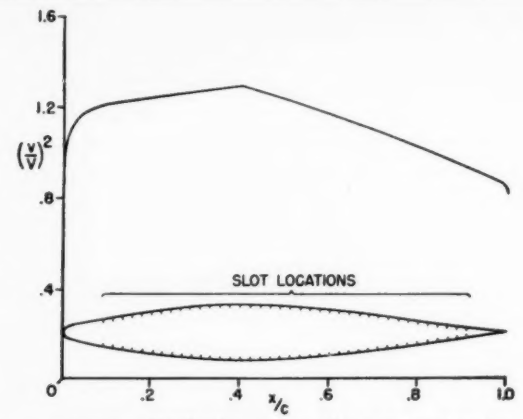

FIG. 2. Pressure distribution and suction-slot locations for an NACA 64A010 airfoil section.

lence pressure tunnel.[12] In order to be reasonably conservative, the design value of the maximum boundary-layer Reynolds Number for the slotted wing section was chosen to be approximately 2,600 at a wing Reynolds Number of 25.0×10^6. Second, the spacing between the slots was determined from suction-power considerations. Although the suction power required to maintain the boundary-layer Reynolds Number decreases continuously with decreasing slot spacing, it was found that the savings of power corresponding to a slot spacing smaller than $^3/_4$ in. on the present model (a Reynolds Number run of 0.5×10^6) were relatively small. Furthermore, a smaller slot spacing would increase considerably the mechanical difficulties of constructing the model. Previous investigations in the Langley low-turbulence tunnel indicated that the slot width should not be greater than the boundary-layer thickness. For the model under consideration this slot width was approximately 0.005 in.

Three parameters—namely, the maximum value of the boundary-layer Reynolds Number, the ratio of the slot width to the boundary-layer thickness, and the Reynolds Number run between slots—are sufficient to determine the design of a slot installation. If the values of these three parameters are held constant, the slot spacing and slot width expressed as fractions of the chord will be functions of the design Reynolds Number. For example, the slot spacing and slot width on the NACA 64A010 airfoil model would be .5 and 0.034 in., respectively, at a Reynolds Number of 25.0×10^6 if the chord of the airfoil were increased to 20 ft. If, however, with the 20-ft. chord the design Reynolds Number were increased to 83×10^6, the slot spacing and slot width would be $1^1/_2$ in. and 0.010 in., respectively, and the number of slots would increase in proportion to the Reynolds Number.

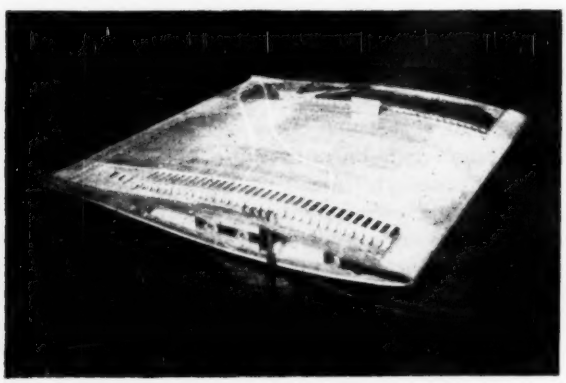

FIG. 3. Model of the N.A.C.A. 64A010 airfoil section equipped with 41 suction slots on upper and lower surfaces.

The theoretical pressure distribution, together with the slot locations, is given in Fig. 2 for the 3-ft. chord NACA 64A010 airfoil model designed for a Reynolds Number of 25.0×10^6. Great pains were taken in the construction of the model to maintain the machined aluminum surfaces in a smooth and fair condition. A photograph of the model partially disassembled is shown in Fig. 3. Preliminary test results indicated that not much difficulty was encountered in obtaining laminar flow over substantially the entire surface of the model up to a Reynolds Number of about 3.0×10^6. As the Reynolds Number was increased, however, the laminar flow in the boundary layer became exceedingly sensitive to minute changes in the shape of the slot entry and flow quantity removed. It was found that honing the edges of the slot slightly with a lead pencil produced sufficient changes in the slot contour to affect markedly the maximum Reynolds Number at which laminar flow could be obtained over the slot. The maximum Reynolds Number at which laminar flow could be obtained over substantially the entire upper surface was 10.0×10^6, whereas the corresponding maximum Reynolds Number for the lower surface was 5.5×10^6. These Reynolds Numbers, although not so high as expected flight values, are considerably higher than those for which complete laminar flow was obtained in the investigations of Holstein[8] and Pfenninger[9] and were obtained only after a great deal of effort had been expended in trying to eliminate minute irregularities from the slot contours. Since the airfoil was symmetrical, the differences in results between the upper and lower surfaces are attributed to small variations in the contours of individual slots. These variations were so slight that they could be observed only with the aid of a powerful magnifying glass. It was also observed that, once transition had occurred, no amount of suction applied downstream of the transition point restored the boundary layer to the laminar state. The conclusion drawn from this investigation is that, although the possible region of laminar flow may be extended to the trailing edge of an airfoil through a region of adverse pressure gradient at fairly high Reynolds Numbers, the laminar layer becomes increasingly sensitive to surface irregularities as the Reynolds Number is increased. This result is entirely consistent with those of a previous flight investigation[13] in which no decrease in sensitivity

of the laminar boundary layer to surface irregularities was observed to result from the installation of a number of suction slots on a wing panel. In view of the observed increasing sensitivity of the laminar layer to surface irregularities with increasing Reynolds Numbers and the difficulties that have been experienced in the past in obtaining the design extent of laminar flow on low-drag airfoils on operational airplanes, the use of suction slots to increase the possible extent of laminar flow does not appear to be attractive. The practicability seems especially limited when consideration is given to the extreme difficulty of manufacturing and maintaining sufficiently accurate slot contours.

Airfoils Designed Especially for Boundary-Layer Control

The second method of overcoming the limitations on the design extent of laminar flow imposed by the consideration of turbulent separation at the rear of the airfoil was suggested by Griffith and discussed in some detail by Goldstein in his Wright Brothers lecture.[14] The original basic idea of this method of approach was to design an airfoil that had favorable pressure gradients over the entire region from leading edge to trailing edge. In order to obtain a closed shape consistent with this condition, it was necessary that the pressure increase discontinuously at some point along the airfoil surface. Suction was to be introduced at this singular point in order to enable the flow to follow the contour without separation. A typical pressure distribution and corresponding airfoil profile, taken from Goldstein's paper,[14] are shown in Fig. 4. Because of the necessarily concave nature of the surface downstream of the pressure discontinuity and the corresponding Goertler type of instability, it was not possible to obtain laminar flow downstream of the suction slot except at extremely low Reynolds Numbers. Consequently, in spite of the favorable pressure gradient over the rear portion of the airfoil, laminar flow could be expected only in the region upstream of the slot. Later, airfoils of this type were, therefore, designed with the pressure discontinuity and associated suction slot at a more rearward position than shown in Fig. 4. More rearward positions of minimum pressure and correspondingly lower drag coefficients would be feasible with this type of airfoil section than, for example, with NACA 6-series sections without boundary-layer control, provided laminar flow were obtained up to the slot. If, however, laminar flow were not obtained up to the slot, it seems unlikely that the suction airfoil would show an appreciably lower drag coefficient than that of a plain airfoil section designed to have minimum pressure at the assumed forward position of transition. Practical airfoils can be designed with the position of minimum pressure as far back as 60 per cent of the chord. Experience with operational airplanes having low-drag wings, however, indicates that laminar flow usually extends over a distance of no more than 15 to 20 per cent of the chord back from the leading edge.[15] The difficulty appears to be not only the presence of inaccuracies in construction but also the accumulation of insects and dirt associated with the necessarily exposed nature of the wing surfaces. There is no reason to expect that the laminar boundary layer over the forward portion of suction airfoils of the Griffith type would be noticeably less sensitive to small surface irregularities than the corresponding region for NACA 6-series airfoils without suction. Unless the certainty of obtaining extensive laminar flow over more than the first 60 per cent of the airfoil chord can be made considerably greater than it is at present, it is not likely that an airplane designer would feel inclined to compromise the design of his airplane to the extent of using this type of suction airfoil. Since the advantages of extensive laminar flow are well known and the drag corresponding to various extents of laminar flow can be calculated theoretically, further research on the design of the Griffith-type airfoils and on their experimental characteristics under ideal conditions is much less urgent than is research on methods of insuring the realization of extensive laminar flow.

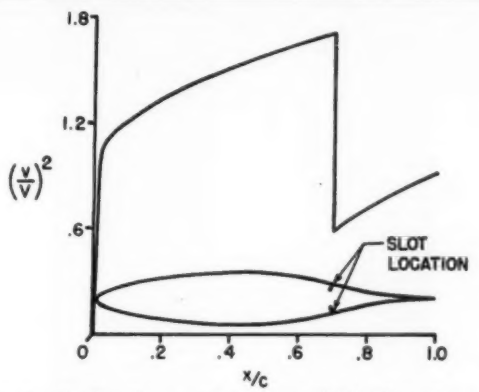

FIG. 4. Profile shape and pressure distribution of a symmetrical suction airfoil section of approximately 16 per cent thickness (reference 14).

Area Suction

A basic difficulty of obtaining laminar flow on airplanes is the sensitivity of the laminar boundary layer at high Reynolds Numbers to surface defects that are sufficiently small so as to be almost unavoidable. The only method of boundary-layer control that offers even any theoretical hope of reducing the sensitivity of the laminar layer to such small disturbances consists of continuous suction through a porous surface. The theory of the stability of laminar boundary layers to small two-dimensional disturbances was developed by Tollmien[16, 17] and Schlichting[18] and checked experimentally for the Blasius velocity distribution by Schubauer and Skramstad.[19] The theory was extended by Schlichting and others[20–25] to include the effects of variations in pressure gradients and the effects of blowing or sucking through a porous surface on the stability of the laminar layer. One of the most important conclusions of this

FIG. 5. Model of the N.A.C.A. 64A010 airfoil section having the center section covered with sintered bronze.

theoretical work (dealing only with small two-dimensional disturbances) is that continuous suction through a porous surface markedly stabilizes the laminar layer with respect to small disturbances and that the quantity of air that has to be removed to achieve this marked stabilizing effect is extremely small. For example, the theory indicates that the lower critical boundary layer Reynolds Number based on the displacement thickness for the flow over a flat plate with zero pressure gradient is increased from a value of approximately 420 without suction[26] to an asymptotic value of 55,000[23] to 70,000,[22] with an amount of suction corresponding to a component of velocity normal to the plate of the order of 0.01 of 1.0 per cent of the free-stream velocity.

An experimental investigation to determine the effects of continuous suction on the drag of an NACA 64A010 airfoil of 3-ft. chord is now being carried out by the N.A.C.A. in the Langley two-dimensional low-turbulence tunnels. The skin of the model is a $^{3}/_{32}$-in.-thick sheet of porous bronze which is made up of powder consisting of approximately spherical particles of such size that all the particles will pass through a 200-mesh screen but none through a 400-mesh screen. The sheet is wrapped in one continuous piece from the trailing edge on the upper surface around the leading edge to the trailing edge on the lower surface. The porous region has a span of 1 ft. situated in the center of the 3-ft. span model. A photograph of the model is shown in Fig. 5. Although some waviness was present in the model, the chordwise waves were actually much less severe than seems to be indicated in this photograph.

Typical results in the form of drag coefficient against flow coefficient are shown in Fig. 6 for a Reynolds Number of 6.0×10^6. Boundary-layer surveys taken near the trailing edge indicated that laminar flow was obtained over virtually the entire porous surface of the model for flow rates corresponding to the lowest drags obtained. These data show that substantial net savings in drag can be obtained and that completely laminar flow can be maintained even when the model is not quite aerodynamically smooth and fair. The fact that the model was not quite aerodynamically smooth and fair is shown by the comparison of the drag coefficient for the boundary-layer control model with sealed surface and the corresponding drag coefficient of the solid, fair, and smooth model of the same airfoil section. In sealing the porous model, the surface texture was not altered. At Reynolds Numbers substantially higher than 6.0×10^6, it was not possible to obtain any net reduction of drag. This adverse scale effect appears to be associated with the particular sample of material used in the investigation. The pressure drop across the porous material is directly proportional to the flow velocity through it, so that the chordwise distribution of inflow velocity becomes increasingly nonuniform not only with decreasing flow coefficient but also with increasing Reynolds Number. The flow coefficient corresponding to $c_{d_{min.}}$ at a Reynolds Number of 6.0×10^6 is somewhat greater than that indicated as theoretically necessary with a uniform inflow velocity to obtain the desired stability. Relative to free-stream velocity, the minimum inflow velocity necessary to avoid local regions of outflow increased with increasing Reynolds Number. At high values of the flow coefficient, it was rather difficult to judge whether the boundary layer was laminar or turbulent. In general, however, the results seem to indicate that complete laminar flow was obtained provided there were no local regions of outflow over the surface. At Reynolds Number much above 6.0×10^6, the flow coefficient necessary to satisfy this condition was so large that no net saving in drag was obtained in spite of the fact that the internal structure of the model was di-

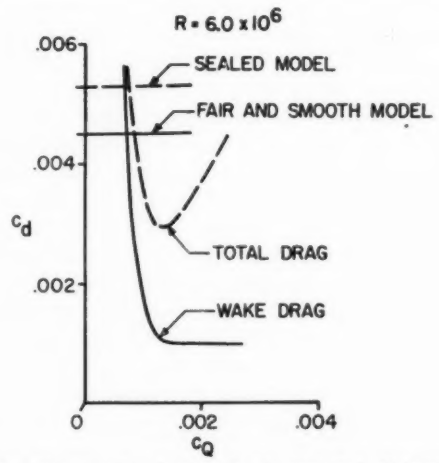

FIG. 6. Drag results obtained for the N.A.C.A. 64A010 airfoil section with and without suction through the surface of sintered bronze. $R = 6.0 \times 10^6$.

vided into a number of compartments with separately adjustable suction pressures. It is planned to continue the investigation using a much more dense porous material. It should be pointed out that the pressure drop through the porous surface itself is sufficiently small compared with the free-stream dynamic pressure for the flow rates of interest that the pressure drop can be increased several fold without materially affecting the suction power requirements.

In addition to the stabilizing effect indicated in the discussion of the data of Fig. 6, a further indication of the stabilizing action was obtained by spanwise drag surveys in the neighborhood of the juncture between the porous and solid portions of the surface of the model. This juncture was not completely smooth. As a result, transition spread inward from the juncture over the porous region and decreased the spanwise extent of the low-drag region behind the model. It was noticed that the spanwise extent of the low-drag region increased with increasing inflow velocity, which indicates that continuous suction decreases the angle of spread of turbulence.

Before any recommendations can be made regarding the use of continuous suction on airplane wings, not only must the feasibility of obtaining substantial reductions in drag be determined at higher Reynolds Number but, more importantly, the effects of surface irregularities such as are likely to be present under practical operating conditions must be found.

Maximum Lift

Usable Maximum Lift Coefficient

One of the earliest applications of boundary-layer control to receive attention was that of increasing the maximum lift coefficient. The gains in performance associated with such an improvement in wing characteristics were thought to be obvious. It is not at all certain, however, that such is the case. For example, a recent analytical investigation of a conventional low-speed airplane having a pay load of 5,000 lbs.[27] has indicated that the gains in take-off performance resulting from increasing the available maximum lift coefficient from values of the order of 3.0, which can be obtained without boundary-layer control, up to a value of approximately 5.0, which can be obtained only with boundary-layer control, did not result in a proportionate decrease in the total take-off distance. The improvement in take-off performance appeared to be relatively unimportant for aspect ratios much less than 15. The results of the analysis are consistent with results of German flight tests of two airplanes incorporating boundary-layer control to increase maximum lift coefficient.[28] It should be pointed out that the take-off distance considered to be of primary importance in these investigations was the distance required to clear a 50-ft. obstacle. In nearly all cases, increases in the maximum lift coefficient resulted in decreases in the ground run, which might be of considerable importance in special problems such as those encountered in the design of aircraft for carrier operation.

These investigations served to clarify considerably current concepts regarding the usefulness of high maximum lift coefficients for the particular take-off problem studied. Similar studies of both take-off and landing performance are badly needed for other types of aircraft, particularly those designed primarily for high-speed performance and having extremely thin wings or wings of unusual plan form. Although the usable maximum lift coefficients for most of the proposed high-speed wing configurations are probably lower than those of wings of more conventional plan form because of the associated high induced drags and low take-off thrusts, there does seem to be a possibility of improving the landing and take-off characteristics of such high-speed configurations by increasing the maximum lift coefficients above the present extremely low values. There appear then to be two possible fields of application for boundary-layer control to increase the maximum lift coefficient: first, to relatively low-speed airplanes having wings of extremely high aspect ratio; and, second, to high-speed airplanes with wings that have extremely low maximum lift coefficients.

Low-Speed Configurations

For conventional wings of high aspect ratio, methods exist for predicting the wing characteristics from airfoil section data. The discussion of methods of improving the maximum lift of conventional wings is, therefore, concerned with results that have been obtained from two-dimensional investigations of airfoils with boundary-layer control and other high-lift devices.

For smooth airfoils at all reasonably high angles of attack, laminar separation occurs near the leading edge, but below the maximum lift coefficient the flow reattaches itself to the surface forming a turbulent boundary layer. The amount of pressure recovery that can occur before the turbulent boundary layer separates depends markedly on the details of the flow conditions associated with the initial forming of the turbulent boundary layer. Turbulent separation near the trailing edge and the laminar separation near the leading edge have a regenerative effect upon each other.[29] Maximum lift finally occurs as a result of either a progressive forward movement of separation from the trailing edge or permanent separation of the laminar boundary layer near the leading edge. Because of the regenerative effect, increases of maximum lift coefficient on almost any given airfoil can be obtained by delaying either form of separation. The larger effect, however, is generally obtained by delaying the type of separation that finally results in complete flow breakdown. For example, the thicker airfoils with blunter leading edges, which have round-top lift curves, generally can be improved most by delaying separation of the turbulent boundary layer; whereas the largest increases in maxi-

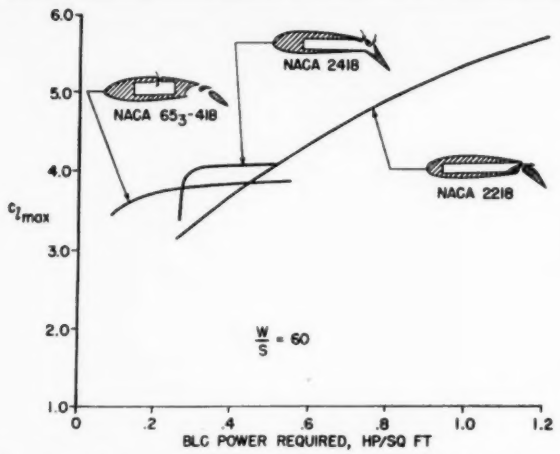

FIG. 7. Effect upon the maximum lift coefficient of boundary-layer control by suction and blowing.

mum lift of the thinner sections can be obtained by controlling separation near the leading edge. In any case, if boundary-layer control is used to prevent one type of separation, maximum lift will then be limited by the other type.

The type of boundary-layer control that has received the most attention has been that which delays turbulent separation over the rear portions of airfoils of 12 per cent thickness and greater. Turbulent separation can be delayed either by removing a portion of the low-energy air in the boundary layer or by injecting high-energy air under the boundary layer. Boundary-layer control is effective in increasing the maximum lift coefficient either with or without other high-lift devices. Their use in connection with boundary-layer control, however, generally has two advantages: First, the values of the maximum lift that can be obtained are greatly increased; and, second, the angles of attack for maximum lift are not excessive when trailing-edge high-lift devices are employed. A comparison of the most common methods of controlling the turbulent boundary layer is given in Fig. 7. The figure shows a plot of maximum lift coefficient as a function of blower power for a given wing loading. The data presented were obtained in the United States,[5] Germany,[30] and England.[31] The choice of the most effective method of boundary-layer control is seen to depend upon the power expenditure per unit wing area. The data indicate that for the lowest power expenditures the mid-chord suction slot, in combination with a trailing-edge double-slotted flap, is most effective. Extremely high maximum lift coefficients can be obtained with an arrangement whereby air is blown over the flap—but only with relatively large expenditure of power. The arrangement whereby air is withdrawn in the neighborhood of the flap hinge may be slightly better than the other two arrangements for intermediate power expenditures.

Some of the results[2, 4–6] of a systematic investigation of boundary-layer control on smooth airfoils of various thickness ratios are given in Fig. 8. In each case boundary-layer control was applied through a single suction slot located at the approximate mid-chord position. The increment of maximum lift coefficient due to boundary-layer control increased progressively with airfoil thickness ratio. The reason for the relatively small increments in maximum lift observed for the thinner sections is that for these airfoils maximum lift was originally limited by permanent laminar separation near the leading edge. In all cases with suction applied, maximum lift finally occurred as a result of permanent laminar separation near the leading edge.

An obvious method of further increasing the maximum lift coefficient is to delay or eliminate leading-edge separation. This can be done by the use of leading-edge slats or flaps or by the use of boundary-layer control. The effect of the addition of a leading-edge slat to the 12 per cent thick airfoil with boundary-layer control and double-slotted flap[4] can be seen in Fig. 9. Substantial increments in maximum lift are gained by the use of the leading-edge slat such that maximum lift coefficients of the order of 4.0 are possible for all of the airfoils of 12 to 24 per cent thickness.

In the hope that some form of boundary-layer control might be more effective or convenient in controlling leading-edge separation than slats or flaps, several investigations have been made. The types of boundary-layer control investigated include the location of slots near the leading edge and the use of a porous leading edge.[14, 32, 33] All data that are available from these investigations are for airfoils employing leading-edge boundary-layer control alone without means for controlling separation over the rear of the airfoil. As might have been expected, the boundary-layer control eliminated leading-edge separation, but turbulent separation

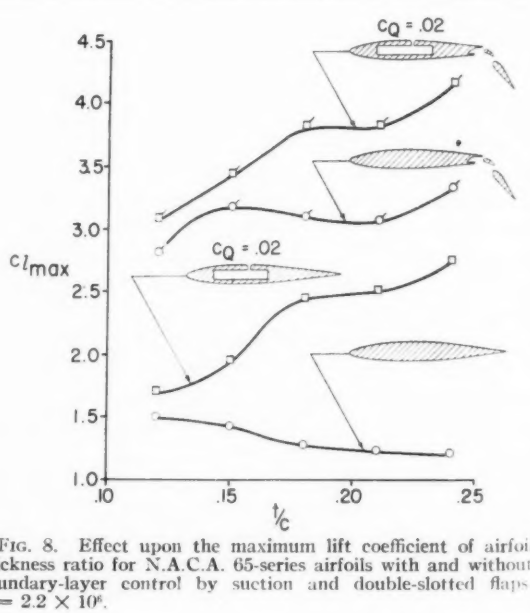

FIG. 8. Effect upon the maximum lift coefficient of airfoil thickness ratio for N.A.C.A. 65-series airfoils with and without boundary-layer control by suction and double-slotted flaps. $R = 2.2 \times 10^6$.

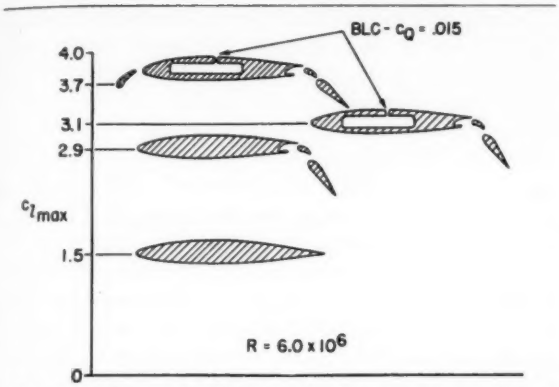

FIG. 9. Influence of a leading-edge slat upon the maximum lift obtained for a 12 per cent thick airfoil equipped with a double-slotted flap and boundary-layer control by suction at the mid-chord position.

over the rear of the airfoil limited the maximum lift to values of the order of those obtainable with a slat. Further research is needed in order to determine whether boundary-layer control applied to the leading edge of the thinner sections will prove more effective than leading-edge slats when used in conjunction with other types of boundary-layer control and high-lift devices. Boundary-layer control by continuous suction near the leading edge may have some advantages over discrete slots or leading-edge slats in that, presumably, detailed investigation of individual sections would not be necessary to obtain optimum configurations.

High-Speed Configurations

Wing configurations that have been designed primarily to obtain good aerodynamic characteristics at high Mach Numbers generally have airfoil section thickness ratios of less than 12 per cent and may have considerable amounts of sweep. Both of these characteristics lead to low values of the maximum lift coefficient. The low maximum lift of the thin sections is caused by relatively early separation of the flow from the leading edge. The largest improvements in the maximum lift would therefore be expected to occur as a result of control of the flow separation near the leading edge. Recent investigations at the N.A.C.A. Langley Aeronautical Laboratory have shown that the use of a plain, drooped leading-edge flap in conjunction with a plain trailing-edge flap increased the maximum lift of a 6 per cent thick airfoil section from 0.78 to 1.89. At least equally large increments in the section maximum lift coefficient could probably be obtained by substituting boundary-layer control for the flap at the leading edge, but the pressure difference through which the boundary-layer control blower would have to operate would be extremely large. This pressure difference would probably be a substantial fraction of the absolute pressure with normal landing speeds for airfoils of the order of 6 per cent thickness. It is questionable whether this application of boundary-layer control would be sufficiently more effective than the simple leading-edge flap to warrant its use. No final conclusion can be reached, however, until data are obtained on the pressure and flow-quantity requirements.

The maximum lift coefficients of the swept-type wings now being used for high-speed aircraft are generally extremely low. Although at the present time there are not generally available any data on the application of boundary-layer control to swept wings, the flow phenomena believed to result in the occurrence of maximum lift on swept wings are briefly discussed in order to indicate by what means the maximum lift of such wings might be improved by the use of boundary-layer control. According to the concepts of simple sweep theory, the characteristics of individual sections of an infinite yawed wing depend upon the component of velocity normal to the leading edge. The characteristics of finite sweptback wings are, however, rather strongly influenced by three-dimensional effects not present in the case of the infinite yawed wing.

The distribution of shed vorticity has two important adverse effects upon the characteristics of the sweptback wing: First, the induced vertical velocity field shifts the spanwise center of pressure outboard as the sweepback is increased; and, second, an effective negative camber is induced in the sections near the tip. The resultant effect upon the flow is that pressure peaks near the leading edge of the outboard sections tend to be accentuated. As a result, the tip sections of sweptback wings would be expected to stall sooner than do those near the root, with the stall originating near the leading edge. Early tip stalling is further provoked by the fact that the spanwise pressure gradient exercises a measure of boundary-layer control on the sections near the root and by the fact that the distribution of shed vorticity induces an effective positive camber in these root sections. Consequently, the first steps in attempting to improve the low-speed characteristics of such wings should be the delay of leading-edge separation on the outboard portions of the wing.

LATERAL CONTROL

The effectiveness of boundary-layer control as a lateral-control device depends upon the sensitivity of the lift of an airfoil section to details of the flow conditions at the trailing edge. Various investigations have been made in Germany[34] of the effect upon the direction of the stream line leaving the trailing edge—and, consequently, the lift—of discharging and withdrawing air through different arrangements of slots located at or near the trailing edge. Several of these devices proved quite effective in changing the lift coefficient at a given angle of attack in much the same way as an aileron acts. Although there is little reason to doubt the effectiveness of these devices, at least at subcritical speeds, or the fact that they might lead to extremely light control forces, it is not evident that they would prove to be

simpler or more reliable than conventional lateral-control devices with boosters where necessary.

Diffusers and Bends

Efficient diffusers are even more important on jet-type airplanes than on airplanes with conventional power plants, because any losses in the diffuser would not only represent an increment of drag but would also greatly decrease the efficiency and output of the jet engine itself. It is extremely difficult to determine any general rules or design criterions for the use of boundary-layer control on diffusers because of the marked effect of the initial conditions of the boundary layer at the entrance of the diffuser on the pressure-recovery characteristics and the rapidity with which the diffusion can be accomplished without encountering serious losses. In many cases, the entrance to the duct is situated well back on a body—as, for example, a scoop inlet on a fuselage. In these cases, improvements in the efficiency of the diffuser can be obtained by removing a portion of the boundary-layer air ahead of the duct as well as within the duct itself. The bypassing of low-energy boundary-layer air from the duct entrance is now general practice for nearly all scoop-type air inlets. The use of suction to avoid separation within a diffuser is not a new principal. Unfortunately, however, generalized data giving the quantity and pressure requirements are not available. Such data for several specific configurations, however, are given in an N.A.C.A. paper by Biebel.[35] In general, it appears that high-efficiency diffusion can be obtained with the use of a single suction slot withdrawing a quantity of air of the order of 5 per cent of the total quantity of air passing through the duct. In many cases, the improvement in airplane performance gained as a result of the improved efficiency of diffusion might more than counterbalance the losses associated with withdrawing the required boundary-layer air. Because, in general, the static pressure within the diffuser is higher than free-stream static pressure, no auxiliary pumping equipment is necessary. This application of boundary-layer control appears attractive and should be considered whenever the problem of efficient diffusion in a short distance arises. Because of the varied nature of individual applications, however, it is difficult to outline a systematic research program that would provide adequate data. Future research would probably most profitably deal with proposed specific installations.

The application of suction to prevent separation in bends does not appear so attractive as that just discussed, because the local pressure at the point where boundary-layer control is required is generally fairly low as compared with free-stream static pressure. Furthermore, considerable improvement in the efficiency of bends can be obtained by the proper use of guide vanes.

Little detailed information is available on the use of blowing slots to improve the flow in diffusers and bends. One such installation has been made, however, in the exit cone of the Langley high-speed 7- by 10-ft. wind tunnel where a comparatively small amount of air, having a total pressure equal to that in the center of the tunnel, is introduced under the boundary layer in the exit cone. It was found that these blowing slots had little effect on the energy ratio of the tunnel, but they eliminated the unsteadiness of the flow in the tunnel. It is possible that a corresponding arrangement in the entrance diffuser of a jet engine installation might have a beneficial influence on the steadiness of the flow entering the compressor.

Boundary-Layer Control at High Mach Numbers

Another possible application of boundary-layer control is the control of separation following a shock at high Mach Numbers. It is fairly well agreed that one of the principal reasons for the rapid increase in drag above the critical Mach Number is the separation of the flow from the surface that accompanies shock formation rather than the losses in the shock itself, at least at low supercritical Mach Numbers. It also seems likely that the position of the shock is strongly affected by boundary-layer conditions. Boundary-layer control as a method for preventing separation following a shock has been investigated to some extent in Germany[36] and England.[37] These tests indicate that the external drag can be reduced at some Mach Numbers, but in many cases the power requirements were about equivalent to the saving in wake drag. These investigations, however, are not necessarily conclusive. In each case boundary-layer control was applied through a single suction slot. If the primary purpose of the boundary-layer control is to eliminate the flow separation associated with shock formation, there is some doubt as to the effectiveness of any single slot configuration because of the large variation of the shock position with Mach Number and angle of attack. The possible reductions in drag coefficient and elimination of buffeting and the fact that boundary-layer control may tend to reduce or at least postpone to higher Mach Numbers the large erratic changes in lift and pitching moment makes further investigations of boundary-layer control at high Mach Numbers seem extremely important. These investigations should include not only the effects of individual suction and blowing slots but also the effects of suction through a porous surface. The purpose of the porous surface in this case would not be so much to maintain extensive laminar flow as to ensure that suction would always be applied in the vicinity of the shock.

The application of boundary-layer control at supersonic speeds is not clear. On the one hand, analysis indicates that for bodies of optimum fineness ratio the skin friction accounts for one-half to two-thirds of the total drag. The investigations of Theodorsen and Regier[38] indicate that the laws for turbulent-boundary-

layer skin friction are not greatly different at supersonic speeds than at subsonic speeds. Reductions of the skin friction drag must, therefore, as at subsonic speeds, come about through an increase in the relative extent of laminar flow. On the other hand, the details of the shock formation at the trailing edge of a supersonic airfoil section appear to have a large effect on the drag. In general, thickening of the boundary layer near the trailing edge appears to increase the trailing-edge pressure and thereby results in a decrease of the pressure drag.[39] Boundary-layer control or any other effect that would tend to increase the extent of laminar flow and decrease the skin friction drag would appear, therefore, to have a tendency to increase the pressure drag. Hence, boundary-layer control at supersonic speeds presents a much more complex problem than at subsonic speeds and is badly in need of thorough investigation.

Suction-Slot Design

The requirements for a good suction slot depend upon whether the slot is to be used for removing a portion of the laminar or turbulent boundary layer. The primary requirement for slots designed to extend laminar flow is that the slots themselves shall not introduce any disturbance that will cause transition. Slots have been designed that satisfy this condition in several investigations,[7–9, 13] and further work on the design of suction slots for laminar layers is discussed by Fage and Sargent.[40] Losses in slots designed to control the laminar boundary layer are usually not of critical importance because the amount of air withdrawn at a single slot is small in a correctly designed installation. Furthermore, the velocity with which the air is withdrawn cannot be very large without disturbing the laminar layer and causing transition. It is necessary, of course, that the flow into the slot be stable, and this question has been investigated by Smith and Roberts.[1]

The conditions affecting the design of slots to operate in a turbulent boundary layer are quite different. In this case the external flow is relatively insensitive to detailed changes in the slot design and is affected primarily by the quantity of air withdrawn. Changes in the design of the suction slot do, however, have a marked effect on the internal losses. These losses are more important than for laminar layers because of the relatively large quantities of air withdrawn in each slot. Investigations to develop efficient slot configurations for turbulent boundary layers have been carried out by Pierpont[41] and Gerber[42]. The problem of reducing the losses following entry of the air into the slot is primarily that of designing efficient diffusers and bends. This problem has been considered in some detail by Rawcliffe.[43]

Conclusions

Consideration of the present status of research on various methods of boundary-layer control indicates the following conclusions:

(1) For relatively low-speed, long-range aircraft, boundary-layer control may be effectively employed to eliminate turbulent separation on thick root-section airfoils such that wings of higher aspect ratio may be employed to give improved values of the lift-to-drag ratio. The data on which the analysis was based were obtained for airfoils having completely turbulent boundary layers extending back from the leading edge.

(2) In order to obtain extensive regions of laminar flow and correspondingly low profile-drag coefficients such as might be obtainable with NACA 6-series airfoils or airfoils of the Griffith type, some means must be found for decreasing the sensitivity of the laminar boundary layer to surface imperfections that are apt to occur under practical operating conditions. The use of multiple slots does not appear to decrease the sensitivity of the laminar boundary layer. Although information regarding the effects of area suction is not sufficiently complete to be conclusive, such data as are available indicate that area suction does have some stabilizing action and that the suction power requirements are small. Further research should be carried out on boundary-layer control by area suction.

(3) By the appropriate use of boundary-layer control maximum lift coefficients of the order of 4.0 can be obtained for airfoil sections of 12 per cent thickness and above without the expenditure of excessive amounts of power. Maximum lift coefficients of the order of 3.0 or 4.0 are effective in decreasing the take-off distance only for airplanes having wings of extremely high aspect ratio.

(4) The use of boundary-layer control as a means of increasing or decreasing the lift of an airfoil independently of the angle of attack has been the subject of several investigations. These methods proved to be effective. It is not clear, however, that they would be any simpler or more effective than conventional control surfaces.

(5) The use of suction to control separation appears to be a particularly convenient method of increasing the efficiency of short diffusers because the pressure at the suction slot usually is sufficiently high to eliminate the need for auxiliary pumping equipment. Because of the varied nature of individual applications, however, future research on this problem would probably most profitably deal with proposed specific installations.

(6) Several short investigations have been made of the effect of boundary-layer control on the drag at supercritical Mach Numbers. These tests showed little net decrease in the drag. The method employed for applying the boundary-layer control, however, did not appear to be the optimum. Further research on boundary-layer control at supercritical speeds is necessary in order to explore more completely the possibilities of the application of boundary-layer control not only for reducing the drag but also for improving the lift and moment characteristics. In particular, it is felt that the

use of continuous or area suction should be investigated at high Mach Numbers.

References

[1] Smith, A. M. O., and Roberts, Howard E., *The Jet Airplane Utilizing Boundary Layer Air for Propulsion.* Journal of the Aeronautical Sciences, Vol. 14, No. 2, pp. 97–109, 128, February, 1947.

[2] Racisz, Stanley F., and Quinn, John H., Jr., *Wind-Tunnel Investigation of Boundary-Layer Control by Suction on NACA 65_3-424 Airfoil with Double Slotted Flap,* N.A.C.A. T.N. No. 1631, 1948.

[3] Schrenk, Oskar, *Experiments with a Wing from which the Boundary Layer Is Removed by Suction,* N.A.C.A. T.M. No. 634, 1931.

[4] Quinn, John H., Jr., *Tests of the NACA 64_1A212 Airfoil Section with a Slat, a Double Slotted Flap, and Boundary-Layer Control by Suction,* N.A.C.A. T.N. No. 1293, 1947.

[5] Quinn, John H., Jr., *Wind-Tunnel Investigation of Boundary-Layer Control by Suction on the NACA 65_3-418, $a = 1.0$ Airfoil Section with a 0.29-Airfoil-Chord Double Slotted Flap,* N.A.C.A. T.N. No. 1071, 1946.

[6] Quinn, John H., Jr., *Wind-Tunnel Investigation of the NACA 65_4-421 Airfoil Section with a Double Slotted Flap and Boundary-Layer Control by Suction,* N.A.C.A. T.N. No. 1395, 1947.

[7] Holstein, Horst, *Messungen zur Laminarhaltung der Grenzschicht durch Absaugung an einem Tragflügel,* Bericht S10 der LGL, pp. 17–27, 1940.

[8] Holstein, Horst, *Messungen zur Laminarhaltung der Reibungsschicht durch Absaugung an einem Tragflügel mit Profil NACA 0012/64,* Forschungsbericht Nr. 1654, Deutsche Luftfahrtforschung (Göttingen), 1942.

[9] Pfenninger, Werner, *Investigations on Reductions of Friction on Wings, in Particular by Means of Boundary-Layer Suction,* N.A.C.A. T.M. No. 1181, 1947.

[10] Ackeret, J., Ras, M., and Pfenninger, W., *Verhinderung des Turbulentwerdens einer Grenzschicht durch Absaugung.* Sonderdruck aus Die Naturwissenschaften, Jahrb. 29, Heft 41, pp. 622–623, 1941.

[11] Wetmore, J. W., Zalovcik, J. A., and Platt, Robert C., *A Flight Investigation of the Boundary-Layer Characteristics and Profile Drag of the NACA 35-215 Laminar-Flow Airfoil at High Reynolds Numbers,* N.A.C.A. M.R., May 5, 1941.

[12] Braslow, Albert L., and Visconti, Fioravante, *Investigation of Boundary-Layer Reynolds Number for Transition on an NACA 65_{216}-114 Airfoil in the Langley Two-Dimensional Low-Turbulence Pressure Tunnel,* N.A.C.A. T.N. No. 1704, 1948.

[13] Zalovcik, John A., Wetmore, J. W., and von Doenhoff, Albert E., *Flight Investigation of Boundary-Layer Control by Suction Slots on an NACA 35-215 Low-Drag Airfoil at High Reynolds Numbers,* N.A.C.A. A.C.R. No. 4B29, 1944.

[14] Goldstein, Sydney, *Low-Drag and Suction Airfoils.* Journal of the Aeronautical Sciences, Vol. 15, No. 4, pp. 189–214, April, 1948.

[15] Zalovcik, John A., *Profile-Drag Coefficients of Conventional and Low-Drag Airfoils as Obtained in Flight,* N.A.C.A. A.C.R. No. L4E31, 1944.

[16] Tollmien, W., *The Production of Turbulence,* N.A.C.A. T.M. No. 609, 1931.

[17] Tollmien, W., *General Instability Criterion of Laminar Velocity Distributions,* N.A.C.A. T.M. No. 792, 1936.

[18] Schlichting, H., *Amplitudenverteilung und Energiebilanz der kleinen Störungen bei der Plattenströmung,* Nachr. d. Ges. d. Wiss. zu Göttingen, Math.-Phys. Kl., Neue Folge, Bd. 1, Nr. 4, pp. 47–78, 1935.

[19] Schubauer, G. B., and Skramstad, H. K., *Laminary-Boundary-Layer Oscillations and Transition on a Flat Plate,* N.A.C.A A.C.R., April, 1943.

[20] Schlichting, H., *Über die Berechnung der kritischen Reynoldsschen Zahl einer Reibungsschicht in beschleunigter und verzögerter Strömung,* Jahrb. 1940 der deutschen Luftfahrtforschung, R. Oldenbourg (Munich), p. I 97.

[21] Schlichting, H., and Ulrich, A., *Zur Berechnung des Umschlages laminar/turbulent,* Bericht S10 der Lilienthal-Gesellschaft für Luftfahrtforschung, Preisausschreiben pp. 75–133, 1940.

[22] Bussman, K., and Munz, H., *Die Stabilität der laminaren Reibungsschicht mit Absaugung,* Jahrb. 1942 der deutschen Luftfahrtforschung, R. Oldenbourg (Munich), pp. I 36–I 39.

[23] Pretsch, J., *Umschlagbeginn und Absaugung,* Jahrb. 1942 der deutschen Luftfahrtforschung, R. Oldenbourg (Munich), pp. I 1–I 7.

[24] Pretsch, J., *Die Stabilität der Laminarströmung bei Druckgefälle und Druckanstieg,* Forschungsbericht Nr. 1343, Deutsche Luftfahrtforschung (Göttingen), 1941.

[25] Iglisch, Rudolf, *Exakte Berechnung der laminaren Grenzschicht an der längsangeströmten ebenen Platte mit homogener Absaugung,* Schriften der Deutschen Akademie der Luftfahrtforschung, Bd. 8B, Heft 1, pp. 1–51, 1944.

[26] Lin, C. C., *On the Stability of Two-Dimensional Parallel Flows, Part I,* Quarterly Appl. Math., Vol. III, No. 2, pp. 117–142, July, 1945; *Part II,* Vol. III, No. 3, pp. 218–234, October, 1945; and *Part III,* Vol. III, No. 4, pp. 277–301, January, 1946.

[27] Horton, Elmer A., and Quinn, John H., Jr., *Analysis of the Effects of Boundary-Layer Control on the Take-Off Performance Characteristics of a Liaison-Type Airplane,* N.A.C.A. T.N. No. 1597, 1948.

[28] Stüper, J., *Flugerfahrungen und Messungen an zwei Absaugeflugzeugen,* Forschungsbericht Nr. 1821, Deutsche Luftfahrtforschung (Göttingen), 1943.

[29] Jacobs, Eastman N., and Sherman, Albert, *Airfoil Section Characteristics as Affected by Variations of the Reynolds Number.* N.A.C.A. Report No. 586, 1937.

[30] Regenscheit, B., and Schrenk, O., *Versuche mit Absaugeklappenflügeln verschiedener Profilwölbung und Wölbungslage,* Forschungsbericht Nr. 1061, Deutsche Luftfahrtforschung (Göttingen).

[31] Lyon, H. M., Barnes, E. G., and Adamson, J. E., *Further Experiments on Boundary-Layer Control as a Means of Increasing Lift,* Report No. B.A. 1669, British R.A.E., April, 1941.

[32] Nuber, Robert J., and Needham, James R., Jr., *Exploratory Wind-Tunnel Investigation of the Effectiveness of Area Suction in Eliminating Leading-Edge Separation over an NACA 64_1A212 Airfoil,* N.A.C.A. T.N. No. 1741, 1948.

[33] McCullough, George B., and Gault, Donald E., *An Experimental Investigation of an NACA 63_1-012 Airfoil Section with Leading-Edge Suction Slots,* N.A.C.A. T.N. No. 1683, 1948.

[34] Seiferth, R., *The Most Important Experimental Research Work of the Last Time and Proposals about Reports Still to be Written.* R. and T. No. 35, British M.A.P. Völkenrode, February 15, 1946.

[35] Biebel, William J., *Low-Pressure Boundary-Layer Control in Diffusers and Bends,* N.A.C.A. A.R.R. No. L5C24, 1945.

[36] Regenscheit, *Research on Diminishing the Drag of an Aerofoil at a High Mach Number by Means of Sucking Away the Boundary Layer behind the Region of Discontinuous Compression,* R. and T. No. 481, British M.A.P. Völkenrode, April, 1946.

[37] Fage, A., and Sargent, R. F., *Effect on Aerofoil Drag of Boundary Layer Suction Behind a Shock Wave,* British R. & M. No. 1913, British A.R.C., 1943.

[38] Theodorsen, Theodore, and Regier, Arthur, *Experiments on Drag of Revolving Disks, Cylinders, and Streamline Rods at High Speeds,* N.A.C.A. Report No. 793, 1944.

[39] Ferri, Antonio, *Experimental Results with Airfoils Tested in the High-Speed Tunnel at Guidonia,* N.A.C.A. T.M. No. 946, 1940.

(*Continued on page 760*)

Heat Transfer in Laminar Compressible Boundary Layer on a Porous Flat Plate with Fluid Injection

SHAO WEN YUAN†

Polytechnic Institute of Brooklyn

SUMMARY

A theoretical investigation was made of flow of hot fluid over a porous flat plate under the condition of uniform fluid injection from the bottom of the plate. The von Kármán integral relation of the momentum equation was derived with the uniform velocity of injection taken into consideration. The velocity profile was assumed as a polynomial of the fourth degree.

Solution of the above equation gave the relationship of length in the direction of flow to the boundary-layer thickness. The velocity profiles and the temperature profiles were then calculated for a Prandtl Number equal to unity.

The relation between wall temperature and the rate of coolant injection were calculated for different Mach Numbers, Reynolds Numbers, and viscosity variation with temperature.

NOMENCLATURE

x	= distance along the plate in the direction of the free stream measured from stagnation point
y	= distance perpendicular to the plate
u	= velocity at any point along the plate
v	= velocity at any point perpendicular to the plate
v_0	= constant injection velocity fluid
U	= velocity outside the boundary layer
δ	= thickness of boundary layer
λ	= $(v_0\delta/6\nu_w) - T_f$ = nondimensional boundary-layer thickness
ξ	= $(Ux/\nu_1)\ (\rho_0 v_0/\rho_1 U)^2$ = nondimensional distance along the plate
c_p	= specific heat at constant pressure
c_t	= coefficient of heat conduction
μ_w, μ_1	= dynamic viscosity at wall and outer boundary layer
ρ_w, ρ_1, ρ_0	= mass fluid density at wall and outer boundary layer, and of coolant
ν_w, ν_1	= kinematic viscosity of fluid at wall and outer boundary layer
T	= fluid temperature
T_1	= fluid temperature at outer boundary layer
T_w	= temperature of the plate
T_0	= temperature of the coolant to be injected
T_a	= $(T_1 - T_w)/T_1$
n_T	= T_1/T_w
η	= y/δ
R_L	= UL/ν_1 Reynolds Number
L	= length of the plate
M	= speed ratio or Mach Number of the free stream
k	= specific heat ratio
T_f	= $\frac{n_T - 1}{12} + \frac{n_T}{12}\frac{k-1}{2} M^2$ for $\mu \sim \sqrt{T}$
T_f	= $\frac{n_T - 1}{8} + \frac{n_T}{8}\frac{k-1}{2} M^2$ for $\mu \sim T^{3/4}$
T_a	= $(n_T - 1)/12$ for $\mu \sim \sqrt{T}$
T_a	= $(n_T - 1)/8$ for $\mu \sim T^{3/4}$
Q	= $\rho_0 v_0$
w	= $\rho_1 U$

Presented at the Heat Transfer and Fluid Mechanics Institute, Pasadena, Calif., June 23, 1948. Received May 16, 1949.

This paper is based on work supported by Project Squid, U. S. Navy. The author's thanks are due to his colleagues, C. Chin and N. Ness, for checking and carrying out the derivation and numerical work.

† Associate Professor in Aeronautical Engineering.

INTRODUCTION

COOLING OF COMBUSTION CHAMBERS in rocket and jet motors, which are subject to extremely high temperature, by means of injecting coolant through a porous wall is a new and effective cooling method. This is the so-called sweat-cooling method. The combustion chamber walls that are to be cooled are built from porous materials, and a cold medium, called coolant in the form of a gas or liquid, is pressed through the pores. On emerging from the wall, the coolant first picks up heat from the wall and lowers the wall temperature, and then it forms a protective layer on the surface exposed to the gas, which diminishes the heat transfer from the hot gas to the wall. Since the magnitude of the boundary-layer thickness along the combustion chamber liner is known to be comparatively small, the problem can be treated by investigating the boundary layer along a flat plate under the same flow condition. It is believed that this approximation will yield some indication of the actual case.

The theoretical study of the aerothermodynamic problems involved was started by the investigation of the flow of a hot fluid over a porous flat plate under the conditions of uniform fluid injection from the bottom of the plate. The assumptions made in the present investigation are: (1) the inverse proportion between mass density and temperature inside the boundary layer is used, and the viscosity is assumed to be proportional to the square root and three-fourths power of the temperature; (2) the Prandtl Number is assumed to be equal to unity; and (3) the flow is assumed to be laminar, and the fluid flowing along the wall and the coolant flowing through the pores are assumed homogenous. It must be borne in mind that in the turbulent

boundary layer that occurs in actual practice, the reduction of heat flow is probably smaller. Moreover, the isolating effect of the coolant film is better in the case of a laminar boundary layer. Hence, the present calculations give an upper limit for the decrease of the heat transfer coefficient by sweat-cooling.

In the solution of the boundary-layer equation, the Prandtl Number was assumed to be equal to unity; then the temperature T could be expressed by a certain parabolic function of the velocity only, which satisfied both the equation of motion and the energy equation. The velocity profile was assumed as a polynomial of the fourth degree.

Knowing that the quantity of heat per unit area removed by the plate is equal to the quantity of heat per unit area absorbed by the coolant at the surface of the plate, a relation between the wall temperature and the amount of coolant needed is established. For a predesignated wall temperature, the amount of coolant required per unit time can be determined provided the temperature of the outer boundary layer and of the coolant are known. A comparison of the above theoretical results with some available experimental data shows only fair qualitative agreement.

The Momentum and Energy Equations for the Boundary Layer

The equation of motion in the boundary layer of a flat plate in steady compressible flow is

$$\rho u\frac{\partial u}{\partial x}+\rho v\frac{\partial u}{\partial y}=\frac{\partial}{\partial y}\left(\mu\frac{\partial u}{\partial y}\right) \tag{1}$$

where the x-axis is taken along the plate in the direction of the free stream, the y-axis is perpendicular to the plate, and u and v indicate the x and y components of the velocity at any point.

The equation of continuity is

$$(\partial/\partial x)\,(\rho u)+(\partial/\partial y)\,(\rho v)=0 \tag{2}$$

The equation that determines the energy balance between the heat produced by viscous dissipation and the heat transferred by conduction and convection is given in the following form:

$$\rho u\frac{\partial}{\partial x}(c_pT)+\rho v\frac{\partial}{\partial y}(c_pT)=\frac{\partial}{\partial y}\left(c_t\frac{\partial T}{\partial y}\right)+\mu\left(\frac{\partial u}{\partial y}\right)^2 \tag{3}$$

In reference 1, it has been shown that, for a Prandtl Number equal to unity, Eqs. (1) and (3) can be satisfied by equating the temperature T to a certain parabolic function of the velocity u only. This relation between T and u is

$$\frac{T}{T_1}=\frac{T_w}{T_1}-\left(\frac{T_w}{T_1}-1\right)\frac{u}{U}+\frac{k-1}{2}M^2\frac{u}{U}\left(1-\frac{u}{U}\right) \tag{4}$$

The perfect gas equation leads to (for zero pressure gradient):

$$\rho/\rho_1=T_1/T \tag{5}$$

It will be assumed that the variation of the viscosity with temperature is given by

$$\mu/\mu_1=(T/T_1)^{1/2} \tag{6}$$

For air at normal temperature, the exponent is about 0.76 instead of $^1/_2$, but it increases slightly with T_1.

Integrating Eq. (1) between the limits $y=0$ and $y=\delta$, utilizing the equation of continuity, and satisfying the boundary conditions, $y=0$; $u=0$, $v=v_0$; $y=\delta$; $v=v(\delta)$, $u=U$, one obtains:

$$\frac{\partial}{\partial x}\int_0^\delta \rho u^2dy-U\frac{\partial}{\partial x}\int_0^\delta \rho\,udy+\rho_wv_0U=\left[\mu\frac{\partial u}{\partial y}\right]_0^\delta \tag{7}$$

where ρ_w is the mass density of the injected coolant.

Solution of Boundary Layer Equation

In order to solve Eq. (7) a polynomial of the fourth degree as an approximation to the velocity profile is assumed:

$$\frac{u}{U}=a\eta+b\eta^2+c\eta^3+d\eta^4 \tag{8}$$

where $\eta=y/\delta$.

The values of the quantities a, b, c, d can be calculated from the following boundary conditions:

$$y=\delta:\quad u=U,\quad \partial^2u/\partial y^2=0,\quad \partial u/\partial y=0$$

$$y=0:\quad u=0,\ v=v_0,\quad \rho_wv_0\left(\frac{\partial u}{\partial y}\right)_w=\mu_w\left(\frac{\partial^2u}{\partial y^2}\right)_w+\left(\frac{\partial\mu}{\partial y}\right)_w\left(\frac{\partial u}{\partial y}\right)_w$$

This gives:

$$a=\frac{2}{1+\lambda},\quad b=\frac{6\lambda}{1+\lambda},\quad c=-\frac{2+8\lambda}{1+\lambda},\quad d=\frac{1+3\lambda}{1+\lambda} \tag{9}$$

and $\lambda=\dfrac{Q\delta}{6\mu_w}-T_f$. Hence, the velocity distribution in the boundary layer is given by

$$\frac{u}{U}=\frac{2}{1+\lambda}\eta+\frac{6\lambda}{1+\lambda}\eta^2-\frac{2+8\lambda}{1+\lambda}\eta^3+\frac{1+3\lambda}{1+\lambda}\eta^4 \tag{10}$$

The density ρ and viscosity μ are expressed as follows:

$$\rho=\rho_1\left[\frac{T_w}{T_1}-\left(\frac{T_w}{T_1}-1\right)\eta+\frac{k-1}{2}M^2\eta(1-\eta)\right]^{-1} \tag{11}$$

and

$$\mu=\mu_1\left[\frac{T_w}{T_1}-\left(\frac{T_w}{T_1}-1\right)\eta+\frac{k-1}{2}M^2\eta(1-\eta)\right]^n \tag{12}$$

where $n=^1/_2$ or $^3/_4$.

Upon substitution of Eqs. (10), (11), and (12) into the first two terms of Eq. (7), one obtains:

$$-U\frac{d}{dx}\int_0^\delta \rho u\,dy = \frac{6w\mu_w U}{Q[(k-1)/2]\,M^2}\Big[(2\alpha - 2\epsilon + 6\beta + 6\gamma)\frac{\lambda}{(1+\lambda)^2} + T_f(2\alpha - 2\epsilon + 6\beta + 6\gamma)\times \frac{1}{(1+\lambda)^2} + (3\alpha + 8\beta + 6\gamma)\frac{\lambda}{(1+\lambda)} + (\alpha + 2\epsilon + 2\beta)\frac{1}{1+\lambda}\Big]\frac{d\lambda}{d\chi} \quad (13)$$

where

$$\epsilon = \frac{1}{2}\Big[\log\frac{T_1}{T_w} + \frac{T_b}{\sqrt{T_b^2+4T_d}}\log\frac{T_b+2T_d-\sqrt{T_b^2+4T_d}}{T_b+2T_d+\sqrt{T_b^2+4T_d}}\Big]$$

$$\gamma = 1 + T_b\epsilon + \frac{T_d}{\sqrt{T_b^2+4T_d}}\log\frac{T_b+2T_d-\sqrt{T_b^2+4T_d}}{T_b+2T_d+\sqrt{T_b^2+4T_d}}$$

$$\beta = -(1/2) - T_b\gamma - T_d\epsilon, \quad \alpha = (1/3) - T_b\beta + T_d\gamma$$

$$T_b = 1 + \Big[(T_1 - T_w)\Big/\Big(T_1\frac{k-1}{2}M\Big)\Big], \quad T_d = T_w\Big/\Big(T_1\frac{k-1}{2}M^2\Big)$$

and

$$-\frac{d}{dx}\int_0^\delta \rho u^2\,dy = \frac{6w\mu_w U}{Q[(k-1)/2]\,M^2}\Big\{(12D + 68E + 156F - 180G + 104H - 24I)\frac{\lambda^2}{(1+\lambda)^3} + [4D + 20E + 36F - 20G - 16H + 24I - 8J + T_f(12D + 68E + 156F - 180G + 104H - 24I)]\times \frac{\lambda}{(1+\lambda)^3} + T_f(4D + 20E + 36F - 20G - 16H + 24I - 8J)\frac{1}{(1+\lambda)^3} + (9D + 48E + 100F - 96G - 36H)\frac{\lambda^2}{(1+\lambda)^2} + (6D + 28E + 44F - 12G - 32H + 24I)\frac{\lambda}{(1+\lambda)^2} + (D + 4E + 4F + 4G - 8H + 4J)\frac{1}{(1+\lambda)^2}\Big\}\frac{d\lambda}{dx} \quad (14)$$

where

$$H = \alpha, \quad I = -\beta, \quad J = 1 + \frac{T_b}{2}\log\frac{T_1}{T_w} + \Big(\frac{T_b^2}{2} + T_d\Big)$$

$$x\frac{1}{\sqrt{T_b^2+4T_d}}\log\frac{T_b+2T_d-\sqrt{T_b^2+4T_d}}{T_b+2T_d+\sqrt{T_b^2+4T_d}} = \gamma, \quad G = \frac{1}{4} + T_b\alpha - T_d\beta$$

$$F = \frac{1}{5} + T_bG + T_d\alpha, \quad E = -\frac{1}{6} - T_bF - T_dG, \quad D = \frac{1}{7} - T_bE + T_dF$$

Hence, Eq. (7) becomes.

$$\frac{6W\mu_w U}{Q[(k-1)/2]M^2}\Big[A_1\frac{\lambda^2}{(1+\lambda)^3} + (B_1 + T_fA_1)\frac{\lambda}{(1+\lambda)^3} + T_fB_1\frac{1}{(1+\lambda)^3} + C_1\frac{\lambda^2}{(1+\lambda)^2} + D_1\frac{\lambda}{(1+\lambda)^2} + (E_1 - T_fH_1)\frac{1}{(1+\lambda)^2} - F_1\frac{\lambda}{(1+\lambda)} - G_1\frac{1}{1+\lambda}\Big]\frac{d\lambda}{dx} - QU\Big[1 + \frac{1}{3(\lambda+1)(\lambda+T_f)}\Big] = 0 \quad (15)$$

Introducing the nondimensional length $\xi = (Q/W)^2(Ux/\nu_1)$, Eq. (15) is then reduced to

$$\frac{d\xi}{d\lambda} = \frac{18}{[(k-1)/2]M^2}\frac{\mu_w}{\mu_1}\Big[\frac{(\lambda+T_f)}{3(\lambda+1)(\lambda+T_f)+1}\Big]\Big[A_1\frac{\lambda^2}{(1+\lambda)^2} + (B_1 + T_fA_1)\frac{\lambda}{(1+\lambda)^2} + T_fB_1\frac{1}{(1+\lambda)^2} + C_1\frac{\lambda^2}{(1+\lambda)} + D_1\frac{\lambda}{(1+\lambda)} + (E_1 - T_fH_1)\frac{1}{1+\lambda} - F\lambda - G\Big] \quad (16)$$

where

$$A_1 = 12D + 68E + 156F - 180G + 104H - 24I$$
$$B_1 = 4D + 20E + 36F - 20G - 16H + 24I + 8J$$

$$C_1 = 9D + 48E + 100F - 96G + 36H$$
$$D_1 = 6D + 28E + 44F - 12G - 32H + 24I - 2\alpha + 2\epsilon - 6\beta - 6\gamma$$
$$E_1 = D + 4E + 4F + 4G - 8H + 4J$$
$$F_1 = 3\alpha + 8\beta + 6\gamma$$
$$G_1 = \alpha + 2\beta + 2\epsilon$$
$$H_1 = 2\alpha + 6\beta - 2\epsilon + 6\gamma$$

Since Eq. (16) is linear, it can be solved by direct integration. The solution is

$$\xi = \frac{18}{[(k-1)/2]M^2}\frac{\mu_w}{\mu_1}\left\{\frac{M_1}{3}\lambda - (1-T_f)^2\frac{P_1}{1+\lambda} + \frac{1-T_f}{2}[3(1-T_f)^2P_1 + Q_1 - T_fR_1] \times \right.$$
$$\log\frac{(1+\lambda)^2}{3\lambda^2 + 3(1+T_f)\lambda + (3T_f+1)} + \sqrt{3}\left[\frac{2}{3}\left(N_1 - \frac{M_1}{3}\right) + (1-T_f)^2(3T_f^2 - 6T_f + 1)P_1 + \right.$$
$$\left.\left.(1-T_f)^2Q_1 - T_f/3\,(3T_f^2 - 6T_f + 1)R_1\right]\frac{1}{\sqrt{1+6T_f-3T_f^2}}\tan^{-1}\frac{\sqrt{3}\{2\lambda + (1+T_f)\}}{\sqrt{1+6T_f-3T_f^2}}\right\} + C' \quad (17)$$

where

$$T_f = \frac{n_T - 1}{12} + \frac{n_T}{12}\frac{k-1}{2}M^2\ (\mu \sim \sqrt{T}),\quad T_f = \frac{n_T - 1}{8} + \frac{n_T}{8}\frac{k-1}{2}M^2\ (\mu \sim T^{3/4})$$

$$M_1 = C_1 - F_1 = A_1 + D_1 - C_1 - G_1$$
$$N_1 = B_1 - 2A_1 + E_1 + C_1 - D_1,\quad P_1 = B_1 - A_1$$
$$Q_1 = 3A_1 - 2B_1 - E_1 - C_1 + D_1,\quad R_1 = A_1 - H_1$$

The constant of integration C' determined from the initial condition $\xi = 0$, $\lambda = -T_f$ is thus,

$$C' = \frac{-18}{[(k-1)/2]M^2}\left(\frac{\mu_w}{\mu_1}\right)\left\{-T_f\frac{M_1}{3} - (1-T_f)P_1 + \frac{(1-T_f)}{2}[3(1-T_f)^2P_1 + Q_1 - T_fR_1] \times \right.$$
$$\log(1-T_f)^2 + \sqrt{3}\left[\frac{2}{3}\left(N_1 - \frac{M_1}{3}\right) + (1-T_f)^2(3T_f - 6T_f + 1)P_1 + (1-T_f)^2Q_1 - \right.$$
$$\left.\left.\frac{T_f}{3}(3T_f^2 - 6T_f + 1)R_1\right]\frac{1}{\sqrt{1+6T_f-3T_f^2}}\tan^{-1}\frac{\sqrt{3}(1-T_f)}{\sqrt{1+6T_f-T_f^2}}\right\}$$

It may be noted that Eq. (17) is not valid for a Mach Number equal to zero. However, a modified equation corresponding to Eq. (17) for Mach Number equal to zero can be derived as follows:

For a Mach Number equal to zero, the differential equation in ξ and λ corresponding to Eq. (16) is reduced to

$$\frac{d\xi}{d\lambda} = -\frac{18}{T_g}\left(\frac{\mu_w}{\mu_1}\right)\left[\frac{\lambda + T_g}{3(\lambda+1)(\lambda+T_g)+1}\right]\left[A_2\frac{\lambda^2}{(1+\lambda)^2} + (B_2 + T_gA_2)\frac{\lambda}{(1+\lambda)^2} + \right.$$
$$\left.T_g\frac{B_2}{(1+\lambda)^2} + C_2\frac{\lambda^2}{(1+\lambda)} + D_2\frac{\lambda}{(1+\lambda)} + (E_2 + T_gH_2)\frac{1}{1+\lambda} - F_2\lambda - G_2\right] \quad (18)$$

where

$$A_2 = 12a_2 + 68b_2 + 156c_2 - 180d_2 + 104e_2 - 24f_2$$
$$B_2 = 4a_2 + 20b_2 + 36c_2 - 20d_2 - 16e_2 + 24f_2 - 8g_2$$
$$C_2 = 9a_2 + 48b_2 + 100c_2 - 96d_2 + 36e_2$$
$$D_2 = 6a_2 + 28b_2 + 44c_2 - 12d_2 - 32e_2 + 24f_2 - 2\alpha_2 + 2\epsilon_2 - 6\beta_2 - 6\gamma_2$$
$$E_2 = a_2 + 4b_2 + 4c_2 + 4d_2 - 8e_2 + 4g_2$$
$$F_2 = 3\alpha_2 + 8\beta_2 + 6\gamma_2$$
$$G_2 = \alpha_2 + 2\beta_2 + 2\epsilon_2$$
$$H_2 = 2\alpha - 2\epsilon + 6\beta + 6\gamma$$

and

$$\epsilon_2 = 1 - \frac{T_w}{T_1 - T_w}\log\frac{T_1}{T_w},\quad \gamma_2 = g_2 = \frac{1}{2} - \frac{T_w}{T_1 - T_w}\epsilon_2$$

$$\beta_2 = -f_2 = -\frac{1}{3} + \frac{T_w}{T_1 - T_w} g_2, \quad \alpha_2 = e_2 = \frac{1}{4} - \frac{T_w}{T_1 - T_w} f_2$$

$$d_2 = \frac{1}{5} - \frac{T_w}{T_1 - T_w} e_2, \quad c_2 = \frac{1}{6} - \frac{T_w}{T_1 - T_w} d_2$$

$$b_2 = -\frac{1}{7} + \frac{T_w}{T_1 - T_w} c_2, \quad a_2 = \frac{1}{8} + \frac{T_w}{T_1 - T_w} b_2$$

The linear differential equation [Eq. (18)] can be solved in a manner similar to that of Eq. (16), and the solution is

$$\xi = \frac{18 n_T}{n_T - 1}\left(\frac{\mu_w}{\mu_1}\right)\left\{\frac{M_2}{3}\lambda - (1 - T_g)^2 \frac{P_2}{1 + \lambda} + \frac{(1 - T_g)}{2}[3(1 - T_g)^2 P_2 + Q_2 - T_g R_2] \times \right.$$

$$\log \frac{(1 + \lambda)^2}{3\lambda^2 + 3(1 + T_g)\lambda + (3T_g + 1)} + \sqrt{3}\left[\frac{2}{3}\left(N_2 - \frac{M_2}{3}\right) + (1 - T_g)^2 (3T_g^2 - 6T_g + 1) P_2 + \right.$$

$$\left.\left.(1 - T_g)^2 Q_2 - \frac{T_g}{3}(3T_g^2 - 6T_g + 1) R_2\right] \frac{1}{\sqrt{1 + 6T_g - 3T_g^2}} \tan^{-1} \frac{\sqrt{3}[2\lambda + (1 + T_g)]}{\sqrt{1 + 6T_g - 3T_g^2}}\right\} + C'' \quad (19)$$

where

$$T_g = (n_T - 1)/12 \text{ for } \mu \sim \sqrt{T}$$
$$T_g = (n_T - 1)/8 \text{ for } \mu \sim T^{3/4}$$
$$M_2 = F_2 - C_2 = C_2 + G_2 - A_2 - D_2, \quad N_2 = 2A_2 + D_2 - B_2 - E_2 - C_2$$
$$P_2 = A_2 - B_2, \quad Q_2 = 2B_2 + C_2 + E_2 - 3A_2 - D_2, \quad R_2 = H_2 - A_2$$

The constant of integration C'' in Eq. (19) is determined from the initial condition $\xi = 0, \lambda = -T_g$, as

$$C'' = -\frac{18 n_T}{n_T - 1}\left(\frac{\mu_w}{\mu_1}\right)\left\{-\frac{M_2}{3} T_g - (1 - T_g) P_2 + \frac{1 - T_g}{2}[3(1 - T_g)^2 P_2 + Q_2 - T_g R_2] \log (1 - T_g)^2 + \right.$$

$$\sqrt{3}\left[\frac{2}{3}\left(N_2 - \frac{M_2}{3}\right) + (1 - T_g)^2(3T_g^2 - 6T_g + 1)P_2 + (1 - T_g)^2 Q_2 - \frac{T_g}{3}(3T_g^2 - 6T_g + 1)R_2\right] \times$$

$$\left.\frac{1}{\sqrt{1 + 6T_g - 3T_g^2}} \tan^{-1} \frac{\sqrt{3}(1 - T_g)}{\sqrt{1 + 6T_g - 3T_g^2}}\right\}$$

The solutions as calculated from Eqs. (17) and (19) are shown in Fig. 1. It was noted that the relation between ξ and λ_1 is linear except in the region $\xi < 1.0$. On examining Eqs. (17) and (19), it is evident that the first term on the right-hand side of the equations is linear in λ, and this dominates the solution when $\xi > 1.0$. This linear relationship between λ and ξ can be shown by their constant slope when $\xi > 1.0$. The growth in boundary-layer thickness with the increase of Mach Number and temperature ratio (outer boundary-layer temperature to wall temperature) are shown in Figs. 1 and 2. Since the effect of compressibility is to increase the heat transfer through the wall and since the amount of heat produced in the boundary layer increases with speed, the effects of both the increase of Mach Number and temperature ratio to the boundary-layer thickness are the same.

In Figs. 3 and 4, velocity profiles were plotted against $y(v_0/\nu_1)$ and yU/ν_1 at various ξ and Mach Numbers, respectively. Because of the injected velocity of the coolant along the plate, inflection points appeared in the velocity profiles. It was found that the larger the value of v_0/U, the farther the inflection point moves outward from the plate. The instability of the laminar boundary layer may be interpreted from the inflection points occurring in these curves.

The temperature distribution at different v_0/U ratios and Mach numbers are shown in Figs. 5 and 6. It is noted that the temperature gradient at the wall increases as the Mach Number increases and decreases as v_0/U increases. This behavior indicates that the heat transfer through the wall increases as the compressibility of the flow becomes more pronounced and decreases as the injection of coolant increases.

In Fig. 7, a comparison of velocity profiles between the present method and the Kármán-Tsien method,[2] based on the similarity law, was made. The results show good agreement, although the present method gives slightly less heat transfer at the wall.

The above calculations are based on the assumption that the viscosity μ is proportional to the square root of the temperature; however, no appreciable differences

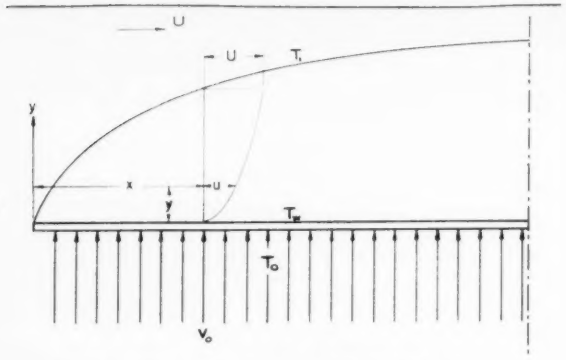

BOUNDARY LAYER ALONG A POROUS FLAT PLATE

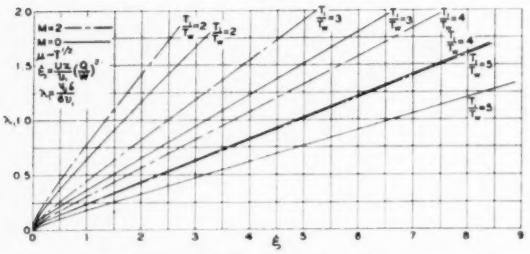

FIG. 1 NON-DIMENSIONAL BOUNDARY LAYER THICKNESS vs NON-DIMENSIONAL LENGTH IN THE DIRECTION OF FLOW

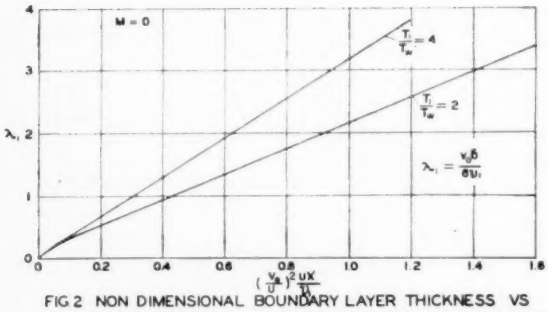

FIG. 2 NON DIMENSIONAL BOUNDARY LAYER THICKNESS VS NON DIMENSIONAL LENGTH IN THE DIRECTION OF FLOW

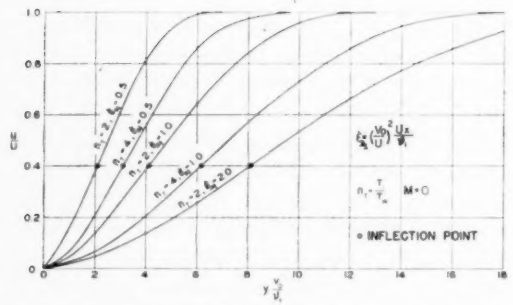

FIG. 3 VELOCITY PROFILES AGAINST $\frac{V_o y}{\nu_i}$ AT DIFFERENT LOCATION ALONG THE PLATE

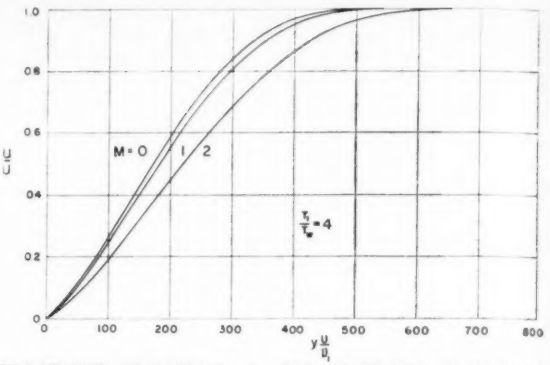

FIG. 4 VELOCITY PROFILES VS. $\frac{yU}{\nu_i}$ FOR DIFFERENT MACH NUMBERS ($\frac{\delta^*}{\nu_i U}$ = .008)

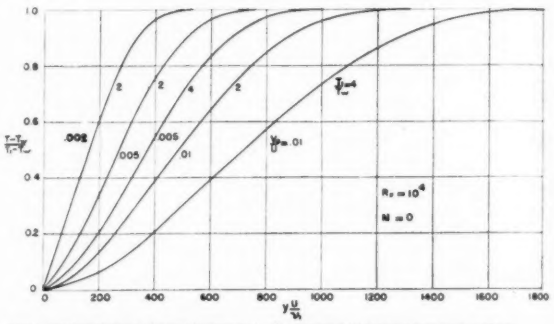

FIG5 TEMPERATURE PROFILES AGAINST $y\frac{U}{\nu_i}$ FOR VARIOUS INJECTION VELOCITIES

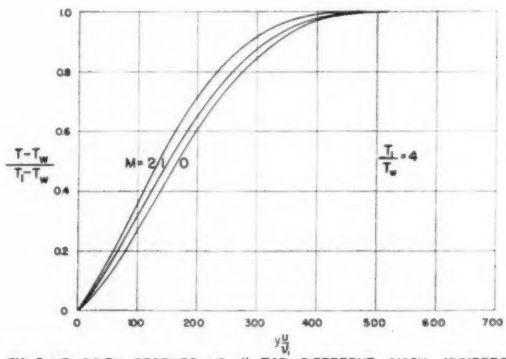

FIG. 6 VELOCITY PROFILES VS. $y\frac{U}{\nu_i}$ FOR DIFFERENT MACH NUMBERS ($\frac{Q}{W}$ = .008)

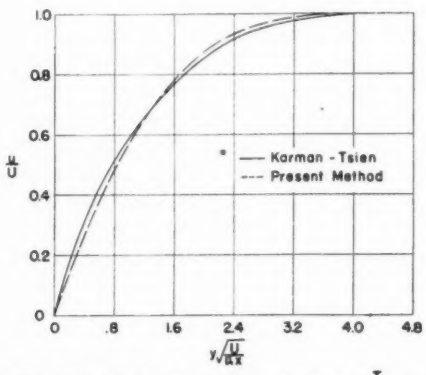

Fig. 7. Velocity Distribution for Impermeable Wall ($\frac{T_i}{T_w}$ = 4, M = 0)

in the results are noted when the viscosity is assumed to vary with the three-fourths power of the temperature ratio, except for large Mach Number.

Wall Temperature and Coolant Discharge

The temperature field in the laminar boundary layer described in the previous section may be used to determine the amount of coolant required to cool the wall to a predesignated temperature from the relation stating that the amount of heat per unit area removed by the plate is equal to the heat absorbed by the coolant. Thus, one obtains

$$\int_0^L c_t \left(\frac{\partial T}{\partial y}\right)_w dx = \rho_w v_0 c_p (T_w - T_0)L \qquad (20)$$

or

$$\frac{T_1 - T_w}{T_w - T_0} = \frac{3L(n_T - 1)\left(\frac{\mu_w c_p}{c_t}\right)}{n_T\left(1 + \frac{k-1}{2}M^2\right) - 1} \times \left[\int_0^L \frac{dx}{(\lambda + 1)(\lambda + T_f)}\right]^{-1} \qquad (21)$$

for $M > 0$, and

$$\frac{T_1 - T_w}{T_w - T_0} = 3L\left(\frac{c_p \mu_w}{c_t}\right) \Big/ \int_0^L \frac{dx}{(\lambda + 1)(\lambda + T_f)} \qquad (22)$$

for $M = 0$, where T_0 is the temperature of the coolant and $n_T = T_1/T_w$. On the substitution of λ for χ from Eqs. (16) and (18) in the above integral, one obtains

$$\int_0^L \frac{dx}{(\lambda + 1)(\lambda + T_f)} = \frac{18\mu_w}{[(k-1)/2]M^2\mu_1}\left[\left(\frac{Q}{W}\right)^2 \frac{U}{\nu_1}\right]^{-1} \int_{-T_f}^{\lambda_L}\left[\frac{1}{3\lambda^2 + 3(1 + T_f)\lambda + (1 + 3T_f)}\right] \times \left[M_1 + (N_1 + T_f R_1)\frac{1}{(1+\lambda)^2} - (1 - T_f)\frac{P_1}{(1+\lambda)^3}\right] d\lambda \qquad (23)$$

for $M > 0$, and

$$\int_0^L \frac{dx}{(\lambda + 1)(\lambda + T_g)} = \frac{18 n_T}{(n_T - 1)}\frac{\mu_w}{\mu_1}\left[\left(\frac{Q}{W}\right)^2 \frac{U}{\nu_1}\right]^{-1} \int_{-T_g}\left[\frac{1}{3\lambda^2 + 3(1 + T_g)\lambda + (1 + 3T_g)}\right] \times \left[M_2 + (N_2 + T_g R_2)\frac{1}{(1+\lambda)^2} - (1 - T_g)\frac{P_1}{(1+\lambda)^2}\right] d\lambda \qquad (24)$$

for $M = 0$.

Substituting the above integral into Eqs. (21) and (22), respectively, the following expressions for the temperature ratios are obtained: for $M > 0$,

$$\frac{T_1 - T_w}{T_w - T_0} = \frac{\left(c_p\frac{\mu_w}{c_t}\right)\left(\frac{k-1}{2}M^2\right)R_L(n_T - 1)}{6\left[n_T\left(1 + \frac{k-1}{2}M^2\right) - 1\right]}\left(\frac{\mu_1}{\mu_w}\right)\left(\frac{Q}{W}\right)^2\Bigg[\Bigg(\Big[3(1 - T_f)^2 P_1 - (N_1 + T_f R_1)\Big]\frac{1}{1+\lambda} + \frac{1 - T_f}{2} \times$$

$$\frac{P_1}{(1+\lambda)^2} + \frac{3}{2}\Big\{(1 - T_f)(N_1 + T_f R_1) + (1 - T_f)\left[1 - 3(1 - T_f)^2\right]P_1\Big\}\log\frac{(1+\lambda)^2}{3\lambda^2 + 3(1 - T_f)\lambda + (3T_f + 1)} +$$

$$\sqrt{3}\Big\{\frac{2}{3}M_1 + (3T_f^2 - 6T_f + 1)(N_1 + T_f R_1) + 3(1 - T_f)^2\left[1 - (3T_f^2 - 6T_f + 1)\right]P_1\Big\} \times$$

$$\frac{1}{\sqrt{1 + 6T_f - 3T_f^2}}\tan^{-1}\frac{\sqrt{3}[2\lambda + (1 + T_f)]}{\sqrt{1 + 6T_f - 3T_f^2}}\Bigg)_{-T_f}^{\lambda_L}\Bigg]^{-1} \qquad (25)$$

and for $M = 0$,

$$\frac{T_1 - T_w}{T_w - T_0} = \frac{c_p\frac{\mu_w}{c_t}R_L(n_T - 1)}{6n_T}\left(\frac{\mu_1}{\mu_w}\right)\left(\frac{Q}{W}\right)^2\Bigg[\Big[3(1 - T_g)^2 P_2 - (N_2 + T_g R_2)\Big]\frac{1}{1+\lambda} + \frac{1 - T_g}{2}\frac{P_2}{(1+\lambda)^2} +$$

$$\frac{3}{2}\Big\{(1 - T_g)(N_2 + T_g R_2) + (1 - T_g)\left[1 - 3(1 - T_g)^2\right]P_2\Big\}\log\frac{(1+\lambda)^2}{3\lambda^2 + 3(1 + T_g)\lambda + (3T_g + 1)} +$$

$$\sqrt{3}\left\{\frac{2}{3}M_2 + (3T_g^2 - 6T_g + 1)(N_2 + T_g R_2) + 3(1 - T_g)^2[1 - (3T_g^2 - 6T_g + 1)]P_2\right\} \times \frac{1}{\sqrt{1 + 6T_g - 3T_g^2}} \tan^{-1}\frac{\sqrt{3}[2\lambda + (1 + T_g)]}{\sqrt{1 + 6T_g - 3T_g^2}}\Bigg)_{-T_g}^{\lambda_L}\Bigg]^{-1} \quad (26)$$

The limit λ_L can be determined from the curves, λ vs. ξ for a corresponding ξ_L, provided the Reynolds Number and Q/W are given.

In Figs. 8, 9, and 10, the temperature ratio $(T_1 - T_w)/(T_w - T_0)$ was plotted against the coolant mass flow ratio at different Mach Numbers, Reynolds Numbers, and viscosity variation with temperature. For predesignated wall temperature, it is shown that the rate of coolant discharge increases as the Mach Number increases and decreases as the Reynolds Number increases. It is also shown that larger amount of coolant is required to cool the wall to a predesignated temperature for $\mu \sim T^{1/2}$ than for $\mu \sim T^{3/4}$. The experimental data, taken from reference 3, were compared with the present calculations (see Fig. 9). The discrepancy between the theoretical calculation and the experimental results is mainly due to the fact that the experimental conditions do not correspond to those assumed in the theories.

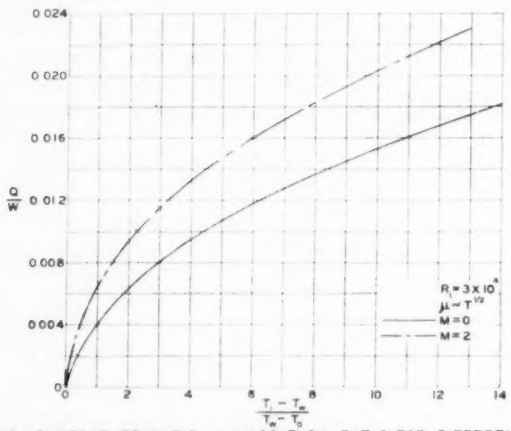

FIG. 8 TEMPERATURE RATIO vs MASS FLOW RATIO FOR DIFFERENT MACH NUMBERS

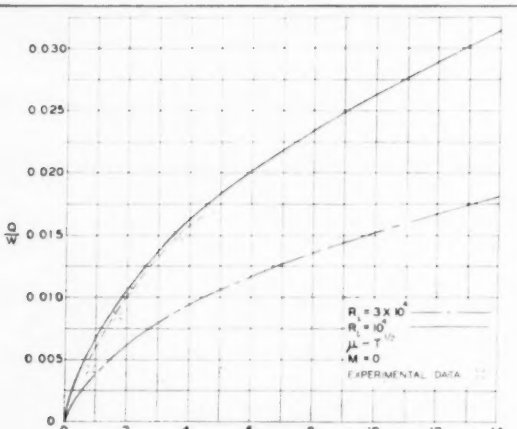

FIG. 9 TEMPERATURE RATIO vs MASS FLOW RATIO FOR DIFFERENT REYNOLDS NUMBERS

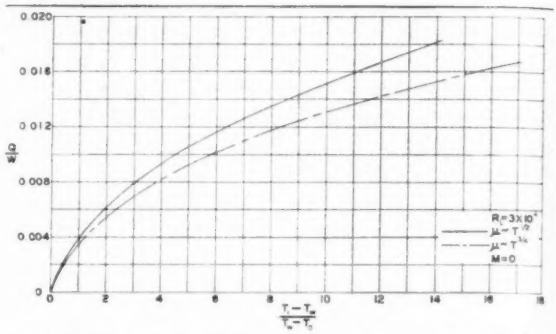

FIG. 10 TEMPERATURE RATIO vs MASS FLOW RATIO FOR $\mu \sim T^{1/2}$ AND $\mu \sim T^{3/4}$

References

[1] von Kármán, Th., The *Problem of Resistance in Compressible Fluids*, v convengo dalla Foundazione Alessandro Volta (Tema, Le Alto Velocita in Avaizione), Realo Accademia D'Italia, Rome.

[2] von Kármán, Th., and Tsien, H. S., *Boundary Layer in Compressible Fluids*, Journal of the Aeronautical Sciences, Vol. 5, No. 6, April, 1938.

[3] Duwez, Pol, and Wheeler, H. L., Jr., *Experimental Study of Cooling by Injection of a Fluid Through a Porous Material*, Journal of the Aeronautical Sciences, Vol. 15, No. 9, pp. 509-521, September, 1948.

[4] Yuan, S. W., *A Theoretical Investigation of the Temperature Field in the Laminar Boundary Layer on a Porous Flat Plate with Fluid Injection*, Project SQUID, Tech. Report No. 4, September, 1947.

Shear Distribution in Beams with Variable Webs

B. E. GATEWOOD*

United States Air Force Institute of Technology

SUMMARY

The general equations for the shear flows in n horizontal panels of a horizontal beam with $n + 1$ stringers are indicated. The three-panel beam with constant stringer areas is solved in detail, and the results are shown by curves in terms of the parameters p (ratio of outer web thicknesses to center web thickness) and b ($b = l\sqrt{t/Ah}$ with l = beam length, t = outer web thickness, A = stringer area, and h = panel height). Tests of a three-panel cantilever beam with a concentrated load verify the calculated results insofar as the test beam represented the assumptions used in the theory.

INTRODUCTION

CONSIDER A CANTILEVER BEAM (Fig. 1) that carries a distributed load $w(x)$ lbs. per unit length. Let the horizontal webs $t_i(x)$ $(i = 1, 2, \ldots, n)$ which connect the horizontal stringers $A_i(x)$ of the beam be thin, so that the webs take only shear stresses with a uniform distribution in each web on a vertical cross section and the stringers take only normal stresses. Let the webs act in diagonal tension, and assume a sufficient number of vertical stiffeners to be present to support the buckled webs and to make any necessary redistribution of shear loads between the horizontal panels. Assume the heights h_i of the horizontal panels to be constant, and let $q_i(x)$ be the shear flow in pounds per inch in the panels.

Ordinarily, in the calculations of the stringer normal stresses and the web shear stresses for the beam of Fig. 1, the bending and shear deflections of the beam are neglected and the usual normal stress formula $s = My/I$ is used. However, in many aircraft beams, especially those with cutouts, the equivalent thickness of the webs may vary widely from panel to panel so that deflections cannot be neglected in the distribution of the loads. Such a beam is the side of a fuselage that has a row of windows with light supporting frames; the frames can be replaced by a thin web of equivalent stiffness, and the analysis carried out on the resulting continuous structure. Local effects of the cutouts can be analyzed separately and combined with the general solution. With suitable modifications, the results are applicable to beams with supports other than cantilever.

DERIVATION OF EQUATIONS FOR THE SHEAR FLOW

From the well-known relations between stresses and displacements, the following relations can be written $(i = 1, 2, \ldots, n)$:

$$s_i = E_i\,(du_i/dx) = (1/A_i)\int (q_{i-1} - q_i)dx \qquad (1)$$

$$q_i = G_i t_i\left[\left(\frac{\partial w_i}{\partial y}\right) + \left(\frac{\partial v_i}{\partial x}\right)\right] \qquad (2)$$

where s_i = the normal stress in stringer i, u_i = horizontal displacement of stringer i, w_i = horizontal displacement of web i, v_i = vertical displacement of web i, E is Young's modulus, and G is the shear modulus.

From the continuity of the structure,

$$\frac{\partial w_i}{\partial y} = (u_{i+1} - u_i)/h_i, \quad v_i = v_1$$

and Eq. (2) can be written

$$S_i q_i - \frac{u_{i+1} - u_i}{h_i} = S_1 q_1 - \frac{u_2 - u_1}{h_1} \qquad (3)$$

with $i = 2, 3, \ldots, n$, where $S_i = 1/G_i t_i$. Differentiate Eq. (3) with respect to x and substitute from Eq. (1) to get

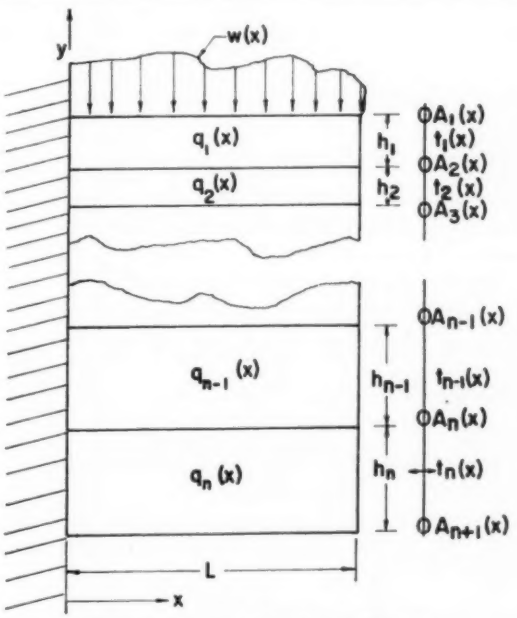

Sketch of General Cantilever Beam

Fig. 1

Received July 6, 1949.

* Associate Professor of Mechanics.

$$\left.\begin{aligned}\frac{d}{dx}(S_iq_i) - B_i\int q_i dx + D_i\int q_{i-1}\,dx + \\ F_i\int q_{i+1}\,dx = \frac{d}{dx}(S_1q_1) - B_1\int q_1 dx + \\ F_1\int q_2 dx, \quad i = 2, 3, \ldots, n\end{aligned}\right\} \quad (4)$$

where

$$h_iB_i = (1/A_iE_i) + (1/A_{i+1}E_{i+1}), \quad D_i = 1/h_iA_iE_i, \quad F_i = 1/h_iA_{i+1}E_{i+1}$$

The n shear flows $q_i (i = 1, 2, \ldots, n)$ can be determined from the $n - 1$ equations in Eq. (4) and the equilibrium condition

$$\sum_{i=1}^{n} h_iq_i = \int w(x)dx = P \quad (5)$$

According to ordinary differential equation theory, the set of n equations in Eqs. (4) and (5) may be expanded into $2(n - 1)$ first-order linear equations plus two zero-order equations, or the set may be reduced to a $2(n - 1)$-order linear equation for one of the variables. For the general case set up here, the equations have variable coefficients so that they are, in general, difficult to solve. It is considered more satisfactory to start directly from Eqs. (4) and (5) for each particular type of problem.

The constants of integration may be determined from the boundary conditions on the beam for the stresses and displacements at the ends.

Beams with Constant Dimensions

For the general case of constant A_i, t_i, E_i, G_i, Eq. (4) may be differentiated a second time with respect to x and written

$$(S_iD^2 - B_i)q_1 + F_iq_2 - (S_iD^2 - B_i)q_i - D_iq_{i-1} - F_iq_{i+1} = 0 \quad (6)$$

$i = 2, 3, \ldots, n$, where $D^2 = d^2/dx^2$. The set of algebraic equations [Eqs. (5) and (6)] may be solved directly for the q_i by determinants or otherwise with the usual interpretation for the operator D.

For the special case of two panels, Eqs. (5) and (6) give

$$q_2 = (P - h_1q_1)/h_2, \quad (D^2 - K^2)q_1 = (K_2^2D^2 - K_1^2)\,P$$

where

$$\begin{aligned}MK^2 &= B_1 + D_2 + h_1(F_1 + B_2)/h_2 \\ MK_2^2 &= S_2/h_2, \quad MK_1^2 = (F_1 + B_2)/h_2 \\ M &= S_1 + (h_1S_2/h_2)\end{aligned}$$

This result for the two-panel case agrees with that on page 9 of reference 1, provided vertical webs are used there.

The Three-Panel Beam

Consider the three-panel case for which Eqs. (5) and (6) give

$$\left.\begin{aligned}h_3q_3 = P - h_1q_1 - h_2q_2 \\ (K_0 - K_4)q_1 = -[(K_1 + K_5)D^2 - (K_2 + K_6)]q_2 + [K_7D^2 - (K_3 + K_8)]\,P \\ (D^4 - L_1D^2 + L_2)q_2 = (L_3D^4 - L_4D^2 + L_5)P\end{aligned}\right\} \quad (7)$$

where

$$\begin{aligned}&h_3S_1K_0 = h_3(B_1 + D_2) - h_1F_2 \\ &h_3S_1K_2 = h_3(F_1 + B_2) + h_2F_2 \\ &h_3S_1K_3 = F_2, \quad h_3JK_4 = h_3B_1 + h_1B_3, \quad S_1K_1 = S_2 \\ &h_3J = h_3S_1 + h_1S_3, \quad h_3JK_5 = h_2S_3 \\ &h_3JK_6 = h_3(D_3 - F_1) + h_2B_3 \\ &h_3JK_7 = S_3, \quad h_3JK_8 = B_3 \\ &(K_1 + K_5)L_1 = K_1K_4 + K_0K_5 + K_2 + K_6 \\ &(K_1 + K_5)L_2 = K_2K_4 + K_0K_6, \quad (K_1 + K_5)L_3 = K_7 \\ &(K_1 + K_5)L_4 = K_0K_7 + K_3 + K_8 \\ &(K_1 + K_5)L_5 = K_0K_8 + K_3K_4\end{aligned}$$

From Eq. (7), for P, a concentrated load at a distance a from the fixed end and a distance b from the free end ($l = a + b$) of the beam,

$$\left.\begin{aligned}q_{2a} = C_{1a}\sinh m_1x + C_{2a}\sinh m_2x + \\ C_{3a}\cosh m_1x + C_{4a}\cosh m_2x + (L_5P/L_2) \equiv \\ f_{1a}(m_1x) + f_{2a}(m_2x) + (L_5P/L_2) \\ q_{2b} = f_{1b}(m_1x) + f_{2b}(m_2x)\end{aligned}\right\} \quad (8)$$

where

$$2m_i^2 = L_1 - (-1)^i\sqrt{L_1^2 - 4L_2}, \quad i = 1, 2$$

Put Eq. (8) into Eq. (7) to get

$$\left.\begin{aligned}q_{1a} &= J_1(m_1)f_{1a}(m_1x) + J_1(m_2)f_{2a}(m_2x) + J_2P \\ q_{1b} &= J_1(m_1)f_{1b}(m_1x) + J_1(m_2)f_{2b}(m_2x)\end{aligned}\right\} \quad (9)$$

$$\left.\begin{aligned}q_{3a} &= H_1(m_1)f_{1a}(m_1x) + H_1(m_2)f_{2a}(m_2x) + H_2P \\ q_{3b} &= H_1(m_1)f_{1b}(m_1x) + H_1(m_2)f_{2b}(m_2x)\end{aligned}\right\} \quad (10)$$

where

$$(K_0 - K_4)J_1(m_i) = -[(K_1 + K_5)m_i^2 - (K_2 + K_6)], \quad i = 1,2$$

$$\begin{aligned}&L_2(K_0 - K_4)J_2 = L_5(K_2 + K_6) - L_2(K_3 + K_8) \\ &h_3H_1(m_i) = -h_2 - h_1J_1(m_i) \\ &h_3H_2 = 1 - h_1J_2 - (h_2L_5/L_2)\end{aligned}$$

The case of A_i, E_i, t_i, h_i, G_i, having different constant values in region a and b can be solved to give similar results.

Constants of Integration

The boundary conditions $u_{ia} = 0$ at $x = 0$, $s_{ib} = 0$ at $x = l$, $u_{ia} = u_{ib}$ at $x = a$, and $s_{ia} = s_{ib}$ at $x = a$ ($i = 1, 2, 3, 4$) give, from Eqs. (1) and (3),

$$\left.\begin{aligned}S_1q_{1a} = S_2q_{2a} = S_3q_{3a}, \quad \text{at } x = 0 \\ S_1q_{1b}' = S_2q_{2b}' = S_3q_{3b}', \quad \text{at } x = l \\ S_1(q_{1a} - q_{1b}) = S_2(q_{2a} - q_{2b}) = S_3(q_{3a} - q_{3b}), \quad \text{at } x = a \\ S_1(q_{1a}' - q_{1b}') = S_2(q_{2a}' - q_{2b}') = S_3(q_{3a}' - q_{3b}'), \quad \text{at } x = a\end{aligned}\right\} \quad (11)$$

Put Eqs. (8), (9), and (10) into Eq. (11) to determine

$$\left.\begin{aligned} MC_{3a} &= M_1(m_2)P, \quad MC_{4a} = -M_1(m_1)P \\ C_{3b} &= C_{3a}\,(1 - \cosh m_1 a) \\ C_{1b} &= -C_{3a}(1 - \cosh m_1 a)\tanh m_1 l \\ C_{1a} &= -C_{3a}\,[(1 - \cosh m_1 a)\tanh m_1 l + \sinh m_1 a] \\ C_{4b} &= C_{4a}\,(1 - \cosh m_2 a) \\ C_{2b} &= -C_{4a}(1 - \cosh m_2 a)\tanh m_2 l \\ C_{2a} &= -C_{4a}\,[(1 - \cosh m_2 a)\tanh m_2 l + \sinh m_2 a] \end{aligned}\right\} \quad (12)$$

where

$$M = \begin{vmatrix} S_1 J_1(m_1) - S_2 & S_1 J_1(m_2) - S_2 \\ S_3 H_1(m_1) - S_2 & S_3 H_1(m_2) - S_2 \end{vmatrix}$$

$$L_2 M_1(m_i) = \begin{vmatrix} S_2 L_b - S_1 L_2 J_2 & S_1 J_1(m_i) - S_2 \\ S_2 L_3 - S_3 L_2 H_2 & S_3 H_1(m_i) - S_2 \end{vmatrix}$$

Special Values for Beam Constants

As a particular case, let

$$\left.\begin{aligned} h &= h_1 = h_2 = 2h_3/3 \\ A &= A_1 = A_2 = A_3 = A_4 \\ 3G &= 3G_1 = 3G_3 = E_1 = E_2 = E_3 = E_4 \\ t &= t_1 = t_3 = pt_2 G_2/G \equiv pt_{2_{\text{eff.}}} \end{aligned}\right\} \quad (13)$$

where p allows for t_2 to be different thickness from t_1 and t_3 and also may allow for a reduced G_2 caused by diagonal tension in t_2.

For this case Eqs. (8), (9), and (10) can be written in the form

$$\left.\begin{aligned} \frac{107hq_{ia}}{P} &= N_{i1}R_a(bk_1x/l) - N_{i2}R_a(bk_2x/l) + Q_i \\ \frac{107hq_{ib}}{P} &= N_{i1}R_b(bk_1x/l) - N_{i2}R_b(bk_2x/l) \\ i &= 1, 2, 3 \end{aligned}\right\} \quad (14)$$

where

$$Q_1 = 26, \quad Q_2 = 36, \quad Q_3 = 30, \quad b = l(t/Ah)^{1/2}$$
$$9(5p + 2)k_i^2 = (13p + 37) - (-1)^i T$$
$$T^2 = (13p + 37)^2 - 321(5p + 2)$$
$$(5p + 2)TN_{2i} = 1170p^2 - 3371p + 1{,}867 + (90p - 71)(-1)^i T$$
$$N_{1i} = [(20/3) - (5p + 2)k_i^2]N_{2i}$$
$$N_{3i} = -[(46/9) - (2/3)(5p + 2)k_i^2]N_{2i}$$
$$R_a(bk_i x/l) = \cosh(bk_i x/l) - U_i \sinh(bk_i x/l)$$
$$R_b(bk_i x/l) = [1 - \cosh(bk_i a/l)][\cosh(bk_i x/l) - \tanh bk_i \sinh(bk_i x/l)]$$
$$U_i = [1 - \cosh(bk_i a/l)]\tanh bk_i + \sinh(bk_i a/l)$$

The Parameters p and b

Eq. (14) presents the shear flows in terms of the two parameters p and $b = l(t/Ah)^{1/2}$. It is noted that a similar result holds for any initial proportions between the constants h_i, A_i, E_i, G_i, and t_i. Since p is a measure of the diagonal tension and of the relative thickness of the t_2 web and since b has the length l in it, as well as t, A, and h, the parameters p and b are considered to represent the most important effects that the deformation of the structure has upon the distribution of the loads. Note that the Q_i in Eq. (14) are the shear flows when all deformation is neglected.

Fig. 2 shows the effects of the parameter p upon the shear distribution for a selected value of b and $a/l = 1$, while Fig. 3 shows the effect of the parameter b for a selected value of p and $a/l = 1$. Fig. 4 shows the shear distribution for the load located at different points on the beam. Note that the shear flows are not zero between the load and the free end. Fig. 5 shows the comparison of the shear flows in this case to the case when the shear flows are taken as zero outboard of the load.

The Test Beam*

In order to compare the theory for a three-panel beam to an actual beam, a test beam, with the beam constants related as in the above sections, was built. For this test beam, $h = 10$ in., $A = 0.62$ sq.in., $E = 3G = 10^7$ lbs. per sq.in., $t = 0.081$ in., $t_2 = 0.020$ in., $l = 100$ in., the material being 24ST extruded angles for the stringers, 24ST Alclad webs, and 24ST extruded angle stiffeners spaced at 8.33 in. Without diagonal tension the factor $p = 4$, and the factor $b = 11.43$. Fig. 6 shows the

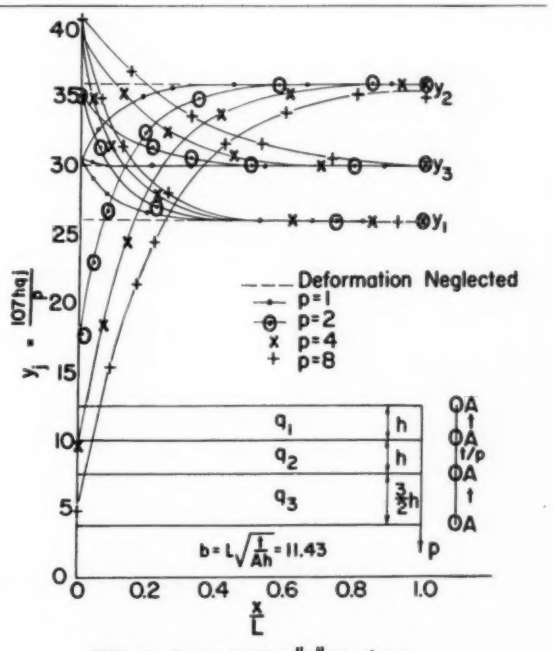

Effect of parameter "p" on shear

Fig. 2

* The author wishes to acknowledge the aid of Asst. Prof. V. A Valey, of the United States Air Force Institute of Technology, in designing and testing the test beam.

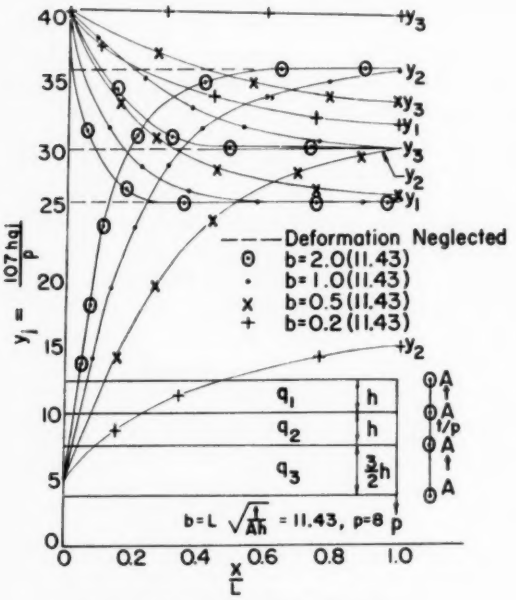

Effect of parameter "b" on shear

Fig. 3

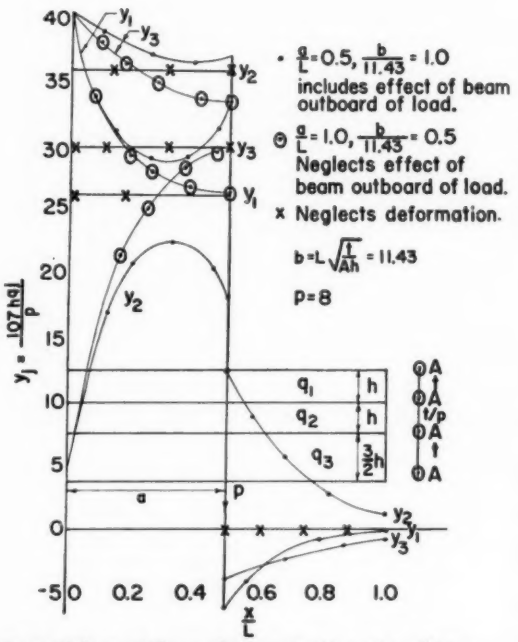

Fig.5 Effect of Beam Outboard of Load on Shear

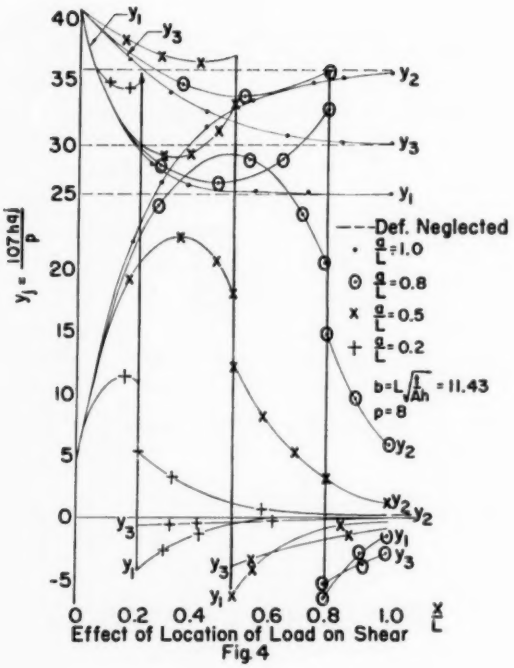

Effect of Location of Load on Shear

Fig. 4

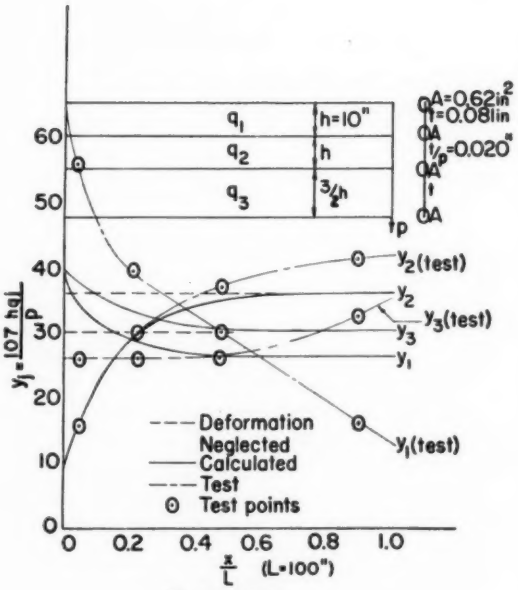

Test Results

Fig.6

test values obtained by the use of SR-4 rosette strain gages as compared to the calculated values. It is noted that q_1 is low at the free end and high at the wall, while q_3 is high at free end and low at the wall. This effect was due to the method of loading and the supporting jig. The load was applied at the free end as a concentrated tension load into a light end stiffener (Fig. 2), which tended to distribute the load to panel 3 first. The load was taken out at the wall through a light stiffener in tension, which tended to concentrate the load in panel 1. q_2 is high toward the free end because of the fact that the assumption that the webs take only shear is not obeyed in this test specimen. The webs $t_1 = t_3 = 0.081$ have areas equivalent in magnitude to the stringer area, so that at low bending stresses near the free end the webs still act as stringer areas, which will necessarily raise the shear stress in the middle web t_2. The strain gages indicated that the t_3 web carried compression stress according to My/I in the outer half of the beam but that this stress was below My/I in the inner half of the beam and actually decreased from its peak value toward the wall. The t_1 web carried tension stresses approximately according to My/I throughout its length.

Considerations on Applicability to Actual Aircraft Structures

In design and stress analysis of an aircraft structure with variable webs, the three-panel beam analysis is considered to be sufficiently good for most cases. Regardless of the number of stringers, the structure can be regarded as made up of three representative sections for the middle, the top, and the bottom. Once the shear flows are obtained for the representative three-panel structure, the analysis may proceed by superposition of the usual section property results—the shear flow in the middle web represents a certain per cent of the bending moment as carried by the beam as an entire unit, while the q_1 and q_3 shears represent the per cent moment carried by the beams with web 1 and 3. The final loads in the various members are obtained by superposition of the results for the three representative beams. Determine the parameters p and b for the structure, and, from curves similar to Figs. 2 and 3 for the type of loading on the structure, divide the bending moment into components for each beam. Calculate the loads in each beam, and add the results.

Conclusions

The use of the usual My/I formulas for aircraft beams with variable webs may lead to misleading results in many cases. The deformation of the structure and the consequent redistribution of loads can be represented in terms of two parameters, p and $b = l\sqrt{t/Ah}$, by families of curves. By judicious use of such curves, a more correct analysis of the structure can be made, and it is believed that lighter and better proportioned structures can be designed.

Reference

[1] Kempner, Joseph, *Recurrence Formulas and Differential Equations for Stress Analysis of Cambered Box Beams*, N.A.C.A. T.N. No. 1466, October, 1947.

Changes of Address

Since the Post Office Department does not as a rule forward magazines to forwarding addresses it is important that the Institute be notified of changes in address 30 days in advance of publishing date to ensure receipt of every issue of the JOURNAL and REVIEW.

Notices should be sent directly to:

Institute of the Aeronautical Sciences, Inc.
2 East 64th Street, New York 21, New York

Services of the Libraries of the Institute of the Aeronautical Sciences

The services of the Libraries are available to all members of the Institute, to Corporate Members, to advertisers in the AERONAUTICAL ENGINEERING REVIEW and AERONAUTICAL ENGINEERING CATALOG, and, under usual library limitations, to the public. Four specialized services are available.

The Paul Kollsman Lending Library

This lending library service makes available, *without charge*, the latest and more important aeronautical books.

Members may request the loan of any aeronautical or technical book they wish to borrow. Through an exchange agreement with the Engineering Societies Library, any book on general engineering may be borrowed from its great collection of over 160,000 volumes.

A photostating service is available at usual library rates.

Applications for membership in the library and further information will be sent on request.

The W. A. M. Burden Reference Library

This reference library contains over 12,000 aeronautical books, magazines, pamphlets, and reports gathered from world-wide sources and is one of the most complete aeronautical libraries in the world. Material from this library is not available for loan but may be used for reference purposes.

The Pacific Aeronautical Library

7660 Beverly Boulevard
Los Angeles 36, California

Established in cooperation with the aircraft companies the library serves. The leading aircraft companies in or near Los Angeles participate in its support and operation.

This service library for aeronautical research is available to the public for reading privileges. Source material includes aerodynamic and structural research reports, as well as books on drafting, production methods, history, and allied sciences. It furnishes books, periodicals, and pamphlet material to the participating aircraft companies to supplement their engineering libraries.

Technical Information Service

This service has experienced personnel under the supervision of trained aeronautical engineers to compile any information desired. The services range from listing specialized reference books to the preparation of exhaustive bibliographies, digesting of reports, and general surveys of any aeronautical subject. Some of the available services are:

Bibliographies on any aeronautical subject.
Reports on any aeronautical subject.
Digests of aeronautical books, papers, periodicals, and references.
Translations.
Engineering investigations of special aeronautical subjects.
Biographies of individuals engaged in aeronautics.
Photostats of any aeronautical or general engineering material.
Microfilms made on special order.
Photographs made from the Institute's photographic collection.
Drawings and tracings made.

In addition to the services mentioned any commission which comes within the scope of the Service will be accepted. Special arrangements may be made for work requiring several weeks or months.

Translators are available for accurate transcriptions of all foreign language data. Translations are carefully edited by trained engineers.

Reproductions of any material in the collections of the Institute may be ordered at standard photostat rates.

INSTITUTE OF THE AERONAUTICAL SCIENCES, INC.
2 EAST 64th STREET, NEW YORK 21, N.Y.

Readers' Forum

BRIEF REPORTS of investigations in the aeronautical sciences and discussions of papers published in the JOURNAL will be presented in this special department. The publication will be completed approximately 6 to 8 weeks after receipt of the material. No proof will be sent to the authors. The Editorial Committee does not hold itself responsible for the opinions expressed by the correspondents. Contributions should not exceed 800 words in length.

Note on Supersonic Wing Pressure Distribution

Ellis Lapin
Douglas Aircraft Company, Inc., Santa Monica, Calif.
September 6, 1949

IF THE PRESSURE DIFFERENCE at any point $p(\xi_0,\eta_0)$ of a flat wing of trapezoidal half-plan form with sweptforward trailing edges is denoted by

$$\frac{\beta}{4\alpha}\,\Delta C_p = \frac{\beta u}{U\alpha} = \frac{\beta u_\Delta}{U\alpha} + \frac{\beta\,\Delta_1 u}{U\alpha} + \frac{\beta\,\Delta_2 u}{U\alpha} \tag{1}$$

where

$\frac{\beta u_\Delta}{U\alpha}$ = pressure difference produced by an infinite delta wing

$\frac{\beta\,\Delta_1 u}{U\alpha}$ = incremental pressure difference induced by the presence of side edges

$\frac{\beta\,\Delta_2 u}{U\alpha}$ = incremental pressure difference induced by the presence of subsonic rear edges

$\beta^2 = M^2 - 1$

η,ξ = coordinates oriented along Mach waves from wing vertex

α = angle of attack, rad.

then by application of the method described by Goodman[1] it may be shown that the incremental pressure difference, $\beta\,\Delta_2 u/U\alpha$, in the regions adjacent to the subsonic edges, as illustrated in Fig. 1, is given by:

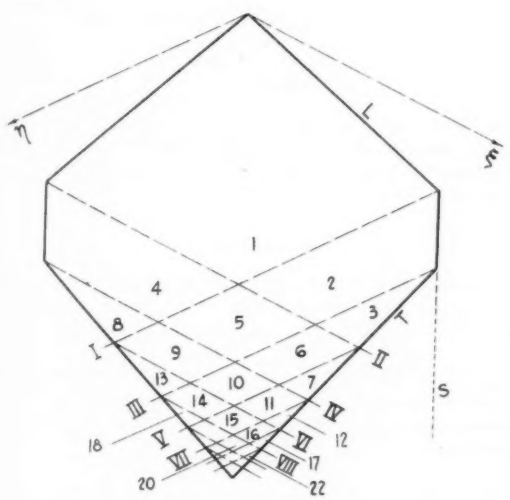

FIG. 1.

$$\left(\frac{\beta\,\Delta_2 u}{U\alpha}\right)_2 = \frac{\sqrt{\eta_0 - \eta_T(\xi_0)}}{\pi}\int_{\eta_S(\xi_0)}^{\eta_T(\xi_0)} \frac{\left(\frac{\beta\,\Delta_1 u}{U\alpha} - \frac{\beta u_\Delta}{U\alpha}\right)d\eta}{(\eta_0 - \eta)\sqrt{\eta_T(\xi_0) - \eta}} \tag{2a}$$

$$(\beta\,\Delta_2 u/U\alpha)_7 = (\beta\,\Delta_2 u/U\alpha)_2 \tag{2b}$$

$$\left(\frac{\beta\,\Delta_2 u}{U\alpha}\right)_{12} = \left(\frac{\beta\,\Delta_2 u}{U\alpha}\right)_2 + \left(\frac{\beta\,\Delta_2 u}{U\alpha}\right)_8 - \frac{\sqrt{\eta_0 - \eta_T(\xi_0)}}{\pi} \times \int_{\eta_{IV}}^{\eta_T(\xi_0)} \frac{(\beta\,\Delta_2 u/U\alpha)_8\,d\eta}{(\eta_0 - \eta)\sqrt{\eta_T(\xi_0) - \eta}} \tag{2c}$$

$$\left(\frac{\beta\,\Delta_2 u}{U\alpha}\right)_{17} = \left(\frac{\beta\,\Delta_2 u}{U\alpha}\right)_{12} - \frac{\sqrt{\eta_0 - \eta_T(\xi_0)}}{\pi} \times \int_{\eta_{VI}}^{\eta_T(\xi_0)} \frac{(\beta\,\Delta_2 u/U\alpha)_{12}\,d\eta}{(\eta_0 - \eta)\sqrt{\eta_T(\xi_0) - \eta}} \tag{2d}$$

$$\left(\frac{\beta\,\Delta_2 u}{U\alpha}\right)_{22} = \left(\frac{\beta\,\Delta_2 u}{U\alpha}\right)_{17} - \frac{\sqrt{\eta_0 - \eta_T(\xi_0)}}{\pi} \times \int_{\eta_{VIII}}^{\eta_T(\xi_0)} \frac{(\beta\,\Delta_2 u/U\alpha)_{18}\,d\eta}{(\eta_0 - \eta)\sqrt{\eta_T(\xi_0) - \eta}} \tag{2e}$$

etc., where $\eta_T(\xi_0)$ is the point on the trailing edge with $\xi = \xi_0$ and $\eta_S(\xi_0)$ is the point on the extension of the side edge with $\xi = \xi_0$. It can be demonstrated that the pressure difference, as computed by means of Eqs. (1) and (2), complies with the Kutta condition, $\Delta C_p = 0$ at the trailing edge. In the regions more remote from, but still influenced by, the trailing edges, the incremental pressure difference, $\beta\,\Delta_2 u/U\alpha$, may be found by application of a superposition principle that accounts for the pressure resulting from the Mach wave reflections:

$$(\beta\,\Delta_2 u/U\alpha)_6 = (\beta\,\Delta_2 u/U\alpha)_2 \tag{3a}$$

$$(\beta\,\Delta_2 u/U\alpha)_{10} = (\beta\,\Delta_2 u/U\alpha)_2 + (\beta\,\Delta_2 u/U\alpha)_8 \tag{3b}$$

$$(\beta\,\Delta_2 u/U\alpha)_{11} = (\beta\,\Delta_2 u/U\alpha)_7 + (\beta\,\Delta_2 u/U\alpha)_8 \tag{3c}$$

$$(\beta\,\Delta_2 u/U\alpha)_{15} = (\beta\,\Delta_2 u/U\alpha)_7 + (\beta\,\Delta_2 u/U\alpha)_{13} \tag{3d}$$

$$\left(\frac{\beta\,\Delta_2 u}{U\alpha}\right)_{16} = \left[\left(\frac{\beta\,\Delta_2 u}{U\alpha}\right)_{12} - \left(\frac{\beta\,\Delta_2 u}{U\alpha}\right)_8\right] + \left(\frac{\beta\,\Delta_2 u}{U\alpha}\right)_{13} \tag{3e}$$

$$\left(\frac{\beta\,\Delta_2 u}{U\alpha}\right)_{20} = \left[\left(\frac{\beta\,\Delta_2 u}{Ua}\right)_{12} - \left(\frac{\beta\,\Delta_2 u}{U\alpha}\right)_8\right] + \left[\left(\frac{\beta\,\Delta_2 u}{U\alpha}\right)_{18} - \left(\frac{\beta\,\Delta_2 u}{U\alpha}\right)_2\right] \tag{3f}$$

etc.

The symbol $(\beta\,\Delta_2 u/U\alpha)_\nu$ is to be construed as meaning "compute the incremental pressure difference $(\beta\,\Delta_2 u/U\alpha)$ at any point $p(\xi_0,\eta_0)$ as though the point lie in region ν."

Since the "basic" pressure difference, $\beta u_\Delta/U\alpha$, and the side edge induced incremental pressure difference, $\beta\,\Delta_1 u/U\alpha$, represent known quantities (cf., reference 2) the computation of the pressure at any point influenced by the trailing edge involves the evaluation of Eq. (2a), the evaluation of interaction terms such as the third term in Eq. (2c), and the application of a special superposition principle. The form of the equations appears suitable for evaluation by means of automatic computing machinery. The restrictions of linearized inviscid supersonic flow theory apply.

REFERENCES

[1] Goodman, T. R., *The Lift Distribution on Conical and Nonconical Flow Regions of Thin Finite Wings in a Supersonic Stream*, Journal of the Aeronautical Sciences, Vol. 16, No. 6, pp. 365–374, June, 1949.

[2] Cohen, Doris, *The Theoretical Lift of Flat Swept-Back Wings at Supersonic Speeds*, N.A.C.A. T.N. No. 1555, March, 1948.

Heat Source in a Uniform Flow*

H. S. Tsien† and Milton Beilock‡
Massachusetts Institute of Technology, Cambridge, Mass.
August 25, 1949

THE PROBLEM OF THE disturbances produced and the forces acting on a heat source in a compressible fluid has been the subject of a recent investigation. The solution obtained is for a line source of heat of strength Q (in mechanical units) per unit length per unit time in a two-dimensional unbounded flow in the x, y plane with the undisturbed velocity U in the x direction. The line source is perpendicular to the x, y plane and is located at the origin. By neglecting the effects of viscosity and heat conduction and by using the Fourier integral technique after linearizing the partial differential equation, the following results are obtained:

M = free-stream Mach Number
p^0 = free-stream static pressure
γ = ratio of specific heats
u' = x-component of disturbance velocity
v' = y-component of disturbance velocity
p' = pressure disturbance, change of static pressure from the value p^0
ρ' = density disturbance
a^0 = velocity of sound in undisturbed flow

For subsonic flow, $M < 1$,

$$u' = \frac{(\gamma - 1)Q}{2\pi\gamma p^0\sqrt{1 - M^2}} \frac{x}{x^2 + (1 - M^2)y^2}$$

$$v' = \frac{(\gamma - 1)\sqrt{1 - M^2}Q}{2\pi\gamma p^0} \frac{y}{x^2 + (1 - M^2)y^2}$$

$$p' = \frac{(\gamma - 1)MQ}{2\pi a^0\sqrt{1 - M^2}} \frac{x}{x^2 + (1 - M^2)y^2}$$

$$\rho' = \frac{(\gamma - 1)MQ}{2\pi a^{03}\sqrt{1 - M^2}} \frac{x}{x^2 + (1 - M^2)y^2} - \frac{(\gamma - 1)Q}{a^{02}U}\delta(y)I(x)$$

where $\delta(y)$ is the δ-function defined as

$$\delta(y) = 0, \quad |y| > 0$$

$$\int_{\epsilon} \delta(y)dy = 1, \quad |\epsilon| \ll 1$$

and $I(x)$ is the unit-step function defined as

$$I(x) = 0 \text{ for } x < 0$$
$$I(x) = 1 \text{ for } x > 0$$

For supersonic flow, $M > 1$, $y > 0$

$$u' = \frac{(\gamma - 1)Q}{2\gamma p^0\sqrt{M^2 - 1}}\delta(x - \sqrt{M^2 - 1}y)$$

$$v' = \frac{(\gamma - 1)Q}{2\gamma p^0}\delta(x - \sqrt{M^2 - 1}y)$$

$$p' = \frac{(\gamma - 1)MQ}{2a^0\sqrt{M^2 - 1}}\delta(x - \sqrt{M^2 - 1}y)$$

$$\rho' = \frac{(\gamma - 1)MQ}{2a^{03}\sqrt{M^2 - 1}}\delta(x - \sqrt{M^2 - 1}y) - \frac{(\gamma - 1)Q}{a^{02}U}\delta(y)I(x)$$

and

$$u'(x, -y) = u'(x, y)$$
$$v'(x, -y) = -v'(x, y)$$
$$p'(x, -y) = p'(x, y)$$
$$\rho'(x, -y) = \rho'(x, y)$$

It is then seen that for subsonic free stream the disturbances are sourcelike, while for supersonic stream the disturbances are essentially limited to a narrow region along the Mach lines. The second terms in the formulas for ρ' are, of course, the heat wake. By taking proper consideration of the linearization, the momentum change due to the heat source is also calculated. This calculation shows that there is no force acting on the heat source.

The above results can be immediately applied to the problem of arbitrary distribution of heat source by the principle of superposition. As an example, let there be a distribution of line sources in the x, y plane along a line inclined at the angle θ with the x axis. In other words, let the heat source be distributed on a plane perpendicular to the x, y plane and making an angle θ with the x, z plane. Let the intensity of the source be q per unit area per unit time. Then for $M < 1$,

$$u' = -\frac{(\gamma - 1)q}{2\gamma p^0}\frac{\sin\theta}{1 - M^2\sin^2\theta}$$

$$v' = \frac{(\gamma - 1)q}{2\gamma p^0}\frac{\cos\theta}{1 - M^2\sin^2\theta}$$

for $M > 1$,

$$u' = -\frac{(\gamma - 1)q}{2\gamma p^0}\frac{\tan\beta \times \sin\beta}{\sin(\beta - \theta)}$$

$$v' = \frac{(\gamma - 1)q}{2\gamma p^0}\frac{\sin\beta}{\sin(\beta - \theta)}$$

where β is the Mach angle, $\sin^{-1}(1/M)$. It is interesting to note that for the subsonic free stream, the disturbance velocity vector is perpendicular to the source surface, while for supersonic free stream it is perpendicular to the Mach wave. In both cases, the flow is decelerated before reaching the heat source. These results have application to the problem of evaluating the true flame propagation speed from flame front photograph.

* This is an abstract from an M.S. thesis (1949) submitted by the junior author to the Department of Aeronautical Engineering, Massachusetts Institute of Technology.

† Professor of Aerodynamics. Now, Robert H. Goddard Professor, California Institute of Technology.

‡ Now at the Aerophysics Laboratory, North American Aviation, Inc.

Action of Viscosity on the Supersonic Wave Drag

E. V. Laitone*
Special Consultant to Hughes Aircraft Company, California
September 1, 1949

SUMMARY

IT IS SHOWN THAT in the case of two-dimensional supersonic flow, viscosity effects can actually decrease the wave drag due to thickness because of the finite boundary layer thickness at the rear of an airfoil.

DISCUSSION

In subsonic flow viscosity effects not only produce a skin friction drag but also directly produce the so-called pressure drag due to the reduction of the pressure recovery at the rear of the body. As shown in Fig. 1, there is a flow compression at the rear of an airfoil which results in zero drag in nonviscous flow but yields a pressure drag whenever viscosity effects produce a boundary layer preventing the stream lines from closing in at the trailing edge.

* Also, Associate Professor, Mechanical Engineering, University of California at Berkeley.

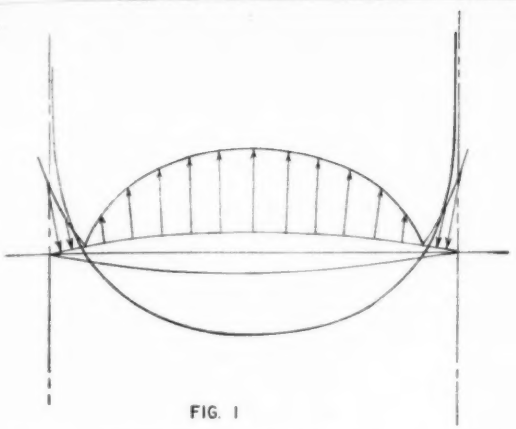

FIG. 1

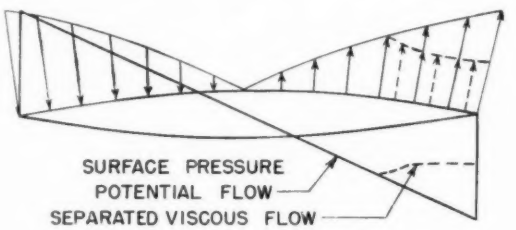

FIG. 2

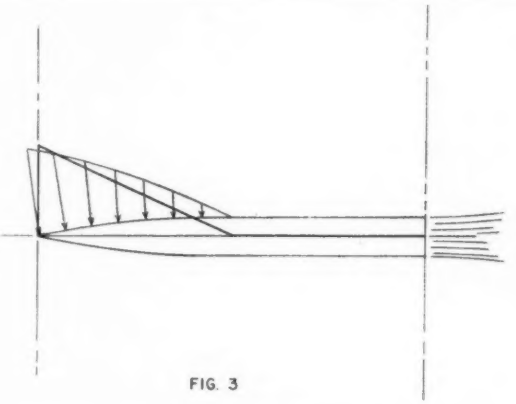

FIG. 3

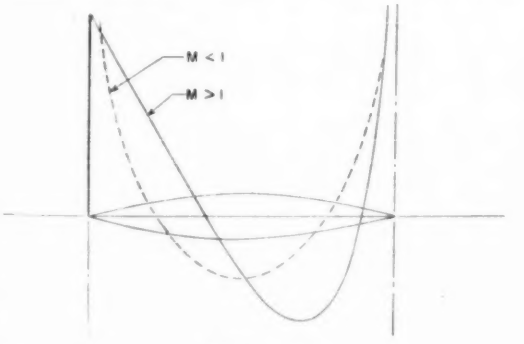

FIG. 4

However, in the two-dimensional supersonic flow over an airfoil, there is no flow compression, the flow continuing to expand over the entire rear portion of the airfoil. The surface pressures as shown in Fig. 2 produce the so-called supersonic wave drag due to thickness (or pressure drag) even in a nonviscous fluid. Any finite boundary-layer thickness would prevent the stream lines from closing in at the trailing edge and would therefore reduce the pressure drag at the rear end. Therefore, in the case of two-dimensional supersonic flow, the viscosity effects create a drag due to skin friction as in the subsonic case but now actually reduce the existing supersonic pressure drag, especially if flow separation takes place.

The two-dimensional supersonic first order lift depends only on the mean inclination of the stream lines along the upper and lower surfaces. Since the lift of a two-dimensional supersonic airfoil does not depend on the flow closing at the trailing edge and the resulting Kutta-Joukowski condition, it is seen that to the first order the supersonic lift is not affected by viscosity if the boundary-layer thickness is the same on the upper and lower surfaces.

Because of this, an improved lift-drag ratio can be obtained for an airfoil shaped as in Fig. 3 and having a jet issuing with at least free-stream velocity from the trailing edge. If, as in Fig. 3, the jet is the same thickness as the airfoil, then the pressure drag would be reduced one-half, allowing a higher lift-drag ratio to be obtained at lower lift. Generally speaking, this is a special case of the Busemann biplane, the total first order lift increment of the upper and lower surfaces being the same as that for a single thin flat plate of the same plan form.

The above effects are not encountered for a body of revolution in supersonic flow because, as shown in Fig. 4, there is again a strong flow compression at the extreme rear of the body of revolution. Then any boundary-layer thickness would increase the drag by decreasing this pressure recovery. As seen in Fig. 4, the pressure gradient at the rear end is greater in supersonic flow than in subsonic flow so that the viscosity effects would produce a greater increase in the surface pressure drag in the supersonic case.

An Experimental Verification of Local Isotropy

Stanley Corrsin
Department of Aeronautics, The Johns Hopkins University, Baltimore, Md.
September 14, 1949

THE MOST SIGNIFICANT IDEA contributed to the problem of turbulent shear flow in many years is the hypothesis of "local isotropy" due to Kolmogoroff.[1, 2] He has suggested that the fine structure in turbulent shear flow may be isotropic.

Recent experiments of Townsend[3, 4] in a wake seem to verify this hypothesis. He found that the skewness and flattening factors of the probability density of $(\partial u/\partial t)$ in the shear flow are closely equal to those in the (effectively isotropic) turbulence far behind a grid. (u = velocity fluctuation in mean flow direction; t = time.)

An independent verification of local isotropy has been obtained by the measurement of the shear correlation coefficient as a function of frequency,

$$ {}_nR_{uv} \equiv \frac{\overline{u_n v_n}}{\sqrt{\overline{u_n^2}}\sqrt{\overline{v_n^2}}} $$

Here, v is the lateral velocity fluctuation; u_n and v_n are the contributions to $u(t)$ and $v(t)$, respectively, in a narrow frequency band of nominal frequency n.

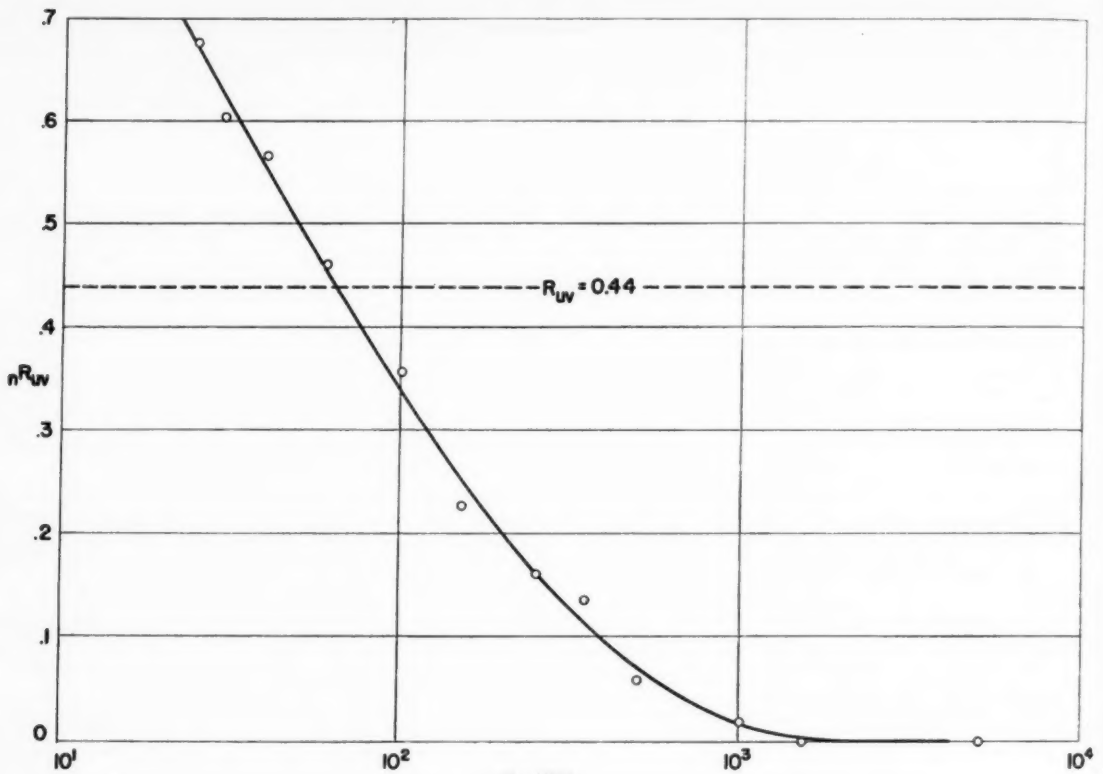

FIG. 1.

The monotonic decrease to zero of ${}_nR_{uv}$ with increasing frequency is a clear indication of the presence of local isotropy (Fig. 1). The overall shear correlation coefficient, also given in the figure, was directly measured by the conventional method. Reasonably good agreement with this value is obtained by computation from ${}_nR_{uv}$ and the power spectrum of u.

These measurements were made in the maximum shear region of a fully developed round turbulent jet. They are part of a broader investigation on turbulent jets[5] sponsored by the National Advisory Committee for Aeronautics.

REFERENCES

[1] Kolmogoroff, A. N., *The Local Structure of Turbulence in an Incompressible Viscous Fluid for Very High Reynolds Numbers*, C. R. Acad. Sci. U.R.S.S. (Doklady), Vol. 30, pp. 301–305, 1941.

[2] Kolmogoroff, A. N., *The Local Structure of Turbulence in an Incompressible Viscous Fluid for Very High Reynolds Numbers*, C. R. Acad. Sci. U.R.S.S. (Doklady), Vol. 32, pp. 16–18, 1941.

[3] Townsend, A. A., *Measurements in the Turbulent Wake of a Cylinder*, Proc. Roy. Soc. (London) A, Vol. 190, pp. 551–561, 1947.

[4] Townsend, A. A., *Local Isotropy in the Turbulent Wake of a Cylinder* Austr. Jour. Sci. Res., A, Vol. 1, pp. 161–174, 1948.

[5] Corrsin, S., and Uberoi, M. S., *Spectra and Diffusion in a Round Turbulent Jet*, N.A.C.A. T.N. (in press), 1949.

Note on Air-Speed Indicator Compressibility Error

Roger D. Schaufele
Douglas Aircraft Company, Inc., Santa Monica, Calif.
September 14, 1949

THE BASIC THEORY of the compressibility error inherent in ordinary air-speed indicators has been well established by previous investigators.[1, 2, 3] The present note extends the theory into the supersonic region.

An air-speed indicator is essentially a differential pressure gage measuring pitot-static pressure, with a dial marked off in arbitrarily chosen speed units. Analysis shows that there is no unique relation between the pitot-static pressure difference and true indicated air speed.* However, at a given pressure altitude, the pitot-static pressure difference is a function only of true indicated air speed, as shown in Fig. 1. An ordinary air-speed indicator, therefore, will read true indicated air speed at only one pressure altitude. Usually air-speed indicator dials are marked off to read true indicated air speed at standard sea-level static pressure. The error in the instrument reading incurred at altitude because of the arbitrary use of this sea-level standard has become significant in recent years as the performance limitations of aircraft have been extended to higher speeds and altitudes. With the advent of supersonic flight, this error becomes increasingly important.

* True Indicated Air Speed (T.I.A.S.) is defined as the true speed times the square root of the density ratio $V_{i_t} = V_t\sigma^{1/2}$; also called Equivalent Air Speed (E.A.S.).

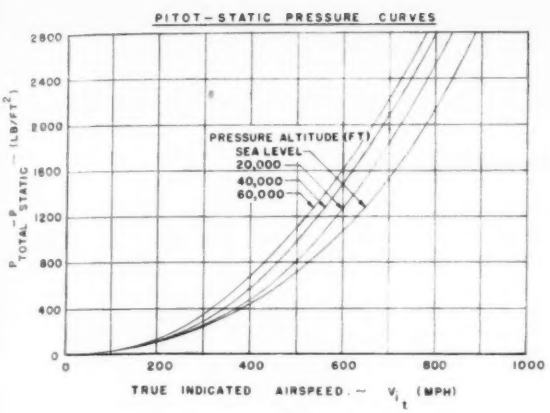

FIG. 1

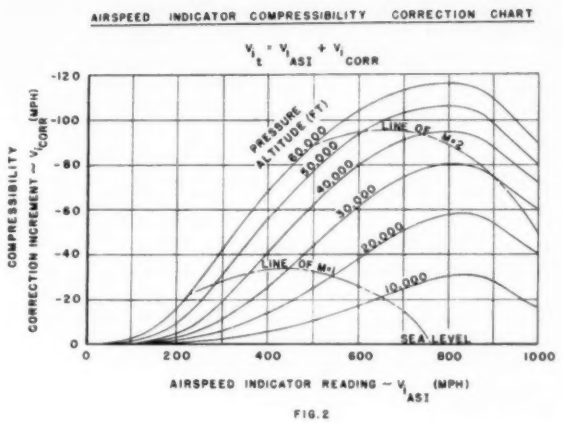

FIG. 2

The analysis is performed for an ideal or "perfect" installation. It is assumed that the meter dial has been marked off to read true indicated air speed at sea level, that there is no lag in pressure readings, and that there is no instrument or position error. The pressures are calculated using the compressible fluid relationships; at supersonic speed, the effect of the bow wave on the total head is included. In addition, it is assumed that the static tap is located in a region of free-stream static pressure behind the shock.

The method of calculation is as follows. At a given pressure altitude, the pitot-static pressure difference, corresponding to a given instrument reading, is converted to a pressure ratio by the identity

$$P_{total}/P_{static} = [P_{total} - P_{static}/P_{static}] + 1$$

From the pressure ratio, it is possible to obtain the Mach Number from the relation

$$P_{total}/P_{static} = \left\{1 + [(\gamma - 1)/2]M^2\right\}^{\gamma/(\gamma-1)}$$

for subsonic flight and

$$\frac{P_{total}}{P_{static}} = \left(\frac{\gamma+1}{2}\right)^{(\gamma+1)/(\gamma-1)} \left(\frac{1}{\gamma}\right)^{1/(\gamma-1)} M^{2\gamma/(\gamma-1)} \times \left[1/\left(M^2 - \frac{\gamma-1}{2\gamma}\right)\right]^{1/(\gamma-1)}$$

for supersonic flight. Fortunately, tables[4] of these pressure ratios as a function of Mach Number have been prepared. Simple interpolation will usually give sufficient accuracy. Once the Mach Number is determined, the true indicated air speed may be found from the equation

$$V_{i_t} = M\sqrt{\gamma g R T \sigma}$$

where

M = flight Mach Number
γ = ratio of specific heats
g = gravitational acceleration
R = gas constant
T = absolute temperature
σ = altitude density ratio

The difference between the instrument dial reading and the true indicated air speed is the compressibility error, and its negative is the compressibility correction increment

The results of the study are presented in Fig. 2. The compressibility correction increment is plotted as a function of the air-speed indicator reading. This is the curve that would be used by pilots to determine the true indicated air speed from the cockpit air-speed indicator reading. Although for present-day aircraft performance the magnitude of the compressibility error is not large, perhaps never more than 10 m.p.h., the study shows that there is a considerable increase in the error at higher speeds and altitudes. For example, an indicator reading of 500 m.p.h. at 50,000 ft. would be in error +78 indicated m.p.h. just from compressibility effects.

There are two additional points that arise in the discussion of the correction curves. First of all, the corrections are valid for any off-standard day so long as pressure altitudes are used and the σ in the equations is defined as the ratio of the density at altitude to sea-level standard density. Secondly, the correction curves have a point of inflection at $M = 1.0$. This change is caused by the formation of the detached shock wave in front of the pitot-static tube and the resulting decrease in total head at the pitot tap. At higher Mach Numbers, and consequently stronger detached shocks, the compressibility error actually decreases.

References

[1] Luskin, Harold, *Charts and Corrections to Airspeed Indicators for Compressibility Effects*, Douglas Aircraft Company, Inc., Report SM-2545, March, 1940.

[2] Kotcher, Ezra, *The Compressibility Factor in Converting Indicated to True Air Speed*, U.S. Air Corps T.R. 4515, February, 1940.

[3] Schoolfield, W. C., *A Simple Method of Applying the Compressibility Correction in the Determination of True Air Speed*, Journal of the Aeronautical Sciences, October, 1942.

[4] Emmons, H. W., Gas Dynamics Tables for Air; Dover Publications, New York, 1947.

Hadamard's Solution for an Inclined Body in Linearized Supersonic Flow

E. V. Laitone*
Associate Professor, Mechanical Engineering, University of California at Berkeley
September 1, 1949

THE INCORRECT SOLUTION mentioned in reference 1 for the velocity potential for linearized supersonic flow about an inclined slender body of revolution had previously been noticed and the correct form given as Eq. (29) of reference 2. This direct analogy to the subsonic doublet was obtained in the supersonic case by introducing Hadamard's concept of the "finite part of the integral."[3]

For example, the potential function given by Eq. (11) of reference 1 should have been written, in the notation of reference 3,

* Special consultant to Hughes Aircraft Company.

as the finite part of the improper integral resulting from the differentiation so that

$$\phi = -\beta^2 \frac{r\cos\theta}{4\pi}\left\{\int_0^{x-\beta r} \frac{g(\xi)d\xi}{[(x-\xi)^2-\beta^2r^2]^{3/2}} = -\beta^2\frac{r\cos\theta}{4\pi}\left\{\int_0^{x-\beta r}\frac{[g(\xi)-g(x-\beta r)]d\xi}{[(x-\xi)^2-\beta^2r^2]^{3/2}} - \frac{(x/\beta^2r^2)g(x-\beta r)}{(x^2-\beta^2r^2)^{1/2}}\right\} \quad (1)$$

as proved directly in Eq. (8) of reference 2.

It is also shown by Eq. (34) of reference 2 that

$$g(x) = 4\alpha U_\infty S(x)\left[1+\beta^2\frac{S''(x)}{2\pi}\log\frac{r}{x}+0(r^2)\right] \quad (2)$$

where $S(x) = \pi r^2$ is the local cross-sectional area of the body of revolution. Therefore to the first order ($r^4 \equiv 0$) we have from Eqs. (1) and (2)

$$\phi = -\frac{\alpha U_\infty\cos\theta}{\pi}\left\{\beta^2 r\int_0^{x-\beta r}\frac{[S(\xi)-S(x-\beta r)]d\xi}{[(x-\xi)^2-\beta^2r^2]^{3/2}} - \frac{(x/r)S(x-\beta r)}{(x^2-\beta^2r^2)^{1/2}}\right\} \quad (3)$$

or by comparison with Eq. (17) of reference 2

$$\phi = -\frac{\alpha U_\infty\cos\theta}{\pi}\frac{1}{r}\int_0^{x-\beta r}\frac{S'(\xi)(\xi-x)d\xi}{\sqrt{(x-\xi)^2-\beta^2r^2}} = -\frac{\alpha U_\infty\cos\theta}{\pi}\beta\int_{\cosh^{-1}(x/\beta r)}^{0} S'(x-\beta r\cosh z)\cosh z\,dz \quad (4)$$

Note that Eq. (4) contains the first derivative of the cross-sectional area, while Eq. (3) only contains S and therefore may be simpler to use in most cases, especially since it is the direct analog to the subsonic doublet. This also shows that Eqs. (10) and (11) of reference 1 are compared incorrectly.

The corresponding Hadamard solutions for the supersonic source distributions for the axial flow along a body of revolution are given in Eqs. (16) and (17) of reference 2.

References

[1] Dorrance, W. H., *Concerning Linearized Supersonic Flow Solutions for Rotationally Symmetric Bodies*, Readers' Forum, Journal of the Aeronautical Sciences, Vol. 16, No. 8, p. 508, August, 1949.

[2] Laitone, E. V., *The Linearized Subsonic and Supersonic Flow about Inclined Slender Bodies of Revolution*, Journal of the Aeronautical Sciences, Vol. 14, No. 11, pp. 631–642, November, 1947.

[3] Hadamard, Jacques, *Lectures on Cauchy's Problem in Linear Partial Differential Equations*; Yale University Press, 1928. (Also see N.A.C.A. T.N. No. 1515 by Heaslet and Lomax.)

Supersonic Airfoil Theory*

Lee S. Wasserman
Wright-Patterson Air Force Base, Dayton, Ohio

September 26, 1949

IT APPEARS that a better physical picture of Ackeret's Supersonic Theory can be obtained by utilizing the particle velocity U set up by the plane wave as shown in Fig. 1.

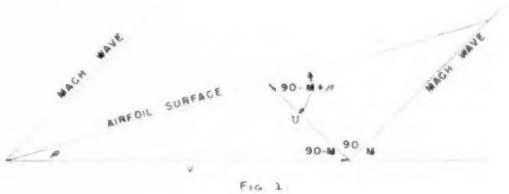

FIG. 1

In order to satisfy the condition normal to the airfoil surface, the following equation is applicable:

$$V\sin\beta = U\sin(90-M+\beta) \quad (1)$$

The value of U for a plane sound wave is given by the well-known equation:

$$\Delta p = \rho C U \quad (2)$$

If U and β are assumed small and cos M is set equal to its value $\sqrt{V^2-C^2}/V$, substitution of Eq. (2) into Eq. (1) yields Ackeret's formula:

$$\Delta p = \rho V^2\beta\sqrt{M^2-1} \quad (3)$$

* Comments on the Readers' Forum item "An Approach to Supersonic Airfoil Theory," by W. E. Strohmeyer and D. R. Gero, Journal of the Aeronautical Sciences, Vol. 16, No. 8, pp. 506–507, August, 1949.

Combustion Problems in Ram-Jet Design

(*Continued from page 713*)

If W_a = the pounds of air per second passing a unit area in the duct and W_f = the pounds of fuel injected per second, then

$$\left.\begin{aligned} W_f &= 2\pi W_a\int_0^\infty f r\,dr \\ &= 2\pi W_a\int_0^\infty (r/ax)e^{-r^2u/4Cx} \\ &= 4C\pi W_a/ua \\ a &= 4\pi CW_a/uW_f \\ f &= (W_fu/4\pi CW_ax)e^{-r^2u/4Cx} \end{aligned}\right\} \quad (6)$$

Present Status of Research on Boundary-Layer Control

(*Continued from page 740*)

[40] Fage, A., and Sargent, R. F., *Design of Suction Slots*, British A.R.C., R. & M. No. 2127, 1944.

[41] Pierpont, P. Kenneth, *Investigation of Suction Slot Shapes for Controlling a Turbulent Boundary Layer*, N.A.C.A. T.N. No. 1292, 1947.

[42] Gerber, Alfred, *Investigation on Removal of the Boundary Layer by Suction*, Translation No. 353, Army Air Corps, Materiel Div., Sept. 26, 1941. (From Mitteilungen aus dem Inst. f. Aerod., November 6, 1938.) Available on request from Air Document Division, Air Materiel Command, Wright Field, Dayton, Ohio.

[43] Rawcliffe, A. G., *Suction Slot Ducting Design*, 10,522, F.M. 1098, Perf. 304, British A.R.C., April 16, 1947.

Index to Volume 16

Journal of the Aeronautical Sciences

Numbers 1–12, January–December, 1949

No. 1, January, 1949, pages 1–64
No. 2, February, 1949, pages 65–128
No. 3, March, 1949, pages 129–192
No. 4, April, 1949, pages 193–256
No. 5, May, 1949, pages 257–320
No. 6, June, 1949, pages 321–384
No. 7, July, 1949, pages 385–448
No. 8, August, 1949, pages 449–512
No. 9, September, 1949, pages 513–576
No. 10, October, 1949, pages 577–640
No. 11, November, 1949, pages 641–704
No. 12, December, 1949, pages 705–768

Material that has appeared in the above volume has been indexed under a general subject heading and by author and has been further cross-indexed under various subheadings.

ADAMS, MAC C. On Shock Waves in Inhomogeneous Flow 685
Aerodynamic hysteresis as a factor in critical flutter speed of compressor blades at stalling conditions 645
Aerodynamics—
Airfoils in Slightly Supersonic Flow, Hsue-Shen Tsien and Judson R. Baron 55
The Analytical Design of an Axially Symmetric Laval Nozzle for a Parallel and Uniform Jet, Kuno Foelsch 161
Applications of the Theory of Free Molecule Flow to Aeronautics, Holt Ashley 95
Base Pressures at Supersonic Velocities, Freeman K. Hill and Ralph A. Alpher 153
The Boundary Layer of Yawed Infinite Wings, J. M. Wild 41
The Drag Problem at High Subsonic Speeds, Adolf Busemann 337
Experiments on a Laminar Suction Airfoil of 17 Per Cent Thickness, W. Pfenninger 227
Flight and Tunnel Test Research on Boundary-Layer Control, H. B. Dickinson 243
Interaction Between Parallel Streams of Subsonic and Supersonic Velocities, H. S. Tsien and M. Finston 515
Interference Between Wing and Body at Supersonic Speeds—Analysis by the Method of Characteristics, Carlo Ferrari 411
Interference Between Wing and Body at Supersonic Speeds—Note on Wind-Tunnel Results and Addendum to Calculations, Carlo Ferrari 542
The Lift Distribution on Conical and Nonconical Flow Regions of Thin Finite Wings in a Supersonic Stream, Theodore R. Goodman 365, Errata, 703
Linearized Theory of Supersonic Control Surfaces, P. A. Lagerstrom and Martha E. Graham 31
Linearized Treatment of Supersonic Flow Through Ducts, H. F. Ludloff and F. Reiche 5
Loads on a Supersonic Wing Striking a Sharp-Edged Gust, M. A. Biot 296
Methods for Predicting Phenomena in the High-Speed Flow of Gases, M. J. Lighthill 69
On a Complete Solution of the One-Dimensional Flow Equations of a Viscous, Heat-Conducting, Compressible Gas, Morris Morduchow and Paul A. Libby 674
On Shock Waves in Inhomogeneous Flow, Mac C. Adams. 685
On the Addition of Heat to a Gas Flowing in a Pipe at Subsonic Speed, Joseph V. Foa and George Rudinger 84
The Oscillating Wedge in a Supersonic Stream, G. F. Carrier 150
The Potential Flow Around Given Wing Sections, Kwei-Lien Chang 306
Present Status of Research on Boundary-Layer Control, A. E. Von Doenhoff and L. K. Loftin, Jr. 729
Problems and Progress in Low-Pressures Research, E. D. Kane and R. G. Folsom 46
Readers' Forum
Action of Viscosity on the Supersonic Wave Drag, E. V. Laitone 756
Aerodynamic Relations with Variable Specific Heat, J. D. Schetzer 190
An Approach to Supersonic Airfoil Theory, W. E. Strohmeyer and D. R. Gero 506, Erratum, 639
Base Pressures at Supersonic Velocities, Ingenieur General Gabeaud 638
Compressibility Correction for Axially Symmetric Bodies, E. V. Laitone 639
Concerning Linearized Supersonic Flow Solution for Rotationally Symmetric Bodies, W. H. Dorrance 508
Determination of Stability Derivatives from Flight Data, Harry Greenberg 62
An Experimental Verification of Local Isotropy, Stanley Corrsin 757
First Order Wing-Body Interference Effects, E. V. Laitone 510
Formulas for the Theoretical Lift of Flat Wings at Supersonic Speeds, Ellis Lapin 381
Hadamard's Solution for an Inclined Body in Linearized Supersonic Flow, E. V. Laitone 759
A Hypothesis Concerning Turbulent Exchange, Wallace D. Hays 316
Lift and Drag of Rectangular Wings of Finite Aspect Ratio in Accelerated, Transonic Flight, C. S. Gardner and H. F. Ludloff 635
Maneuvering Horizontal Tail Loads, Innes Bouton 440
A Note on Detached Shock Waves, E. V. Laitone 441
Note on Supersonic Wing Pressure Distribution, Ellis Lapin 755
Note on the Perturbation Theory for Axially Symmetric Flows, C. C. Lin and E. Reissner 318
A Note on the Velocity of Sound, Morris Morduchow 635
On Damping in Pitch for Delta Wings, John W. Miles 574
On Nonsteady Motion of Delta Wings, John W. Miles 568
On the Compressibility Correction Factor for Axially Symmetric Bodies, W. H. Dorrance 443, 703
On the Hodograph Method, Y. H. Kuo 189
On the Oscillating Aileron at Supersonic Speeds, John W. Miles 511
On the Oscillating Rectangular Airfoil at Supersonic Speeds, John W. Miles 381, Errata, 702

Oscillating Airfoils at Mach Number I, N. Rott..... 380
Quasi-Stationary Airfoil Theory in Compressible Flow, John W. Miles..... 509
Quasi-Stationary Thin Airfoil Theory, John W. Miles.. 440
The Rolling and Yawing Moments Due to Yaw of Unswept Wings, R. F. Anderson.....445, Errata, 573
The Shock-Boundary Condition, B. Etkin..... 318
A Simple Method of Calculating the Subsonic Rolling Characteristics of Sweptback Wings, Edward N. Spryer..... 702
Spanwise Lift Distribution for Sweptback Wings, Alan Pope and William R. Haney, Jr..... 505
Supersonic Airfoil Theory, Lee S. Wasserman..... 760
Transform and Variational Methods in Supersonic Aerodynamics, John W. Miles..... 252
Transient Phenomena at Sonic Speed, N. Rott..... 439
On Transient Two-Dimensional Flows at Supersonic Speeds, Charles E. Watkins..... 569
Relations Between the Characteristics of a Wing and Its Reverse in Supersonic Flow, A. H. Flax..... 496
A Solution for the Lift and Drag of Airfoils with Air Inlets and Suction Slots, C. B. Smith..... 581
Temperature and Velocity Profiles in the Compressible Laminar Boundary Layer with Arbitrary Distribution of Surface Temperature, Dean R. Chapman and Morris W. Rubesin..... 547
Two-Dimensional Airfoils in Hypersonic Flows, Richard D. Linnell..... 22
Two-Dimensional Jet Mixing of a Compressible Fluid, S. I. Pai..... 463
A Unit Solution for the Load Distribution of a Nonrigid Wing by Matrix Methods, Samuel Pines..... 470
Airfoil, in subsonic incompressible potential flow, the instability of pitching oscillations of an..... 691
Airfoil, laminar suction, of 17 per cent thickness, experiments on a..... 227
Airfoils in slightly supersonic flow..... 55
Airfoils, two-dimensional, in hypersonic flows..... 22
Airfoils, with air inlets and suction slots, a solution for the lift and drag of..... 581
ALPHER, RALPH A., AND FREEMAN K. HILL. Base Pressures at Supersonic Velocities..... 153
ANDERSON, R. F. The Rolling and Yawing Moments Due to Yaw of Unswept Wings (Readers' Forum)..... .....445, Errata, 573
ASHLEY, HOLT. Applications of the Theory of Free Molecule Flow to Aeronautics..... 95
AUGENSTEIN, BRUNO W. The Simulation of Combustion Models in Wind Tunnels (Readers' Forum)..... 191

BARON, JUDSON R., AND HSUE-SHEN TSIEN. Airfoils in Slightly Supersonic Flow..... 55
BARRY, FRANK W., AND C. DARBY FULTON. Gas Flow in Ducts (Readers' Forum)..... 379
Base pressures at supersonic velocities..... 153
BATDORF, S. B. Theories of Plastic Buckling..... 405
Beam, multicell box, in pure bending, the optimum proportions of..... 653
Beams with variable web, shear distribution in..... 749
BECKER, HERBERT. The Optimum Proportions of a Multicell Box Beam in Pure Bending..... 653
BEILOCK, MILTON, AND H. S. TSIEN. Heat Source in a Uniform Flow (Readers' Forum)..... 756
BEST, G. C. Notes on Column End-Fixity Coefficients... 117
———— The Theory of Beam Columns with Continuous Support Applied to the Problem of Stringer Roll 289
BIJLAARD, P. P. Stability of Sandwich Plates (Readers' Forum)..... 573
———— Theory and Tests on the Plastic Stability of Plates and Shells..... 529
BIOT, M. A. Loads on a Supersonic Wing Striking a Sharp-Edged Gust..... 296
BOLEY, BRUNO A., N. J. HOFF, AND VITO L. SALERNO. Shear Stress Concentration and Moment Reduction Factors for Reinforced Monocoque Cylinders Subjected to Concentrated Radial Loads..... 277
Boundary Layer, compressible laminar, with arbitrary distribution of surface temperature, temperature and velocity profiles in..... 547
Boundary-layer control, flight and tunnel test research on.. 243
Boundary-layer control, present status of research on..... 729
Boundary layer of yawed infinite wings..... 41
BOUTON, INNES. Maneuvering Horizontal Tail Loads (Readers' Forum)..... 440
BRANCHFLOWER, DALE R. A Method of Least Square Adjustment for Measured Wing Deflections..... 375
BUCHERT, KENNETH P. Stringer Panel and Multicell Wing Construction (Readers' Forum)..... 124
Buckling, plastic, theories of..... 405
BUSEMANN, ADOLF. The Drag Problem at High Subsonic Speeds..... 337

CARRIER, G. F. The Oscillating Wedge in a Supersonic Stream..... 150
CARTER, ARTHUR W. Recent N.A.C.A. Research on High Length-Beam Ratio Hulls..... 167
CHANG, KWEI-LIEN. The Potential Flow Around Given Wing Sections..... 306
CHAPMAN, DEAN R., AND MORRIS W. RUBESIN. Temperature and Velocity Profiles in the Compressible Laminar Boundary Layer with Arbitrary Distribution of Surface Temperature..... 547
Column curves for magnesium-alloy sheet..... 301
Column end-fixity coefficients, notes on..... 117
Column, *n*-section, matrix solution of the..... 623
Columns, beam, with continuous support applied to the problem of stringer roll, the theory of..... 289
Columns, a simple approximate formula for effective end-fixity of..... 116
Combustion problems in ram-jet design..... 707
Compressible fluid, two-dimensional jet mixing of a..... 463
Compression tests of curved panels with circular hole reinforced with circular doubler plates..... 354
Compressor blades at stalling conditions, aerodynamic hysteresis as a factor in critical flutter speed of..... 645
Compressors, centrifugal, performance analysis of..... 435
Control surfaces, supersonic, linearized theory of..... 31
Control System—
Equations for the Approximate Solution of Dynamic Problems for Stable Linear Systems, Kurt H. Hohenemser.. 723
Convertible aircraft design, some aspects of..... 611
CORRSIN, STANLEY. An Experimental Verification of Local Isotropy (Readers' Forum)..... 757
COX, H. L. Structural Design for Minimum Weight (Readers' Forum)..... 444
Cylinders, reinforced monocoque, subjected to concentrated radial loads, shear stress concentration and moment reduction factors for..... 277

DAVIS, HUNT, D. G. TRAVER, AND A. M. G. MOODY. Rotary Compressors (Readers' Forum)..... 124
Design—
Landing-Gear Oscillations Due to Unstable Skidding Friction, J. E. Wignot and Frederic M. Hoblit..... 491
Some Aspects of Convertible Aircraft Design, Robert L. Lichten..... 611

Readers' Forum
Suitability of Flying Wings as Jet Airplanes, J. V. Foa 253
Recent N.A.C.A. Research on High Length-Beam Ratio Hulls, Arthur W. Carter 167
DICKINSON, H. B. Flight and Tunnel Test Research on Boundary-Layer Control 243
DORRANCE, W. H. Concerning Linearized Supersonic Flow Solutions for Rotationally Symmetric Bodies (Readers' Forum) 508
——— On the Compressibility Correction Factor for Axially Symmetric Bodies (Readers' Forum) 443
Drag problem at high subsonic speeds 337
DRAPER, C. S., AND Y. T. LI. A New High-Performance Engine Indicator of the Strain-Gage Type 593
DRUCKER, D. C. A discussion of the Theories of Plasticity (Readers' Forum) 567
DUBERG, JOHN E. A Numerical Procedure for the Stress Analysis of Stiffened Shells 451
——— Reinforced Monocoque Cylinders (Readers' Forum) 377
Duct of constant cross-sectional area, mixing of any number of streams in a 697
Ducts, supersonic flow through, linearized treatment of 5
DUKE, JAMES B., AND M. J. TURNER. Propeller Flutter (Readers' Forum) 638
——— Propeller Flutter 323

Elastic stability of simply supported flat rectangular plates under critical combinations of transverse compression and longitudinal bending 272
Engine indicator, of the strain-gage type, a new high performance 593
ETKIN, B. The Shock-Boundary Condition (Readers' Forum) 318

FERRARI, CARLO. Interference Between Wing and Body at Supersonic Speeds—Note on Wind-Tunnel Results and Addendum to Calculations 542
——— Interference Between Wing and Body at Supersonic Speeds—Analysis by the Method of Characteristics 411
FETTIS, HENRY E. The Calculation of Coupled Modes of Vibration by the Stodola Method 259
——— Effect of Rotary Inertia on Higher Modes of Vibration (Readers' Forum) 445
——— A Modification of the Holzer Method for Computing Uncoupled Torsion and Bending Modes 625
FINSTON, M., AND H. S. TSIEN. Interaction Between Parallel Streams of Subsonic and Supersonic Velocities 515
Flame stabilization, basic studies on 714
FLAX, A. H. Relations Between the Characteristics of a Wing and Its Reverse in Supersonic Flow 496

Flight Propulsion—
Aerodynamic Hysteresis as a Factor in Critical Flutter Speed of Compressor Blades at Stalling Conditions, Alexander Mendelson 645
Basic Studies on Flame Stabilization, Glenn C. Williams 714
Combustion Problems in Ram-Jet Design, J. P. Longwell 707
Generalized Charts for Determination of Pressure Drop of a High-Speed Compressible Fluid in Heat-Exchanger Passages, Michael F. Valerino 311
Heat Transfer in Laminar Compressible Boundary Layer on a Porous Flat Plate with Fluid Injection, Shao Wen Yuan 741
Mixing of Any Number of Streams in a Duct of Constant Cross-Sectional Area, Roger Weatherston 697
A New High-Performance Engine Indicator of the Strain-Gage Type, C. S. Draper and Y. T. Li 593
On the Addition of Heat to a Gas Flowing in a Pipe at Subsonic Speed, Joseph V. Foa and George Rudinger 84
Performance Analysis of Centrifugal Compressors, Shao-Pan Liang 435
Readers' Forum
Addition of Heat to a Gas Flowing in a Pipe at Sonic and Subsonic Speeds, Maurice Roy 566
Effect of Disposable Load on Range of Turbojet Airplanes, W. F. Savage 637
Gas Flow in Ducts, Frank W. Barry and C. Darby Fulton 379
Heat Addition in a Pipe, D. G. Samaras 699
Heat Addition to a Flowing Gas, Newman A. Hall 317
Heat Addition to a Flowing Gas, J. V. Foa and G. Rudinger 566
Heat Source in a Uniform Flow, H. S. Tsien and Milton Beilock 756
Importance of Intermolecular Forces at Low Specific Volumes in the Steady, One-Dimensional Flow of a Gas, Lester Lees 447
Induced Deflection Angle in Cascades, W. R. Hawthorne 252
On Sweat-Cooling, E. A. Richardson 62
On Unsteady One-Dimensional Flows with Heat Addition, William Swartz 571
Porous Cooling, Lester Lees 255
Rotary Compressors, Hunt Davis, D. G. Traver, and A. M. G. Moody 124
Research on Aircraft Propulsion Systems, Abe Silverstein 197
The Simulation of Combustion Models in Wind Tunnels, Bruno W. Augenstein 191
Flutter, propeller 323
FOA, J. V., AND G. RUDINGER. Heat Addition to a Flowing Gas (Readers' Forum) 566
——— On the Addition of Heat to a Gas Flowing in a Pipe at Subsonic Speed 84
FOA, J. V. Suitability of Flying Wings as Jet Airplanes, (Readers' Forum) 253
FOELSCH, KUNO. The Analytical Design of an Axially Symmetric Laval Nozzle for a Parallel and Uniform Jet 161
FOLSOM, R. G., AND E. D. KANE. Problems and Progress in Low-Pressures Research 46
Flutter analysis, station functions and air density variations in 315
Free molecule flow, applications of the theory of to aeronautics 95
FULTON, C. DARBY, AND FRANK W. BARRY. Gas Flow in Ducts (Readers' Forum) 379

GABEAUD, INGENIEUR GENERAL. Base Pressures at Supersonic Velocities (Readers' Forum) 638
GARDNER, C. S., AND H. F. LUDLOFF. Lift and Drag of Rectangular Wings of Finite Aspect Ratio in Accelerated, Transonic Flight (Readers' Forum) 635
Gas, Viscous, heat-conducting, compressible, on a complete solution of the one-dimensional flow equations of a 674
Gases, methods for predicting phenomena in the high-speed flow of 69
GATEWOOD, B. E. Shear Distribution in Beams with Variable Web 749
GERARD, GEORGE. Efficient Applications of Stringer Panel and Multicell Wing Construction 35
——— Note on Life Expectancy Analysis of Structures (Readers' Forum) 572
GERO, D. R., AND W. E. STROHMEYER. An Approach to Supersonic Airfoil Theory (Readers' Forum) 506, Errata, 639
GOLAND, MARTIN, AND YUDELL L. LUKE. A Study of the Bending-Torsion Aeroelastic Modes for Aircraft Wings 389
GOODMAN, THEODORE K. The Lift Distribution on Conical and Nonconical Flow Regions of Thin Finite Wings in a Supersonic Stream 365, Errata, 703

GRAHAM, MARTHA E., AND P. A. LAGERSTROM. Linearized Theory of Supersonic Control Surfaces 31
GREENBERG, HARRY. Determination of Stability Derivatives from Flight Data (Readers' Forum) 62
GREIDANUS, J. H. Low Speed Flutter (Readers' Forum) .. 127
GROSSMAN, NORMAN. Elastic Stability of Simply Supported Flat Rectangular Plates Under Critical Combinations of Transverse Compression and Longitudinal Bending 272
Gust, sharp-edged, loads on a supersonic wing striking a .. 296

HALL, NEWMAN A. Heat Addition to a Flowing Gas (Readers' Forum) 317
HANEY, WILLIAM R., JR., AND ALAN POPE. Spanwise Lift Distribution for Sweptback Wings (Readers' Forum) ... 505
HAWTHORNE, W. R. Induced Deflection Angle in Cascades (Readers' Forum) 252
HAYS, WALLACE D. A Hypothesis Concerning Turbulent Exchange (Readers' Forum) 316
Heat-exchanger, passages, generalized charts for determination of pressure drop of a high-speed compressible fluid in 311
Heat transfer in laminar compressible boundary layer on a porous flat plate with fluid injection 741
HILL, FREEMAN K., AND RALPH A. ALPHER. Base Pressures at Supersonic Velocities 153
HISCOCKS, R. D. Analysis of an Unsymmetrical Pin Pattern (Readers' Forum) 317
HOBLIT, FREDERIC M., AND J. E. WIGNOT. Landing-Gear Oscillations due to Unstable Skidding Friction 491
HOFF, N. J., VITO L. SALERNO, AND BRUNO A. BOLEY. Shear Stress Concentration and Moment Reduction Factors for Reinforced Monocoque Cylinders Subjected to Concentrated Radial Loads 277
HOHENEMSER, KURT H. Equations for the Approximate Solution of Dynamic Problems for Stable Linear Systems 723
Holzer method for computing uncoupled torsion and bending modes, a modification of the 625
Hulls, high length-beam ratio, recent N.A.C.A. research on 167
Hypersonic flows, two-dimensional airfoils in 22

Instruments—
A New High-Performance Engine Indicator of the Strain-Gage Type, C. S. Draper and Y. T. Li 593
Readers' Forum
Note on Air-Speed Indicator Compressibility Error, Roger D. Schaufele 758
Interference between wing and body at supersonic speeds—analysis by the method of characteristics 411
Interference between wing and body at supersonic speeds—note on wind-tunnel results and addendum to calculations 542
ISAKSON, GABRIEL. A Method for Accelerating the Convergence of an Iteration Procedure (Readers' Forum) ... 443

Jet, the analytical design of an axially symmetric laval nozzle for a parallel and uniform 161
Jet, two-dimensional, mixing of a compressible fluid 463
Joints, eccentrically loaded riveted or bolted, analysis of ... 120

KANE, E. D., AND R. G. FOLSOM. Problems and Progress in Low-Pressures Research 46
KROLL, WILHELMINA D., AND A. E. MCPHERSON. Compression Tests of Curved Panels with Circular Hole Reinforced with Circular Doubler Plates 354
KUO, Y. H. On the Hodograph Method (Readers' Forum) 189

LAGERSTROM, P. A., AND MARTHA E. GRAHAM. Linearized Theory of Supersonic Control Surfaces 31
LAITONE, E. V. Action of Viscosity on the Supersonic Wave Drag (Readers' Forum) 756
———— Compressibility Correction for Axially Symmetric Bodies (Readers' Forum) 639
———— First Order Wing-Body Interference Effects (Readers' Forum) 516
———— Hadamard's Solution for an Inclined Body in Linearized Supersonic Flow (Readers' Forum) .. 759
———— A Note on Detached Shock Waves (Readers' Forum) 441
Landing-gear oscillations due to unstable skidding friction 491
LAPIN, ELLIS. Formulas for the Theoretical Lift of Flat Wings at Supersonic Speeds (Readers' Forum) 381
———— Note on Supersonic Wing Pressure Distribution (Readers' Forum) 755
LEES, LESTER. Importance of Intermolecular Forces at Low Specific Volumes in the Steady, One-Dimensional Flow of a Gas (Readers' Forum) 447
———— Porous Cooling (Readers' Forum) 255
LI, Y. T., AND C. S. DRAPER. A New High-Performance Engine Indicator of the Strain-Gage Type 593
LIANG, SHAO-PAN. Performance Analysis of Centrifugal Compressors 435
LIBBY, PAUL A., AND ROBERT C. SAUER. Comparison of the Rayleigh-Ritz and Complementary Energy Methods in Vibration Analysis (Readers' Forum) 700
LIBBY, PAUL A., AND MORRIS MORDUCHOW. On a Complete Solution of the One-Dimensional Flow Equations of a Viscous, Heat-Conducting, Compressible Gas 674
LICHTEN, ROBERT L. Some Aspects of Convertible Aircraft Design 611
Lift distribution on conical and nonconical flow regions of thin finite wings in a supersonic stream 365
Lifting surfaces, low aspect ratio, with particular regard to planing craft, an empirical study of 184
LIGHTHILL, M. J. Methods for Predicting Phenomena in the High-Speed Flow of Gases 69
LIN, C. C. AND E. REISSNER. Note on the Perturbation Theory for Axially Symmetric Flows (Readers' Forum) .. 318
LINNELL, RICHARD D. Two-Dimensional Airfoils in Hypersonic Flows 22
LOCKE, F. W. S., JR. An Empirical Study of Low Aspect Ratio Lifting Surfaces with Particular Regard to Planing Craft 184
LOFTIN, L. K., JR., AND A. E. VON DOENHOFF. Present Status of Research on Boundary-Layer Control 729
LONGWELL, J. P. Combustion Problems in Ram-Jet Design 707
Low-pressures research, problems and progress in 46
LUDLOFF, H. F., AND C. S. GARDNER. Lift and Drag of Rectangular Wings of Finite Aspect Ratio in Accelerated, Transonic Flight (Readers' Forum) 635
LUDLOFF, H. F., AND F. REICHE. Linearized Treatment of Supersonic Flow Through Ducts 5
LUKE, YUDELL L., AND MARTIN GOLAND. A Study of the Bending-Torsion Aeroelastic Modes for Aircraft Wings .. 389

Magnesium-alloy sheet, column curves for 301
Materials—
Column Curves for Magnesium-Alloy Sheet, Evan H. Schuette 301
MCPHERSON, A. E., AND WILHELMINA D. KROLL. Compression Tests of Curved Panels with Circular Hole Reinforced with Circular Doubler Plates 354
MENDELSON, ALEXANDER. Aerodynamic Hysteresis as a Factor in Critical Flutter Speed of Compressor Blades at Stalling Conditions 645
MICHIELSEN, H. F. The Stress Analysis of Arbitrarily Shaped Wing Structures with Shear Stressed Skin and Walls 659

MILES, JOHN W. A Formulation of the Aeroelastic Problem for a Swept Wing 477
——— Induction Effects in Aeroelasticity (Readers' Forum) ..... 63, Errata, 126
——— On Chordwise Divergence (Readers' Forum) 126
——— On Damping in Pitch for Delta Wings (Readers' Forum) 574
——— On Harmonic Motion at Supersonic Speeds (Readers' Forum) 378
——— On Nonsteady Motion of Delta Wings (Readers' Forum) 568
——— On the Oscillating Aileron at Supersonic Speeds (Readers' Forum) 511
——— On the Oscillating Rectangular Airfoil at Supersonic Speeds (Readers' Forum) ..... 381, Errata, 702
——— Quasi-Stationary Airfoil Theory in Compressible Flow (Readers' Forum) 509
——— Quasi-Stationary Thin Airfoil Theory (Readers' Forum) 440
——— Transform and Variational Methods in Supersonic Aerodynamics (Readers' Forum) 252
MONROE, G. M. Analysis of Eccentrically Loaded Riveted or Bolted Joints 120
MOODY, A. M. G., HUNT DAVIS, AND D. G. TRAVER. Rotary Compressors (Readers' Forum) 124
MORDUCHOW, MORRIS. A Note on the Velocity of Sound (Readers' Forum) 635
MORDUCHOW, MORRIS AND PAUL A. LIBBY. On a Complete Solution of the One-Dimensional Flow Equations of a Viscous, Heat-Conducting, Compressible Gas 674

NEWELL, JOSEPH S. End-Fixity Coefficients for Columns (Readers' Forum) 319
NEWMARK, N. M. A Simple Approximate Formula for Effective End-Fixity of Columns 116
Nozzle, for a parallel and uniform jet, the analytical design of an axially symmetric laval 161

PAI, S. I. Two-Dimensional Jet Mixing of a Compressible Fluid 463
PAI, S. I., AND W. R. SEARS. Some Aeroelastic Properties of Swept Wings 105
Panels, curved, with circular hole reinforced with circular doubler plates, compression tests of 354
Plates, and shells, theory and tests on the plastic stability of 529
Plates, simply supported flat rectangular, elastic stability of, under critical combinations of transverse compression and longitudinal bending 272
Panel, stringer, and multicell wing construction, efficient applications of 35
PFENNINGER, W. Experiments on a Laminar Suction Airfoil of 17 Per Cent Thickness 227
PINES, SAMUEL. A Unit Solution for the Load Distribution of a Nonrigid Wing by Matrix Methods 470
PINSKER, W. Structural Damping (Readers' Forum) 699
Pipe at subsonic speed, on the addition of heat to a gas flowing in a 84
Planing craft, an empirical study of low aspect ratio lifting surfaces with particular regard to 184
POPE, ALAN, AND WILLIAM R. HANEY, JR. Spanwise Lift Distribution for Sweptback Wings (Readers' Forum) 505
Pressure, drop of a high-speed compressible fluid in heat-exchanger passages, generalized charts for determination of 311
Propellers—
Propeller Flutter, M. J. Turner and James B. Duke 323
Readers' Forum
Propeller Flutter, M. J. Turner and James B. Duke 638
Ram-jet design, combustion problems in 707
RAUSCHER, MANFRED. Station Functions and Air Density Variations in Flutter Analysis 345
REICHE, F., AND H. F. LUDLOFF. Linearized Treatment of Supersonic Flow through Ducts 5
REISSNER, ERIC. Complementary Energy Procedure for Flutter Calculations (Readers' Forum) 316
REISSNER, E., AND C. C. LIN. Note on the Perturbation Theory for Axially Symmetric Flows (Readers' Forum) 318
Research on aircraft propulsion systems 197
RICHARDSON, E. A. On Sweat-Cooling (Readers' Forum) 62
ROTT, N. Oscillating Airfoils at Mach Number 1 (Readers' Forum) 380
——— Transient Phenomena at Sonic Speed (Readers' Forum) 439
ROY, MAURICE. Addition of Heat to a Gas Flowing in a Pipe at Sonic and Subsonic Speeds (Readers' Forum) 566
RUBESIN, MORRIS W., AND DEAN R. CHAPMAN. Temperature and Velocity Profiles in the Compressible Laminar Boundary Layer with Arbitrary Distribution of Surface Temperature 547
RUDINGER, G., AND J. V. FOA. Heat Addition to a Flowing Gas (Readers' Forum) 566
——— On the Addition of Heat to a Gas Flowing in a Pipe at Subsonic Speed 84

SALERNO, VITO L., N. J. HOFF, AND BRUNO A. BOLEY. Shear Stress Concentration and Moment Reduction Factors for Reinforced Monocoque Cylinders Subjected to Concentrated Radial Loads 277
SAMARAS, D. G. Heat Addition in a Pipe (Readers' Forum) 699
SANDORFF, PAUL E. The Problem of Stringer Roll (Readers' Forum) 571
SAUER, ROBERT C., AND PAUL A. LIBBY. Comparison of the Rayleigh-Ritz and Complementary Energy Methods in Vibration Analysis (Readers' Forum) 700
SAVAGE, W. F. Effect of Disposable Load on Range of Turbojet Airplanes (Readers' Forum) 637
SCHAUFELE, ROGER D. Note on Air-Speed Indicator Compressibility Error (Readers' Forum) 758
SCHETZER, J. D. Aerodynamic Relations with Variable Specific Heat (Readers' Forum) 190
SCHOLZ, N. An Empirical Study of Low Aspect Ratio Lifting Surface with Particular Regard to Planing Craft (Readers' Forum) 637
SCHUETTE, EVAN H. Column Curves for Magnesium-Alloy Sheet 301
Seaplanes and Flying Boats—
An Empirical Study of Low Aspect Ratio Lifting Surfaces with Particular Regard to Planing Craft, F. W. S. Locke, Jr. 184
Readers' Forum
An Empirical Study of Low Aspect Ratio Lifting Surface with Particular Regard to Planing Craft, N. Scholz 637
Recent N.A.C.A. Research on High Length-Beam Ratio Hulls, Arthur W. Carter 167
SEARS, W. R., AND S. I. PAI. Some Aeroelastic Properties of Swept Wings 105
Servo-controlled aircraft, the flutter of 397
SHANLEY, F. R. Principles of Structural Design for Minimum Weight 133
——— Simplified Analysis of General Instability of Stiffened Shells in Pure Bending 590
Shells, stiffened, a numerical procedure for the stress analysis of 451
Shells, stiffened, in pure bending, simplified analysis of general instability of 590

Shells, theory and tests on the plastic stability of plates and 529
Shock waves in inhomogeneous flow 685
SILVERSTEIN, ABE. Research on Aircraft Propulsion 197
SMILG, BENJAMIN. The Instability of Pitching Oscillations of an Airfoil in Subsonic Incompressible Potential Flow 691
SMITH, C. B. A Solution for the Lift and Drag of Airfoils with Air Inlets and Suction Slots 581
——— Wind-Tunnel Wall Corrections for Wing-Body Combinations 237
SOROKA, WALTER W. Note on the Relations Between Viscous and Structural Damping Coefficients 409
SPRYER, EDWARD N. A Simple Method of Calculating the Subsonic Rolling Characteristics of Sweptback Wings (Readers' Forum) 702
Stodola Method, the calculation of coupled modes of vibration by the 259
Stress Analysis and Structures—
Analysis of Eccentrically Loaded Riveted or Bolted Joints, G. M. Monroe 120
Compression Tests of Curved Panels with Circular Hole reinforced with Circular Doubler Plates, Wilhelmina D. Kroll and A. E. McPherson 354
Efficient Applications of Stringer Panel and Multicell Wing Construction, George Gerard 35
Elastic Stability of Simply Supported Flat Rectangular Plates Under Critical Combinations of Transverse Compression and Longitudinal Bending, Norman Grossman 272
Matrix Solution of the n-Section Column, William T. Thompson 623
Notes on Column End-Fixity Coefficients, G. C. Best 117
A Numerical Procedure for the Stress Analysis of Stiffened Shells, John E. Duberg 451
The Optimum Proportions of a Multicell Box Beam in Pure Bending, Herbert Becker 653
Principles of Structural Design for Minimum Weight, F. R. Shanley 133
Readers' Forum
Analysis of an Unsymmetrical Pin Pattern, R. D. Hiscocks 317
A Discussion of the Theories of Plasticity, D. C. Drucker 567
End-Fixity Coefficients for Columns, Joseph S. Newell 319
End-Fixity of Columns, George Winter 573
Note on Life Expectancy Analysis of Structures, George Gerard 572
The Problem of Stringer Roll, Paul E. Sandorff 571
Reinforced Monocoque Cylinders, John E. Duberg 377
Stability of Sandwich Plates, P. P. Bijlaard 573
Stringer Panel and Multicell Wing Construction, Kenneth P. Buchert 124
Structural Design for Minimum Weight, H. L. Cox 444
Shear Distribution in Beams with Variable Web, B. E. Gatewood 749
Shear Stress Concentration and Moment Reduction Factors for Reinforced Monocoque Cylinders Subjected to Concentrated Radial Loads, N. J. Hoff, Vito L. Salerno, and Bruno A. Boley 277
A Simple Approximate Formula for Effective End-Fixity of Columns, N. M. Newmark 116
Simplified Analysis of General Instability of Stiffened Shells in Pure Bending, F. R. Shanley 590
The Stress Analysis of Arbitrarily Shaped Wing Structures with Shear Stressed Skin and Walls, H. F. Michielsen 659
Theories of Plastic Buckling, S. B. Batdorf 405
Theory and Tests on the Plastic Stability of Plates and Shells, P. P. Bijlaard 529
The Theory of Beam Columns with Continuous Support Applied to the Problem of Stringer Roll, G. C. Best 289
Stringer roll, the theory of beam columns with continuous support applied to the problem of 289
STROHMEYER, W. E., AND D. R. GERO. An Approach to Supersonic Airfoil Theory (Readers' Forum) 506, Errata, 639
Structural damping coefficients, note on the relations between viscous and 409
Supersonic flow, relations between the characteristics of a wing and its reverse in 496
Supersonic flow, slightly, airfoils in 55
Supersonic flow through ducts, linearized treatment of 5
Supersonic speeds, interference between wing and body at—analysis by the method of characteristics 411
Supersonic speeds, interference between wing and body at,—note on wind-tunnel results and addendum to calculations 542
Supersonic stream, the lift distribution on conical and nonconical flow regions of thin finite wings in a 365
Supersonic stream, the oscillating wedge in a 150
Supersonic velocities, base pressures at 153
Supersonic velocities, interaction between parallel streams of subsonic and 515
SWARTZ, WILLIAM. On Unsteady One-Dimensional Flows with Heat Addition (Readers' Forum) 571

THOMSON, WILLIAM T. Matrix Solution of the n-Section Column 623
TRAVER, D. G., HUNT DAVIS, AND A. M. G. MOODY. Rotary Compressors (Readers' Forum) 124
TSIEN, H. S., AND MILTON BEILOCK. Heat Source in a Uniform Flow (Readers' Forum) 756
TSIEN, H. S., and M. FINSTON. Interaction Between Parallel Streams of Subsonic and Supersonic Velocities 515
TSIEN, HSUE-SHEN, AND JUDSON R. BARON. Airfoils in Slightly Supersonic Flow 55
TURNER, M. J., AND JAMES B. DUKE. Propeller Flutter 323
——— Propeller Flutter (Readers' Forum) 638

VALERINO, MICHAEL F. Generalized Charts for Determination of Pressure Drop of a High-Speed Compressible Fluid in Heat-Exchanger Passages 311
Vibration and Flutter—
The Calculation of Coupled Modes of Vibration by the Stodola Method, Henry E. Fettis 259
A Formulation of the Aeroelastic Problem for a Swept Wing, John W. Miles 477
The Flutter of Servo-Controlled Aircraft, Jonathan Winson 397
The Instability of Pitching Oscillations of an Airfoil in Subsonic Incompressible Potential Flow, Benjamin Smilg 691
A Method of Least Square Adjustment for Measured Wing Deflections, Dale R. Branchflower 375
A Modification of the Holzer Method for Computing Uncoupled Torsion and Bending Modes, Henry E. Fettis 625
Note on the Relations Between Viscous and Structural Damping Coefficients, Walter W. Soroka 409
The Oscillating Wedge in a Supersonic Stream, G. F. Carrier 150
Readers' Forum
Comparison of the Rayleigh-Ritz and Complementary Energy Methods in Vibration Analysis, Paul A. Libby and Robert C. Sauer 700
Complementary Energy Procedure for Flutter Calculations, Eric Reissner 316
Effect of Rotary Inertia on Higher Modes of Vibration, Henry E. Fettis 445
Induction Effects in Aeroelasticity, John W. Miles 63, Errata, 126

Low-Speed Flutter, J. H. Greidanus 127
A Method for Accelerating the Convergence of an Iteration Procedure, Gabriel Isakson 443
On Chordwise Divergence, John W. Miles 126
On Harmonic Motion at Supersonic Speeds, John W. Miles 378
Structural Damping, W. Pinsker 699
Some Aeroelastic Properties of Swept Wings, S. I. Pai, and W. R. Sears 105
Station Functions and Air Density Variations in Flutter Analysis, Manfred Rauscher 345
A Study of the Bending-Torsion Aeroelastic Modes for Aircraft Wings, Martin Goland and Yudell L. Luke 389
A Unit Solution for the Load Distribution of a Nonrigid Wing by Matrix Methods, Samuel Pines 470
VON DOENHOFF, A. E., AND L. K. LOFTIN, JR. Present Status of Research on Boundary-Layer Control 729

WASSERMAN, LEE S. Supersonic Airfoil Theory (Readers' Forum) 760
WATKINS, CHARLES E. On Transient Two-Dimensional Flows at Supersonic Speeds (Readers' Forum) 569
WEATHERSTON, ROGER. Mixing of Any Number of Streams in a Duct of Constant Cross-Sectional Area 697
Wedge, oscillating, in a supersonic stream 150
Weight, minimum, principles of structural design for 133
WIGNOT, J. E., AND FREDERIC M. HOBLIT. Landing-Gear Oscillations Due to Unstable Skidding Friction 491
WILD, J. M. The Boundary Layer of Yawed Infinite Wings 41
WILLIAMS, GLENN C. Basic Studies on Flame Stabilization 714
Wind Tunnels—
Problems and Progress in Low-Pressure Research, E. D. Kane and R. G. Folsom 46
Readers' Forum
The Stimulation of Combustion Models in Wind Tunnels, Bruno W. Augenstein 191
Wind-Tunnel Wall Corrections for Wing-Body Combinations, C. B. Smith 237
Wing, and its reverse in supersonic flow, relations between the characteristics of a 496
Wing-body combinations, wind-tunnel wall corrections for .. 237
Wing construction, multicell, and efficient applications of stringer panel 35
Wing, deflections, measured, a method of least square adjustment for 375
Wing, nonrigid, a unit solution for the load distribution of a, by Matrix methods 470
Wing sections, given, the potential flow around 306
Wing structures, arbitrarily shaped, with shear stressed skin and walls, the stress analysis of 659
Wing, supersonic, striking a sharp-edged gust, loads on a ... 296
Wing, swept, a formulation of the aeroelastic problem for a 477
Wings, aircraft, a study of the bending-torsion aeroelastic modes for 389
Wings, swept, some aeroelastic properties of 105
Wings, thin finite, in a supersonic stream, the lift distribution on conical and nonconical flow regions of 365
Wings, yawed, infinite, the boundary layer of 41
WINSON, JONATHAN. The Flutter of Servo-Controlled Aircraft 397
WINTER, GEORGE. End-Fixity of Columns (Readers' Forum) 573

YOUNG, A. D. On the Compressibility Correction Factor for Axially Symmetric Bodies (Readers' Forum) 703
YUAN, SHAO WEN. Heat Transfer in Laminar Compressible Boundary Layer on a Porous Flat Plate with Fluid Injection 741

SUGGESTIONS *for* CONTRIBUTORS *to the Publications of the* INSTITUTE *of the* AERONAUTICAL SCIENCES

The Institute of the Aeronautical Sciences invites both members and nonmembers from any country to submit papers for publication in the JOURNAL OF THE AERONAUTICAL SCIENCES and the AERONAUTICAL ENGINEERING REVIEW. The Institute, following the practice of other societies, does not pay for contributions.

The following directions for the preparation of papers, if followed by authors, will save correspondence, avoid the return of papers for changes, minimize the work of preparation for the printer, and save the expense due to the charges made for "author's corrections."

MANUSCRIPTS: The original typewritten copy of the paper desired, double or triple spaced on one side of white paper sheets, consecutively numbered. There should be wide margins to allow for the marking of directions to the printer. Correcting, changing, or adding to papers after they are in type is costly. It is, therefore, imperative that papers submitted be in final form. Typographical errors may be corrected on proofs, but if authors wish to add material, they may do so at their own expense. In mailing, drawings may be rolled, but manuscripts should be sent flat. Send by first class mail (register, if you wish, for your own protection) to the Editorial Office, Institute of the Aeronautical Sciences, 2 East 64th Street, New York 21, N.Y. All manuscripts will be examined by the Editorial Committee and by the Editor. Authors will be advised as promptly as possible whether the paper is acceptable for publication.

TITLES: The title of the paper should be brief. The name and initials of the author should be written as he prefers. The use of the full name of an author is advocated because of the frequent duplication of initials and surnames which sometimes makes it difficult to establish the identity of the author. This is particularly important for large annual indexing and abstracting services. All titles and degrees or honors are omitted. The name of the organization with which the author is associated should be placed after his name on a separate line. The date on which the paper is received will be inserted by the Editor. The author's title should be indicated in a footnote.

SUMMARIES OR ABSTRACTS: An abstract to be printed at the beginning should accompany each article. It should be adequate as an *index* and as a *summary*. It should contain a statement of major conclusions reached, since summaries in many cases constitute the only source of information used in compiling scientific reference indexes. Abstracts printed in other journals, especially foreign, in most cases, consist of summaries from printed papers. The summary should explain as adequately as possible the major conclusions to a nonspecialist in the subject and should contain from 100 to 300 words, depending on the length of the paper.

SUBHEADINGS: Subheadings should be inserted by the author at frequent intervals. The work of editorial preparation will be simplified by the author providing many subheadings.

MATTER USUALLY DELETED: Photographs or illustrations of little technical interest and not showing advances in general practice. Too detailed tabular matter (general results of such tables may be included in the text). Lengthy descriptions of materials or processes or of preliminary experiments or theories that preceded final results; salient features only are of interest.

REFERENCES AND FOOTNOTES: References should appear as footnotes only, numbered consecutively, grouped together at the end of the manuscript. The arrangement should be as follows: (for books)—[1] Durand, W. F., *Aerodynamic Theory*, 1st Ed., Vol. 1, p. 23. Julius Springer, Berlin, 1934. (For magazines)—[1] Englund, C. R., Crawford, A. B., and Mumford, W. W. *Some Results of a Study of Ultra-Short-Wave Transmission Phenomenon*, Proc. I. R. E., Vol. 20, No. 12, pp. 481 and 482, March, 1933. Please give author, title, edition, volume, page, publisher, and date of publication as indicated. Omission of one required fact causes much extra editorial work and possible inaccuracies.

ILLUSTRATIONS: Illustrations should accompany manuscripts and each should always be referred to in the text, by number. Drawings or graphs should not be larger than 12 × 16 inches, and must be made with jet black India Ink on white paper or tracing cloth, the latter being preferred. *Do not use typewriter for lettering.* The smallest lettering on 8 × 10 inch figures should be no less than $^1/_4$ inch high. Cross-section paper (white with black lines) may be used, but should not have more than 4 lines per inch. If finer ruled paper is used, the major division lines should be drawn in with black ink, omitting the finer divisions. In the case of finely ruled paper, only blue-lined paper can be accepted. *Tracing paper and blueprints* are not acceptable. Lettering and all markings must be large enough to be readable after reduction. Mail rolled or flat, never fold. Drawings that cannot be reproduced (including pencil drawings) will be returned to the author for redrawing, thus delaying publication of the paper. Photographs should be distinct and show clear black and white contrasts. They must be on glossy white paper. Avoid round and oval photographs.

CAPTIONS AND LEGENDS: Legends or captions must accompany each drawing or photograph submitted. If written on the drawing or photograph, they should be placed below and well outside the part to be reproduced. Each table should have a caption such as Table 1, Table 2, Table 3, etc. Captions should be complete in themselves so as to make the data intelligible to the reader without reference to the text. A duplicate list of captions for figures should be included as the last page of the manuscript. Use "Fig. 1" (not Figure 1), Figs. 3 and 4, etc., in both the text and the numbering of illustrations. In the text, "Eq. (1)," or "Eqs. (1) and (2)" are preferable to "Equation (1)." In captions and legends, except for "Fig." and "Eq.," and in table headings, write all words in full; do not abbreviate.

MATHEMATICAL WORK: Only the simplest formulas should be typewritten, all others should be carefully written in pen and ink, the writing to be large enough so that ample room is provided to mark mathematical matter for the printer. A considerable space for marking should be allowed above and below all equations. All complicated equations should be repeated on separate sheets with plenty of space left for marking. The solidus should be used for simple fractions appearing within the text. Make all expressions clear to the typesetter. Greek letters used in formulas should be clearly designated by name on the margin of the manuscript. All symbols should be clearly written and carefully checked. The difference between capital and lower-case letters should be clearly distinguished and care taken to avoid confusion between zero (0) and the letter (o), between the numeral (one) and the letter (ell) and the prime ('), between alpha and a, kappa and k, u and mu, v and nu, n and eta. All subscripts and exponents should be clearly marked and dots and bars over letters or mathematical expressions should be avoided. Avoid complicated exponents and subscripts. When it is necessary to repeat a complicated expression, it should be represented by some convenient symbol.

NOMENCLATURE AND ABBREVIATIONS: Standard abbreviations should be used, and it should be noted that most abbreviations are lower case such as m.p.h., b.m.e.p., i.hp., b.hp., hp., . . . etc.